Studies on the Interaction between Retinoschisin and the Retinal Na/K-ATPase

Towards Elucidating the Molecular Pathomechanism of X-linked Juvenile Retinoschisis

Dissertation

zur Erlangung des Doktorgrades

der Biomedizinischen Wissenschaften

(Dr. rer. physiol.)

der

Fakultät für Medizin

der Universität Regensburg

vorgelegt von

Karolina Plößl

aus

Nabburg

im Jahr

2017

Studies on the Interaction between Retinoschisin and the Retinal Na/K-ATPase

Towards Elucidating the Molecular Pathomechanism of X-linked Juvenile Retinoschisis

Dissertation

zur Erlangung des Doktorgrades

der Biomedizinischen Wissenschaften

(Dr. rer. physiol.)

der

Fakultät für Medizin

der Universität Regensburg

vorgelegt von

Karolina Plößl

aus

Nabburg

im Jahr

2017

Dekan: Prof. Dr. Dr. Torsten E. Reichert

Betreuer: Prof. Dr. Bernhard H.F. Weber

Tag der mündlichen Prüfung:

Parts of this work have already been published in peer-reviewed journals in an open access format

Plössl, K., Weber, B. H. F., & Friedrich, U. (2017). The X-linked juvenile retinoschisis protein retinoschisin is a novel regulator of mitogen-activated protein kinase signalling and apoptosis in the retina. *Journal of Cellular and Molecular Medicine*, *21*(4), 768–780. (a)

Plössl, K., Royer, M., Bernklau, S., Tavraz, N. N., Friedrich, T., Wild, J., Weber, BHF, Friedrich, U. (2017). Retinoschisin is linked to retinal Na/K-ATPase signaling and localization. *Molecular Biology of the Cell*, mbc.E17-01-0064. (b)

Table of Contents

Zusammenfassung

Bei der X-gebundenen juvenilen Retinoschisis (engl. X-linked juvenile retinoschisis, XLRS) handelt es sich um eine degenerative Erkrankung der Netzhaut, welche auf Grund ihres X-chromosomalen Vererbungsmusters vorwiegend bei Männern auftritt (George et al., 1995). Charakteristisch für die XLRS ist eine Aufspaltung der retinalen Schichten (Schisis) und eine defekte Signalweiterleitung von Photorezeptor- zu Bipolarzellen. Ursächlich für diese Erkrankung sind Mutationen im *RS1*-Gen (Sauer et al., 1997). Das vom *RS1*-Gen kodierte Protein, Retinoschisin, wird in der Retina spezifisch von Photorezeptoren und Bipolarzellen exprimiert und bindet an die Plasmamembranen dieser Zelltypen. Die Verankerung von Retinoschisin an der Plasmamembran wird dabei von der retinalen Na/K-ATPase vermittelt (Friedrich et al., 2011), welche bereits in einer früheren Studie als ein Interaktionspartner von Retinoschisin identifiziert wurde (Molday et al., 2007).

Der molekulare Pathomechanismus der XLRS und inwiefern die retinale Na/K-ATPase in der XLRS-Pathogenese involviert ist, ist bisher nicht bekannt. Ziel dieser Arbeit war es daher, funktionelle Konsequenzen sowie die strukturelle Basis der Retinoschisin-Na/K-ATPase Interaktion zu untersuchen.

Für die folgenden Studien wurden zunächst die kodierenden Sequenzen für Retinoschisin und eine pathogene Retinoschisin-Variante, RS1-C59S, mit einem Myc-Tag fusioniert und in einen Expressionsvektor kloniert, was die Aufreinigung rekombinanten Retinoschisins ermöglichte. Die aufgereinigten Retinoschisin-Varianten wurden in die weiteren Versuche zur Retinoschisin-Na/K-ATPase Interaktion eingesetzt.

Das erste Projekt hatte zum Ziel, einen möglichen Einfluss von Retinoschisin auf Proteinmengen oder Membranstabilität der Na/K-ATPase in Netzhautexplantaten des *RS1*-Knock out (*Rs1h^{-/Y}*) Mausmodells oder in Hek293 Zellen, welche heterolog die retinale Na/K-ATPase exprimierten, aufzuklären. Rekombinantes Retinoschisin hatte in keinem der beiden Modellsysteme einen Einfluss auf Na/K-ATPase Proteinmengen, weder in Gesamtzelllysaten noch in angereicherten Membranfraktionen.

Ein weiteres Projekt befasste sich mit einem möglichen Effekt von Retinoschisin auf die aktive Ionenpumpfunktion der Na/K-ATPase. Rekombinantes Retinoschisin hatte dabei keinen Einfluss auf die ATP-Hydrolyserate oder Substrataffinitäten der Na/K-ATPase in *Rs1h^{-/Y}*-Netzhautexplantaten. Ebenso hatte es keinen Einfluss auf die Ionentransportaktivität der heterolog in *Xenopus leavis* Oozyten exprimierten, humanen retinalen Na/K-ATPase.

Im Rahmen des dritten Projekts wurde untersucht, ob Retinoschisin die Na/K-ATPase abhängige Signaltransduktion beeinflussen kann. Die Zugabe von Retinoschisin, nicht aber von RS1-C59S, verminderte die Aktivität von c-RAF und ERK1/2, zentraler Komponenten des MAPK

(Mitogen-aktivierten Proteinkinase) Signalweges, in *Rs1h⁻/Y* Netzhautexplantaten sowie in der humanen Retinoblastom-Zelllinie Y-79. Außerdem verminderte Retinoschisin die Expression der MAPK Zielgene *c-FOS* und *EGR1* in beiden retinalen Modellsystemen. Weitere Studien zur Retinoschisin-abhängigen Regulation von Signalkaskaden fokussierten sich auf *Rs1h⁻/Y* Netzhautexplantate. Es zeigte sich, dass die Zugabe von rekombinantem Retinoschisin, nicht aber von RS1-C59S, die Aktivität von Src, welches als initialer Signaltransmitter der Na/K-ATPase beschrieben wurde (Cui und Xie, 2017), mindert. Ebenso verminderte Retinoschisin die Aktivität des Ca^{2+} Signalweg-Markers Camk2. Die Aktivität des PI3K/AKT Signalwegs, repräsentiert durch Akt, wurde von Retinoschisin nicht beeinflusst. Immunhistochemische Analysen muriner, wildtypischer Netzhäute zeigten überlappende Signale des Retinoschisin-Na/K-ATPase-Komplexes mit Signalen von Gerüstproteinen und Transmittern, denen eine Beteiligung an der Na/K-ATPase-Signalweiterleitung zugesprochen wird.

Des Weiteren wurde der Einfluss von Retinoschisin auf die zelluläre Homöostase untersucht. Die Behandlung von Y-79-Zellen mit rekombinantem Retinoschisin hatte keinen Einfluss auf deren Überlebensrate, Zellgröße oder Proliferation. Jedoch zeigte sich nach Zugabe von re-kombinantem Retinoschisin eine Minderung der apoptotischen Aktivität sowohl in Y-79-Zellen als auch in *Rs1h⁻/Y* Netzhautexplantaten. Die Expression des pro-apoptotischen Markergens *BAX* wurde in beiden Modellsystemen beeinflusst und nach unten reguliert. Ebenso zeigten Y-79 Zellen nach Behandlung mit Retinoschisin eine verminderte Caspase-3-Aktivität. Netzhautexplantate der *Rs1h⁻/Y* Maus, die für eine Woche in Gegenwart von Retinoschisin *ex vivo* kultiviert wurden, zeigten eine deutlich reduzierte Photorezeptordegeneration.

Das letzte Projekt befasste sich mit der Identifikation der Retinoschisin-Interaktionsfläche der Na/K-ATPase. Neun verschiedene Na/K-ATPase-Isozymkombinationen (ATP1A1, ATP1A2, und ATP1A3 in Kombination mit ATP1B1, ATP1B2, oder ATP1B3) wurden hinsichtlich ihrer Fähigkeit, Retinoschisin zu binden, untersucht. Eine Retinoschisin-Bindung fand nur an Na/K-ATPasen, welche die ATP1B2-Untereinheit enthielten, statt. Die Herstellung chimärer ATP1B2-ATP1B1-Untereinheiten ermöglichte es, die Interaktionsstelle weiter auf die extrazelluläre Domäne der ATP1B2-Untereinheit einzuschränken. Mit Hilfe bioinformatischer Analysen wurden anschließend zwei mögliche Protein-Interaktionsregionen auf ATP1B2 identifiziert. Durch gerichtete Mutagenese wurden diese Regionen gezielt entfernt, in dem die entsprechenden Aminosäuresequenzen von ATP1B1 eingefügt wurden. Retinoschisin-Bindeversuche an diese chimären ATP1B2-Mutanten ergaben eine Kandidatenregion für die Retinoschisin-Interaktionsstelle in der zweiten Interaktionsregion, an Aminosäure T240.

Zusammenfassend liefert diese Arbeit neue Einblicke in initiale pathologische Prozesse der XLRS, was die Erforschung neuer therapeutischer Strategien für diese bisher unheilbare Krankheit vorantreiben könnte.

Summary

X-linked juvenile retinoschisis (XLRS) is a degenerative disease of the retina which primarily affects males due to an X-chromosomal recessive mode of inheritance (George et al., 1995). Mutations in the *RS1* gene were shown to be causative for XLRS (Sauer et al. 1997) which is characterized by a splitting of the retinal layers (schisis) as well as defects in signal transduction between photoreceptors and bipolar cells (Molday et al. 2012). The protein encoded by *RS1,* retinoschisin, is specifically expressed and secreted by photoreceptors and bipolar cells in the retina and was found to bind to plasma membranes of these cell types. Membrane anchorage of retinoschisin was shown to be mediated by the retinal Na/K-ATPase (Friedrich et al., 2011), which had been identified as a retinoschisin interacting protein before (Molday et al., 2007).

The molecular pathomechanism of XLRS and a putative involvement of the Na/K-ATPase in XLRS pathogenesis remain elusive. Therefore, aim of this study was to investigate functional consequences and the structural basis of retinoschisin-binding to the Na/K-ATPase.

To this end, the coding sequences for retinoschisin and a pathogenic retinoschisin variant, RS1-C59S, were fused to a Myc-tag and cloned into expression vectors, enabling purification of the recombinant proteins. These purified proteins were then used in further studies addressing the interaction between retinoschisin and the Na/K-ATPase.

The first project aimed to delineate whether retinoschisin influences Na/K-ATPase levels or membrane stability in murine retinal explants of an *RS1* knock out (*Rs1h$^{-/Y}$*) mouse model or in Hek293 cells heterologously expressing retinal Na/K-ATPase subunits ATP1A3 and ATP1B2. Recombinant retinoschisin had no effect on Na/K-ATPase protein levels in total cell lysates or enriched plasma membrane fractions from both model systems.

A second project assessed the effect of retinoschisin on the active ion pump function of the Na/K-ATPase. Retinoschisin treatment did not affect Na/K-ATPase catalysed (pump function dependent) ATP cleavage or substrate affinities in *Rs1h$^{-/Y}$* retinal explants. Neither did it affect ion transport activity of the heterologously expressed human retinal Na/K-ATPase in *Xenopus leavis* oocytes.

The third project investigated an influence of retinoschisin on Na/K-ATPase mediated signaling. Recombinant retinoschisin, but not RS1-C59S, was shown to reduce the activity of mitogen activated protein kinase (MAPK) signaling constituents c-RAF and ERK1/2 in *Rs1h$^{-/Y}$* retinal explants as well as the human retinoblastoma cell line Y-79. MAPK pathway target genes *EGR1* and *c-FOS* were also downregulated upon retinoschisin treatment in both model systems. Further studies on signal regulation by retinoschisin focused on *Rs1h$^{-/Y}$* retinal explants as model system. Recombinant retinoschisin, but not C59S, was found to decrease

the activity of the non-receptor tyrosine kinase Src, an initial signal transmitter in Na/K-ATPase mediated signaling (Cui and Xie, 2017). Retinoschisin also decreased the activity of Ca^{2+} signaling marker Camk2, but not activation of PI3K/AKT signaling marker Akt. Immunohistochemistry in murine wildtype retinae showed overlapping signals of the retinoschisin-Na/K-ATPase complex and scaffolding proteins as well as signal transmitters involved in Na/K-ATPase mediated signal transduction.

The next project assessed the effect of retinoschisin on cellular homeostasis. Retinoschisin treatment did not influence cell viability, cell size or proliferation of Y-79 cells. However, retinoschisin but not RS1-C59S treatment lead to decreased apoptotic activity in Y-79 cells and *Rs1h*$^{-/Y}$ retinal explants: Expression of the pro-apoptotic marker gene *BAX* was down regulated in both model systems. In Y-79 cells, retinoschisin reduced the activity of apoptosis marker Caspase-3. *Rs1h*$^{-/Y}$ retinal explants, cultivated in the presence of retinoschisin for one week *ex vivo*, exhibited significantly decreased photoreceptor degeneration.

The last project focused on the identification of the Na/K-ATPase interaction site to retinoschisin. Retinoschisin binding to nine different Na/K-ATPase isozyme combinations (ATP1A1, ATP1A2, and ATP1A3 in combination with ATP1B1, ATP1B2, or ATP1B3) was tested and revealed that retinoschisin specifically binds to ATP1B2. Applying ATP1B2-ATP1B1 chimera, the interaction site was further narrowed down to the extracellular domain of ATP1B2. Next, bioinformatics analyses identified two putative protein-interaction sites on the extracellular domain of ATP1B2. These two "docking patches" patches on ATP1B2 were each mutated by introducing the respective sequences of ATP1B1. Analysis of retinoschisin binding to ATP1B2 docking-patch mutants revealed a candidate region in docking patch II, in specific the amino acid (aa) T240, putatively involved in retinoschisin binding.

Taken together, this work provides novel insight into initial pathological processes of XLRS and could thus enhance the development of novel therapeutic options for this currently untreatable disease.

1 Introduction

1.1 X-linked Juvenile Retinoschisis (XLRS) – Clinical Features

X-linked juvenile retinoschisis (XLRS) is a hereditary retinal dystrophy and represents one of the most common forms of early onset macular degeneration in males (George et al., 1995). XLRS was first described in two brothers by the Austrian ophthalmologist Josef Haas in 1898 (Haas, 1898) and later identified to be of X-linked inheritance (Pagenstecher, 1913). Due to the X-chromosomal recessive mode of transmission, mostly males are affected. Female carriers, in general, are asymptomatic, with few documented cases of subtle retinal changes (Wu et al., 1985, Rodriguez et al., 2005, Saldana et al., 2007). The worldwide estimated prevalence of XLRS ranges between 1:5000 and 1:20000 with hotspots of elevated prevalence for example in Finland, where XLRS was found to be the most common X-linked disease due to three founder mutations in the Finish population (Tantri et al., 2004). XLRS is almost fully penetrant (~ 98 %), and shows a juvenile onset in most patients (Molday et al., 2012). Affected boys often present for ophthalmologic examination at school age when reading difficulties are detected, but symptoms of XLRS were also found in patients being under one year of age, suggesting a congenital onset of the disease (George et al., 1995, Prasad et al., 2006, Renner et al., 2008, Lee et al., 2009).

The clinical manifestations of XLRS are highly variable even within families, but there are phenotypic changes characteristic for a specific diagnosis. As the name "X-linked juvenile retinoschisis" suggests, the disease is characterized by retinal "schisis", i.e. a splitting of retinal layers mainly affecting ganglion cell layer and inner nuclear layer, which can be visualized by spectral domain optical coherence tomography (OCT-SD) (**Figure 1 A**). Retinal schisis is mainly found to affect the fovea in a majority of XLRS patients, but peripheral manifestations are also seen in around 50 % of affected individuals (George et al., 1995, Molday et al., 2012). Alongside with retinal schisis goes the development of large, fluid-filled cysts, also known as schisis cavities. The presence of foveal cysts causes a distinctive spoke-wheel like schisis pattern which is characteristic for XLRS and is used as a main indicator for diagnosis (**Figure 1 B)**. Retinal schisis was shown to be more pronounced in young patients and decreases when patients grow older (George et al., 1995, Molday et al., 2012). A further characteristic feature of XLRS is the so called "negative" electroretinogram (ERG). Compared to healthy individuals, XLRS patients show a lower b-wave response, whereas the a-wave remains almost normal (**Figure 1 C**). The decreased b-wave indicates a defective transmission of visual signals from photoreceptor to bipolar cells (Khan et al., 2001). Since there have been reports of XLRS patients showing normal ERG responses (e.g. Eksandh et al., 2005, Vincent et al., 2013) and clinical manifestation of XLRS is highly variable with regard to disease onset, progression and

severity even in siblings, a combined approach of fundus autofluorescence imaging, OCT imaging, ERG measurement, and molecular-genetic testing is nowadays used to diagnose XLRS (Renner et al., 2008).

Secondary complications like vitreous haemorrhages or retinal detachment can occur in addition to the characteristic clinical features of XLRS. Approximately 5 % of all patients are affected by these secondary complications which in most cases develop in the first decade of life (Molday et al., 2012). Macular holes have also been reported to arise as side effects of XLRS (Brasil et al., 2011; Shukla et al., 2006).

A) Fundus autofluorescence   **B) Optical coherence tomography**   **C) Electroretinogram**
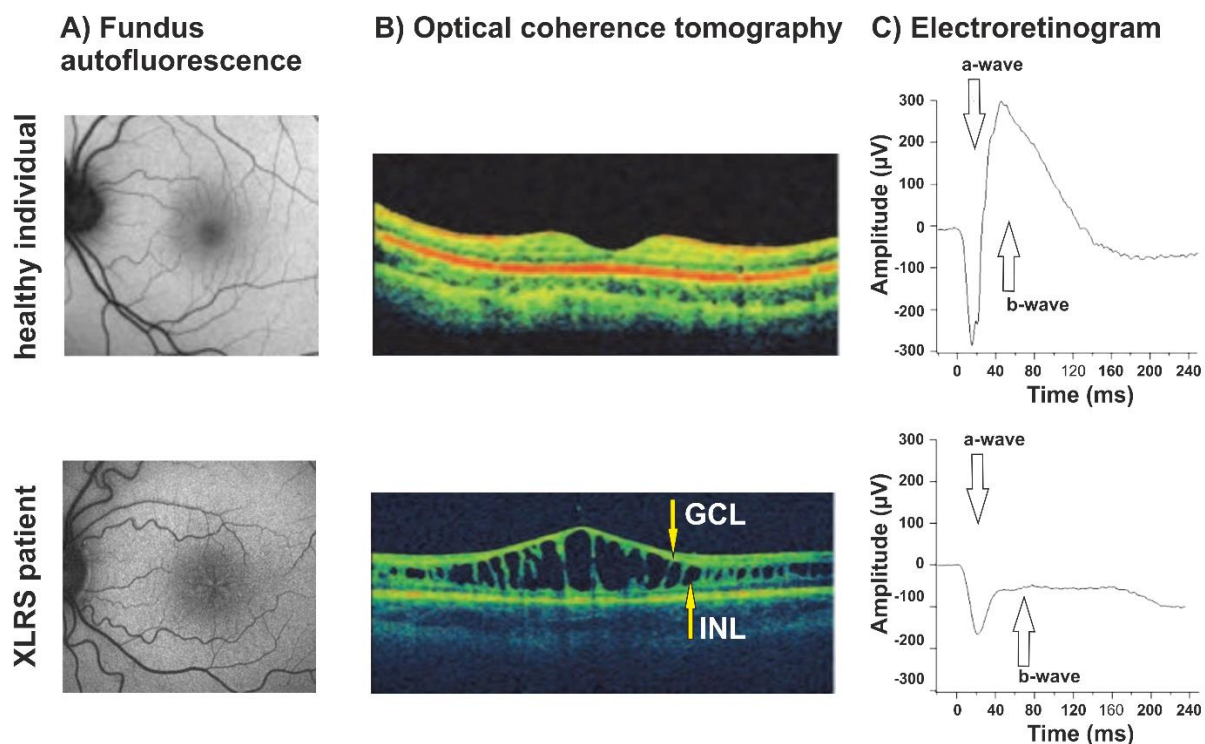
Figure 1: Clinical features of XLRS
A) Fundus autofluorescence images of a healthy individual and a XLRS patient. A spoke-wheel like foveal schisis can be detected in the patient's image. **B)** SD-OCT images of a healthy individual and a XLRS patient. A marked splitting of retinal layers is seen in the foveal area of the XLRS patient's retina between the ganglion cell layer (GCL) and inner nuclear layer (INL) **C)** ERG recordings from a healthy individual and a XLRS patient. The patient's ERG exhibits a strongly reduced b wave (Images adapted from Molday et al., 2012 (A, XLRS patient), Cuba and Gomez-Ulla, 2011 (A, healthy individual), Sergeev et al., 2011 (B) and Bowles et al., 2011 (C)).

1.2 Mutations in the RS1 Gene are Causative for XLRS

After localizing the XLRS-locus in close proximity to Xg blood group markers in 1984 (Wieacker et al., 1984), it was not until 1997 that the XLRS gene was identified by a positional cloning approach (Sauer et al., 1997). The identified gene was termed *RS1* and localizes to the short, distal arm of the X-chromosome at Xp22.2. The *RS1* gene is 32.4 kb in length and is organized in 5 introns and 6 exons. The mRNA transcript arising from *RS1* is 3.1 kb long and encodes a 224 amino acid (aa) long protein named retinoschisin. *RS1* expression was found to be

exclusive to photoreceptor and bipolar cells of the retina (Sauer et al., 1997, Grayson et al., 2000, Molday et al., 2001,) as well as to the pinealocytes of the pineal gland (Takada et al., 2006). Its specific expression is controlled by an upstream CpG island and two opposing CRX (Cone-Rod Homeobox) transcription factor binding regions (Langmann et al., 2008, Kraus et al., 2011). *RS1* expression in murine retina is detectable already at postnatal day 1 (p1) and reaches adulthood levels at p5 to p7 which then stay constant throughout life (Weber and Kellner, 2007). Due to the X-chromosomal recessive mode of inheritance, the lack of correlation of mutation type and disease phenotype, and various biochemical studies on mutant retinoschisin, it is thought that XLRS arises as a result of a functional loss of the retinoschisin protein (e.g. Wang et al., 2002, Wu and Molday, 2003, Vijayasarathy et al., 2010; reviewed by Molday; 2007).

1.3   *Rs1h* Knock Out Mice – A Model System for XLRS

Identification of the *RS1* gene has not only facilitated XLRS diagnostics but also provided the possibility to generate a mouse model for XLRS. Murine retinoschisin is termed Rs1h and shares 96% sequence identity with its human homologue. *Rs1h* knock out mouse lines were generated and characterized independently by several groups (Weber et al., 2002, Zeng et al., 2004, Jablonski et al., 2005). The phenotype resulting from $Rs1h^{-/Y}$ knock out models reflects the human condition of XLRS in the independent mouse lines: Retinal structures are disorganized and a marked retinal splitting is observable in the inner nuclear layer. Also, the characteristic negative ERG is comparable to the human condition (Molday et al., 2012). Together, these features render the retinoschisin-deficient mice excellent model systems for studies on XLRS pathomechanisms as well as treatment options.

1.4   Prospect on Therapeutic Strategies for XLRS

To date, there is no cure for XLRS. Prescription of low-vision aids is still the most common treatment for XLRS patients and the only drug which is under testing for XLRS treatment is 2 % dorzolamide, a carbonic anhydrase inhibitor (CAI). CAIs such as dorzolamide and acetozolomide have been used to successfully treat macular oedema, where inhibition of carbonic anhydrase in the retinal pigment epithelium leads to acidification of the retina and elevated fluid extrusion. This, in turn, results in a lowered intraocular pressure (Wolfensberger, 1999). Because of this known beneficial effects on macular oedema, CAIs were also suggested to reduce schisis cavities in XLRS. Studies have analysed the effects of CAI treatment in 8 or 9 XLRS patients and observed positive effects on foveal thickness, cystic spaces and/or visual acuity in 7 or 5 of these, respectively (Apushkin and Fishman 2006, Verbakel et al., 2016). Successful CAI treatment of XLRS patients was also shown to be

irrespective of the class of disease-associated mutation (Walia et al., 2009). However, there are also studies that have reported no improvement in visual acuity after CAI treatment, but only a decrease in retinal splitting (Genead et al., 2010, Khandhadia et al., 2011). For a subset of XLRS patients, CAI treatment had no effect at all (Apushkin and Fishman 2006, Genead et al., 2010, Khandhadia et al., 2011, Verbakel et al., 2016). A clinical evaluation on the use of 2 % dorzolamide or 1 % brinzolamide, another CAI, in 66 XLRS patients for 18 months has been completed in October 2016 (https://clinicaltrials.gov/ct2/show/NCT02331173, accessed August 31st 2017), but final data on the outcome of this study are not yet available. Due to the few and partially conflicting studies on XLRS patients treated with CAIs, this type of medication is not routinely used in XLRS treatment.

RS1 gene replacement using AAV (adeno-associated virus) vectors in the *Rs1h$^{-/y}$* mouse model has successfully reduced XLRS phenotypes and opened up gene replacement therapy as a novel way to cure XLRS (Zeng et al., 2004, Janssen et al., 2008, Park et al., 2009, Ou et al., 2015, Ye et al., 2015, Bush et al., 2016a). Pre-clinical evaluations had already confirmed that the vectors are well tolerated in both mice and *Cynomolgus* macaques: vector DNA was only detectable in eyes and there were no antibodies against the exogenously expressed retinoschisin (Ye et al., 2015a, Ye et al., 2015b). Currently there is a Phase I clinical trial ongoing on gene replacement therapy for XLRS using AAV based vectors (https://clinicaltrials.gov/ct2/show/NCT02317887, accessed August 2nd 2017). Solid Lipid Nanoparticles (SLNs) have also been used to deliver *RS1* to the eyes of *Rs1h$^{-/Y}$* mice resulting in reduced photoreceptor loss and schisis formation (Apaolaza et al., 2015, Apaolaza et al., 2016). SLNs may thus provide an alternative approach to viral gene replacement therapies.

For all three XLRS therapeutic approaches, however, further studies and especially long-term follow up of patients will be needed to evaluate their value for XLRS treatment.

1.5   The Retinoschisin Protein

Due to the very limited therapeutic options for XLRS, several research groups aim to dissect the basic pathomechanisms caused by retinoschisin deficiency, and thus the function of retinoschisin in the retina. Retinoschisin is a 24 kDa protein and highly conserved among species. It exhibits four distinct domains: an N-terminal signal peptide (23 aa), a discoidin domain (157 aa), an RS1 domain (39 aa), and a short C-terminal fragment of 5 aa (Sauer et al., 1997, Molday, 2007) (**Figure 2 A**).

The signal peptide is responsible for retinoschisin secretion and is cleaved off during this process. Two cleavage sites, between aa 21-22 and aa 23-24 have been identified within the signal peptide, resulting in two mature retinoschisin isoforms which differ by two aa in length in mouse (Vijayasarathy et al., 2006). Next follows the RS1 domain, which has been given its

name due to the lack of sequence homology with any other known protein (Molday et al., 2012). The subsequent discoidin domain, however, is highly conserved and found in many other proteins. After the discoidin domain, the last element to follow in the retinoschisin protein is the short C-terminal segment.

The discoidin domain makes up about 75 % of the mature retinoschisin protein and is thought to be the major functional unit of retinoschisin (Wu et al., 2003, Molday, 2007). A discoidin domain was first identified in the discoidin I protein of *Dictyostelium discoideum* (Poole et al., 1981) and later found as a recurrent motif in a huge variety of eukaryotic and prokaryotic proteins (Baumgartner et al., 1998, reviewed by Kiedzierska et al., 2007). Discoidin domain containing proteins are involved in a plethora of cellular processes such as cellular adhesion, fertilization, migration, signaling and development (reviewed by Kiedzierska et al., 2007). Discoidin domains are organized in a core domain which is highly conserved, and so called spike or loop regions which, in contrast, are highly variable (reviewed by Kiedzierska et al., 2007). The core domain of discoidin domains consists of a five-stranded antiparallel ß-sheet which is tightly packed up against a three-stranded antiparallel ß-sheet forming a distorted barrel like structure. From this core barrel two or more of the highly variable spike regions are protruding. The spike regions form a groove which serves as the recognition site for discoidin domain's interaction partners. Since the spike regions are highly variable, discoidin domains can bind to a variety of ligands including lipids, carbohydrates and proteins which goes along with the diverse functions they have been attributed (reviewed by Kiedzierska et al., 2007). Even though the 3-D structure of the retinoschisin discoidin domain has not been determined yet, the availability of high resolution structures of many other discoidin domains allowed for modelling of the retinoschisin discoidin domain. In case of the retinoschisin discoidin domain, three spikes protrude from one end of a core hydrophobic structure of eight ß-strands (Wu and Molday, 2003).

Retinoschisin is secreted from photoreceptors and bipolar cells as a homo-octameric complex (**Figure 2 B**). Oligomerization was shown to take place before the protein is secreted from the endoplasmatic reticulum (ER) (Molday et al., 2001, Wu and Molday, 2003, Wu et al., 2005). Intensive studies on known pathogenic retinoschisin variants determined the cystein residues responsible for retinoschisin oligomerisation: While two retinoschisin monomers are linked together by a disulfide bond between their cystein residues at aa position 40 (C40), octamerization is achieved by disulfide bonds between cystein at position 59 (C59) in the RS1 domain and cystein at position 223 (C223) in the C-terminal segment of two retinoschisin monomers (Wu and Molday, 2003, Wu et al., 2005). Recently, technical advances enabled the determination of the structure of the retinoschisin octamer. Using single particle electron microscopy, Bush and colleagues were the first to present retinoschisin to be arranged in a cog-wheel like ring structure, with the RS1 domains facing the inside of the ring and the

discoidin domains and especially their spikes facing outwards (Bush et al., 2016). Using cryoelectron microscopy, Tolun and colleagues refined the structure and Ramsay and colleagues analysed the influence of XLRS associated mutants on the octamer structure (Tolun et al., 2016, Ramsay et al., 2016). Tolun and colleagues also provided evidence that two retinoschisin octamers assemble in a back-to-back fashion, forming a hexadecamer (**Figure 2 C**).
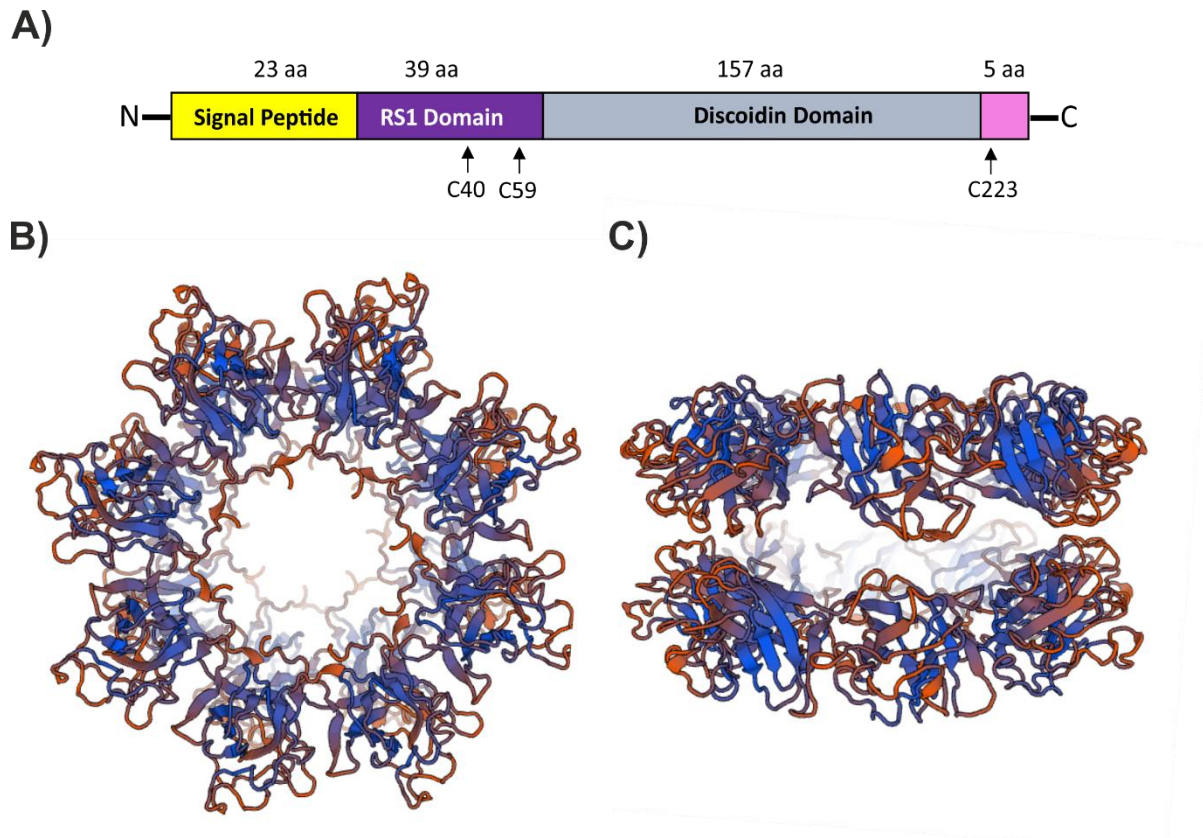
Figure 2: Schematic presentation of retinoschisin domains and 3D structure of hexadecameric complexes
A) Schematic representation of the retinoschisin domains, arrows depict cystein residues which are essential for retinoschisin oligomerization. **B)** Top view onto a retinoschisin double-octamer organized into a cog-wheel like structure. **C)** Side view onto two retinoschisin octamers organized into a hexadecamer in a back-to-back fashion. Subfigures **B)** and **C)** were created using the 3D structure of retinoschisin provided by Ramsay et al., 2016 as a template with the EXPASY swissmodell tool available at https://swissmodel.expasy.org/repository/uniprot//O15537.

Immunolabelling experiments detected retinoschisin on the inner segments of both rod and cone photoreceptors, as well as in plexiform layers with most intensive staining found in photoreceptor inner segments (**Figure 3**) (Grayson et al., 2000, Molday et al., 2001, Reid et al., 2003, Takada et al., 2004).
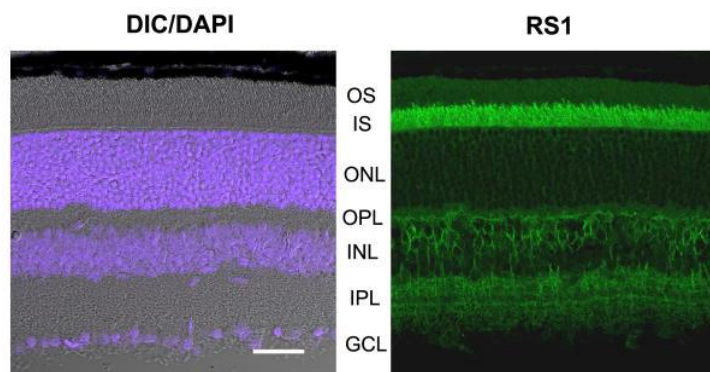
Figure 3: Immunolabeling of a murine retinal cryosection showing retinoschisin localization
Left: DIC/DAPI (differential interference contrast/ 4′,6-Diamidin-2-phenylindol) visualisation of nuclei in retinal layers. Right: Immunohistochemistry (IHC) with an anti-retinoschin antibody OS/IS: outer/inner segments; OPL/IPL outer/ inner plexiform layers; ONL/INL: outer/inner nuclear layer; GCL: ganglion cell layer. (Molday et al., 2012**)**

1.6   Categorization of XLRS Associated Mutations

To date, 197 pathogenic variants of the *RS1* gene have been reported (https://databases.lovd.nl/shared/genes/RS1, accessed August 3rd 2017). In 2012, a review by Molday and colleagues categorized the then known 191 XLRS-associated mutations as follows: 13 % were deletions, 3 % duplications, 1.5 % insertions, 1.5 % insertions/deletions and the majority of 80 % were single nucleotide polymorphisms (SNPs) which may result in pre-mature stop-codons, aa changes or alterations of splice sites. Around 40 % of these mutations are expected to be true null alleles, not allowing translation (Molday et al., 2012). The rest is represented by missense mutations categorized into three different classes with regard to their position in the retinoschisin protein and thus their effects on retinoschisin protein folding, secretion and stability/octamerization.

The first class of missense mutations is represented by mutations in the discoidin domain which seems to be a hotspot for missense mutations and harbours 85 % of all *RS1* missense mutations. The discoidin domain missense mutations biochemically characterized so far in general led to defects in retinoschisin secretion caused by ER retention (Wang et al., 2002, Wu et al., 2003, Iannaccone et al., 2006, Wang et al., 2006, Walia et al., 2009, Gleghorn et al., 2010). As shown by Gleghorn and colleagues, misfolded retinoschisin does not induce the unfolded protein response (UPR), which suggests that it is rather the null phenotype that causes disease than cellular stress induced by UPR (Gleghorn et al., 2010).

Missense mutations in the signal peptide of retinoschisin represent the second class of distinctive *RS1* mutations. These mutations (e.g. RS1-L12H (NM_000330.3(RS1):c.35T>A [p.Leu12His] and RS1-L13P (NM_000330.3(RS1):c.38T>C [p.Leu13Pro]) were shown to prevent translocation of the nascent protein into the ER, resulting in complete absence of mature retinoschisin and thus a null phenotype (Wang et al., 2002, Vijayasarathy et al., 2010).

The third class of *RS1* mutations leads to protein variants which are still secreted, but exhibit abnormal oligomerization. As shown by Wu and colleagues the cystein residues C59 and C223 are essential for assembly of retinoschisin octamers and mutations at both of these residues

have been reported in XLRS patients (Wu et al., 2005). Pathogenicity of these mutations led to the suggestion that octamer formation is necessary for correct retinoschisin function.

There are few known mutations which have also been characterized biochemically, and do not fit into any of the mutation categories described above. The retinoschisin variants RS1-R141H (NM_000330.3(RS1):c. 422G>A [p.Arg141His]), RS1-R141G (NM_000330.3 (RS1):c.421>T/G [p.Arg141Gly]), RS1-H207Q (NM_000330.3(RS1):c. 621C>G [p.His207Gln]), and RS1-R209H (NM_000330.3(RS1):c.626G>A [p.Arg209His]) have been shown to be secreted as octameric complexes. Ramsay and colleagues analysed the structural changes introduced into the retinoschisin octamer by mutations R141H and H207Q. Whereas H207Q was reported to destabilize both the retinoschisin monomer and octamer, R141H did not affect overall protein stability. It was suggested that the pathomechanism underlying the R141H mutation potentially arises from defective interaction of the mutant protein with its interaction partners (Ramsay et al., 2016).

1.7 Towards Retinoschisin Function – Proposed Interaction Partners

In spite of the clinical features being well defined and the disease causing gene being known for 20 years, the pathomechanism of XLRS still remains elusive. Efforts have been made to identify the molecular mechanisms underlying retinoschisin function and determine why retinoschisin deficiency has such tremendous consequences for retinal integrity. Retinoschisin has been proposed to interact with galactose, phosphatidylserine, extracellular matrix proteins like laminin, L-type voltage gated ion channels, as well as the retinal Na/K-ATPase (Fraternali et al., 2003, Steiner-Champliaud et al., 2006, Vijayasarathy et a., 2007, Molday et al., 2007, Dyka et al., 2008, Shi et al., 2009, Kotova et al., 2010, Friedrich et al., 2011, Shi et al., 2017), each interaction partner providing room for speculations towards retinoschisin function.

1.7.1 Phospholipids

One of the molecules retinoschisin was proposed to interact with is phosphatidylserine. Phosphatidylserine is an acidic membrane phospholipid which is found in the plasma membrane. A possible interaction of retinoschisin and phosphatidylserine was assumed because other discoidin domain containing proteins were also shown to interact with phosphatidylserine (Ortel et al., 1992, Zwaal et al., 1998). An initial study addressing the interaction between retinoschisin and phosphatidylserine was conducted by Fraternali and colleagues in 2003. Bioinformatical evaluation of XLRS associated mutations leading to aa exchanges at Y89, V90, W92, Y93, F108, and I144 revealed that these aas may form a hydrophobic and exposed region on retinoschisin similar to sites on Factor V and Factor VIII which mediate interactions with phospholipid bilayers (Fraternali et al., 2003). Later studies

showed retinoschisin to co-purify with phosphatidylserine (Vijayasarathy et al., 2007) and atomic force microscopy analyses by the same group detected retinoschisin binding to phosphatidylserine containing planar lipid bilayers (Kotova et al., 2010). However, other groups were not able to verify an interaction between retinoschisin and phosphatidylserine (Molday et al., 2007, Friedrich et al., 2011). In addition to the contradictory experimental data obtained by different *in vitro* systems, the physiological relevance of an interaction between retinoschisin and phosphatidylserine is also questionable. In a native cellular system phosphatidylserine mostly localizes to the inner leaflet of plasma membranes whereas retinoschisin binds to the outer plasma membrane, hence the proposed interaction might not be feasible in a native system (Molday et al., 2012).

1.7.2 Galactose

Discoidin proteins from *Dictyostelium discoideum* were shown to function as lectins and exhibit a high affinity for galactose residues to promote cell aggregation (Poole et al., 1981, Valencia et al., 1989). This finding encouraged Dyka and colleagues to analyse whether retinoschisin is capable of binding to immobilized carbohydrates. They found efficient retinoschisin binding to agarose-coupled galactose and lactose, whereas no retinoschisin binding was observed to agarose-coupled N-acetylgalactosamine, N-acetylglucosamine, mannose or heparin (Dyka et al., 2008). To date, there are no further studies addressing the physiological relevance of the interaction between retinoschisin and galactose. Nevertheless, its high affinity to galactose has been used to purify recombinant retinoschisin (e.g. Bush et al., 2016).

1.7.3 Extracellular Matrix Proteins

In an affinity chromatography based approach to identify retinoschisin binding proteins, the extracellular matrix component β2-laminin and αB crystalline were found to bind to immobilized retinoschisin (Steiner-Champliaud et al., 2006). Interaction with extracellular matrix proteins would strengthen the notion that retinoschisin is involved in cell-cell contact formation, but no further investigations with regard to a physiological relevance of these interactions have been conducted so far.

1.7.4 L-Type Voltage Gated Calcium Channels

In 2009, Shi and colleagues performed co-immunoprecipitations and Yeast-2-Hybrid experiments which identified L-Type Voltage Gated Calcium Channels (L-VGCCs) as novel retinoschisin interaction partners (Shi et al., 2009). L-VGCCs are heteromeric complexes of four different subunits which span the plasma membrane and function as Ca^{2+} specific channels (De Waard et al., 1996). Mutations in the gene encoding the Cav1.4 α1 subunit of L-

VGCCs (*CACNA1F*) were shown to cause X-linked stationary night blindness. *Cacna1f* knock out in mice resulted in a negative ERG, highlighting the importance of L-VGCCs in photoreceptor bipolar synapse integrity (Mansergh et al., 2005). As a negative ERG is also a clinical hallmark of XLRS, an involvement of L-VGCCs in XLRS pathogenesis, possibly due to misregulation in a retinoschisin deficient retina, might be conclusive. A more recent study by Ou and colleagues also showed that retinoschisin is needed to maintain the synaptic localization of L-VGCC in retina (Ou et al., 2015). The latest publication by Shi and colleagues described successful co-immunoprecipitation of retinoschisin and Cav1.3 and Cav1.4 from porcine retinae. Furthermore, retinoschisin was shown to increase L-VGCC currents in transfected Hek293 cells. The same study also presented immunohistochemical analyses indicating that Cav1.4 expression is reduced in retina of *Rs1h$^{-/Y}$* mice, but does not provide quantification (Shi et al., 2017). This finding is contradictory to results from Ou and colleagues, who did not observe any differences in Cav1.4 expression (quantification given) when comparing *Rs1h$^{-/Y}$* and wildtype murine retinae. In addition, Cav1.4 α1 subunits are only expressed and located at release sites of mammalian photoreceptors in the outer plexiform layer, additionally exhibiting a punctate immunostaining in the mouse inner plexiform layer (Boycott et al., 2000, Ball and Greg, 2002, Berntson et al., 2003, Baumann et al., 2004). Retinoschisin signals in contrast are most abundant in the photoreceptor inner segments. Finally, immunohistochemical analyses reveal poor colocalization of Cav1.4 and retinoschisin in the plexiform layers. (Shi et al., 2017). Further analysis will be needed to gain deeper insight into possible effects of retinoschisin on L-VGCC regulation.

1.7.5 The Retinal Na/K-ATPase

Another proposed protein interaction partner of retinoschisin is the retinal Na/K-ATPase consisting of Na/K-ATPase subunits α3 and ß2. This complex was first identified by co-immunoprecipitation of human (and bovine) retina by Molday and colleagues in 2008 (Molday et al., 2008). This study also showed a perfect colocalization of retinoschisin and the retinal Na/K-ATPase in retinal cryosections (Molday et al., 2008). Later studies at the Institute of Human Genetics at the University of Regensburg confirmed the importance of the Na/K-ATPase for membrane anchorage of retinoschisin (Friedrich et al., 2011). Heterologous expression of ATP1A3 and ATP1B2 in Hek293 cells was sufficient to enable retinoschisin binding to Hek293 membranes. Western blot and immunohistochemical analyses demonstrated that retinoschisin no longer binds to retinal membranes in Atp1b2 deficient mice. In return, immunostaining of the Na/K-ATPase subunits α3 and ß2 in *Rs1h$^{-/Y}$* retinae revealed retinal Na/K-ATPase localization different from that in wildtype mice, suggesting an effect of retinoschisin on Na/K-ATPase localization and/or stabilization in the membrane (Friedrich et al., 2011).

1.8   The Na/K-ATPase

1.8.1   Structure of the Na/K-ATPase

The Na/K-ATPase is a plasma membrane spanning ion pump which is ubiquitously expressed. The minimal functional unit of this enzyme is a heterodimeric complex composed of an α and a ß subunit (**Figure 4**).
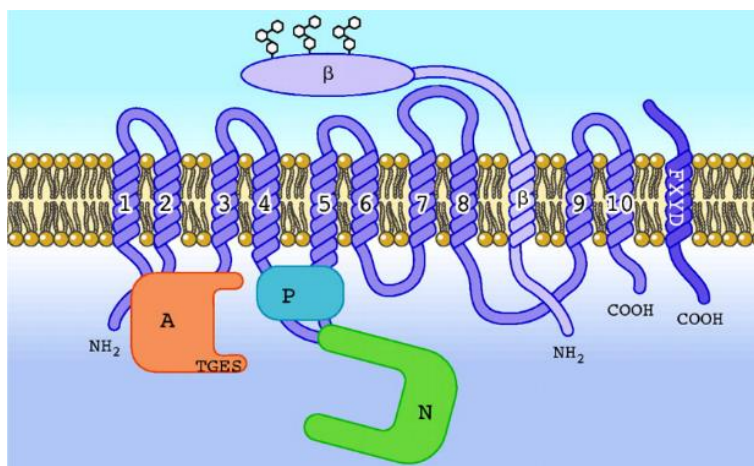
Figure 4: Schematic overview of the Na/K-ATPase structure.
The α subunit is shown in medium purple, numbers 1-10 represent the 10 transmembrane domains; The actuator (A) domain is shown in orange, the phosphorylation (P) domain in blue and the nucleotide binding (N) domain in green. The ß subunit is depicted in light purple, N-linked glycosylation of the extracellular domain is indicated by white hexagons; shown in dark purple is an auxiliary FXYD subunit (modified after Horisberger 2004).

The α subunit is the catalytic subunit of the complex, responsible for ion transport as well as ATP cleavage (Skou et al., 1957). It is also responsible for signal transmission upon binding of cardiac glycosides (reviewed in Cui and Xie, 2017). The α subunit is an integral membrane protein of 110-130 kDa which has 10 transmembrane domains, 5 short extracellular loops, and 4 cytosolic domains. Specific functions have been attributed to the first and second intracellular loops and three domains have been named accordingly: the first loop comprises the nucleotide (ATP) binding domain (N domain), while the second loop contains the phosphorylation domain (P domain) and the actuator domain (A domain) which is responsible for occlusion of cargo ions in the transmembrane binding sites and for dephosphorylation of the P-domain (Kühlbrandt, 2004) (**Figure 4**).

Four different isoforms of the Na/K-ATPase α subunit have been identified and were shown to be expressed in a tissue specific manner. The α1 isoform is omnipresent in all tissues and the predominant isoform in epithelial and heart tissue. The α2 isoform is mainly expressed in heart and skeletal muscle, as well as in astrocytes and glial cells of the brain. The α3 isoform is most strongly expressed in neuronal tissue and α4 was exclusively detected in testis (summarized in Kaplan 2002, Cui and Xie, 2017, Clausen et al., 2017). The α1, α2, and α3 isoforms share about 87 % aa sequence identity while α4 is about 78 % identical to the other three α isoforms (Shamraj and Lingrel, 1994). Even though there are sequence differences, the overall three dimensional structure of all four α isozymes seems to be identical and mainly the extracellular surface of the protein differs between the individual isoforms (Clausen et al., 2017). However,

there are functional differences in the catalytic activity of the isoforms, affecting substrate affinities, voltage dependency and pump activity (Crambert et al., 2000, Blanco, 2005).

Within the retina, different α isoforms were attributed to different retinal cell types. In rodent retina, α1 was found in Müller cells, horizontal cells and to a small extent in photoreceptors, α2 only in some Müller cells, and α3 in photoreceptors and other neuronal cells (Wetzel et al., 1999, Schneider and Kraig, 1990).

The ß subunit does not have any catalytic properties, but is responsible for correct assembly, membrane integration and stability of the α-ß heterodimeric Na/K-ATPase complex (Ackermann and Geering, 1990, Geering 2001, Reinhard et al., 2013). Further, the ß subunit was also shown to modulate activity of the α subunit (Jaisser 1994, Horisberger and Rossier 1992; Eakle et al. 1994; Blanco et al. 1995) and is also involved in mediating intracellular adhesion (e.g. Antonicek et al., 1987, Shoshani et al., 2005, Vagin et al., 2012, Tokhtaeva et al., 2016).

The ß subunit consists of a short cytosolic N-terminal part, a single transmembrane domain and a large extracellular domain (reviewed in Kaplan 2002, Reinhard et al., 2013) (**Figure 4**). Three different isoforms of the ß subunit have been identified, which in contrast to the α isoforms, show only little aa sequence identity (35-47 % in humans) (Reinhard et al., 2013). A common feature of all three ß isoforms is post-translational modification by N-linked glycosylation: ß1 has three glycosylation sites, while ß2 has eight and ß3 two glycosylation sites, respectively (Miller and Farley, 1988, Malik et al., 1996, Tokhtaeva et al., 2010).

Similar to the α subunits, the different ß subunits also show a tissue specific expression pattern. Expression of ß1 has been detected in brain, heart, and kidney, ß2 subunits are expressed predominantly in brain, pineal gland and retina and ß3 expression has been detected in lung, liver and testis (Shyjan and Levenson, 1989, Shyjan et al., 1990, Arystarkhova and Sweadner, 1997). In rodent retina, ß1 is expressed in photoreceptors, horizontal, amacrine and ganglion cells, ß2 is expressed in bipolar cells, photoreceptors and Müller cells, while ß3 is restricted to photoreceptors (Wetzel et al., 1999, Schneider and Kraig, 1990).

In several tissues, members of the FXYD proteins build accessory subunits of the Na/K-ATPase. FXYD proteins are type I membrane proteins, which have a single membrane spanning domain (Swaender and Rael, 2000). The FXYD protein family consists of seven members, five of which are associated with the Na/K-ATPase complex. FXYD1 (phospholemman), FXYD2 (γ-subunit of Na-K-ATPase), FXYD3 (Mat-8), FXYD4 (CHIF), and FXYD7 were shown to interact with the Na/K-ATPase *via* their transmembrane domain and are capable of regulating its function (reviewed by Geering, 2006). FXYD family members exhibit a distinct, tissue specific expression, but, until now, there is no data on FXYD protein expression in the retina.

1.8.2 The Na/K-ATPase as an Ionpump

The most crucial function of the Na/K-ATPase is the maintenance of a steep gradient of Na$^+$ and K$^+$ ions across the cellular plasma membrane. This gradient is essential for many processes such as neuronal excitability, cellular uptake of ions, nutrients, or neurotransmitters, but also for regulation of cell volume and intracellular pH (reviewed by Reinhard et al., 2013). At the expense of one molecule of ATP, the Na/K-ATPase transports three Na$^+$ ions out of and two K$^+$ ions into the cell. For a single cell, this process may consume up to 80 % of the energy stored in ATP molecules. At baseline activity, Na/K-ATPases go through an average of 60-80 phosphorylation-dephosphorylation cycles per minute (reviewed by Orlov et al., 2017). The Na/K-ATPase is a member of the so called P-Type ATPase family of proteins, which all share the presence of a phosphorylated enzyme intermediate during their reaction cycle (Pedersen and Carafoli, 1987). The reaction cycle of the Na/K-ATPase confers two major steps and enzyme conformations, E1 and E2, and is described by the Albers-Post scheme (**Figure 5**). The E1 state is also referred to as the Na$^+$-bound state and the E2 as K$^+$-bound state. The change from one state to the other is accompanied by many intermediate states and conformational changes.
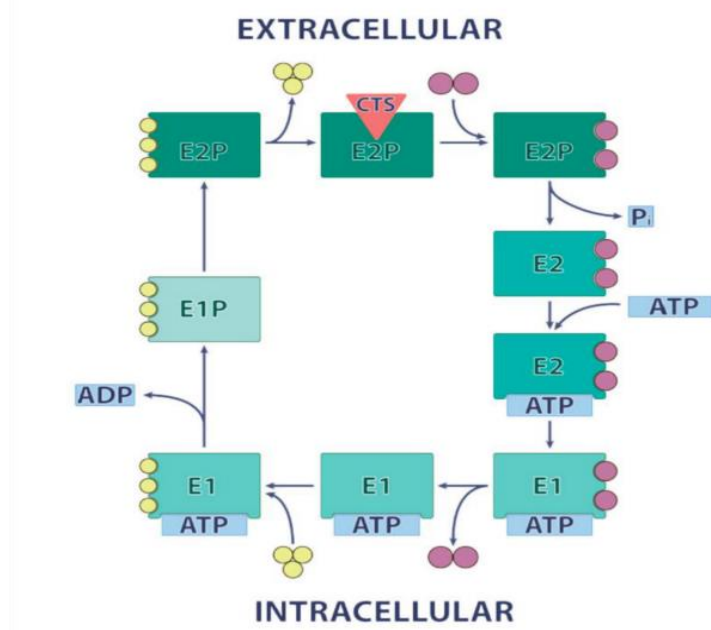
Figure 5: Schematic picture of the Albers-Post reaction cycle of the Na/K-ATPase
Per reaction cycle the Na/K-ATPase transports three Na+ ions (yellow circles) out of the cell and two K+ ions (purple circles) inside. During this reaction cycle one molecule of ATP is hydrolysed and the Na/K-ATPase becomes phosphorylated. E1: Na$^+$-bound conformation, E2: K$^+$-bound conformation, E1P/E2P: phosphate-bound states of E1/E2.
The Na/K-ATPase specific class of cardiotonic steroid inhibitors (CTS, orange triangle) binds to the Na/K-ATPase in its E2P conformation and puts the reaction cycle to a halt at this stage.
(Figure adapted from Orlov et al., 2017)

The transition of the Na/K-ATPase through its reaction cycle can be prevented by the application of a variety of inhibitors. The most commonly used and best studied Na/K-ATPase inhibitors are so called cardiotonic steroids (CTS). Low levels of endogenously produced CTS digoxin, ouabain and marinobufagenin have been detected in mammalian tissue and biological fluids (Schoner and Schreiner-Bobis, 2005, Aperia et al., 2016). For decades, the main medical use of CTS has been for treatment of congestive heart failure. Most frequently used CTS are the plant-derived digoxin, ouabain and the vertebrate-derived bufalin and marinobufagenin

(Schoner and Schreiner-Bobis, 2007). CTS bind to the Na/K-ATPase from the extracellular side and enter the putative ion-exchange pathway with highest affinities for the E2P state (Laursen et al., 2015). By putting the pump to a halt in this position, no more Na^+ ions are transported out of the cell and intracellular Na^+ levels rise, which leads to an inhibition of the Na^+/Ca^{2+} exchanger (NCX). In patients suffering from congestive heart failure, CTS treatment *via* NCX inhibition leads to raised cytoplasmic Ca^{2+} levels, which allows for enhanced contractility of the diseased cardiac muscle (reviewed in Kaplan 2002, Clausen et al., 2017).

1.8.3 Na/K-ATPase Mediated Signaling

There is growing evidence that the Na/K-ATPase also functions as a receptor for signal transduction *via* CTS as hormones (summarized in Aperia et al., 2016, Cui and Xie, 2017). First findings were made in the 1970s, when several studies showed effects of low (sub-pump-inhibitory) nM concentrations of ouabain on gene expression, differentiation and proliferation (Cuff and Lichtman, 1975, Kaplan, 1978, summarized in Cui and Xie, 2017). Later studies from many laboratories then showed that CTS treatment could stimulate different intracellular signaling pathways in various cell types and by that also affect cellular processes like proliferation, development, or apoptosis (e.g. Huang et al., 1997, Kometiani et al., 1998, Xie et al., 1999, Haas et al., 2000, Haas et al., 2002, Dmitrieva and Doris, 2003, Golden and Matrin, 2006, Ramirez-Ortega et al., 2006, Kulikov et al., 2007, Wang et al. 2015). Until today, there is experimental evidence that CTS can trigger the activation of the mitogen activated protein kinase (MAPK) signaling pathway, the phosphoinositide 3-kinase/ Protein kinase B (PI3K/AKT) pathway as well as Ca^{2+} dependent signaling cascades (reviewed in Aperia et al., 2016, Cui and Xie, 2017, Orlov et al., 2017).

The extracellular signal-regulated (ERK) pathway, one of the four MAPK pathways (Lewis et al., 1998, Chang and Karin, 2001), was the first Na/K-ATPase activated signaling pathway to be discovered by Kometiani and colleagues (Kometiani et al., 1998). Upon binding of CTS, various cell types show a strong activation of intracellular ERK signaling. The non-receptor tyrosine kinase SRC is widely accepted to be involved in activation of MAPK signaling through the Na/K-ATPase. However, the exact mechanism of how SRC is implicated in this pathway is discussed controversially (Haas et al., 2000, Haas et al., 2002, Tian et al., 2005, Weigand et al., 2012, Gable et al., 2014, Yosef et al., 2016). Despite the discrepancies on the mechanism of SRC activation by the Na/K-ATPase, SRC is thought to act as the initial, Na/K-ATPase associated signal transmitter which gets activated upon CTS binding to the Na/K-ATPase. Activated SRC stimulates the endothelial growth factor receptor (EGFR), which then signals on towards the MAPK cascade through RAS and RAF (**Figure 6**).

The PI3K/AKT pathway has also been shown to be activated by CTS-bound Na/K-ATPases, in a manner independent of SRC kinase activation (Liu et al., 2007). It was described to be induced by a physical interaction of the p85 subunit of phosphatidyl inositol 3 kinase (PI3K) with the Na/K-ATPase α subunit, which then causes AKT activation (Liu et al., 2007, Wu et al., 2013) (**Figure 6**).

The third signaling cascade activated upon CTS binding to the Na/K-ATPase is Ca^{2+} dependent signaling. Two different mechanisms were suggested to be responsible for Ca^{2+} pathway activation *via* the Na/K-ATPase. Several studies described a direct interaction of the Na/K-ATPase α subunit with the inositol trisphosphate receptor (IP3R). Upon CTS binding to the Na/K-ATPase structural alterations of the Na/K-ATPase α subunit are suggested to act on the IP3R and induce Ca^{2+} oscillations from the ER, leading to variable Ca^{2+} dependent cellular responses (Aizman et al., 2001, Miakawa-Naito et al., 2003, Yuan et al., 2005) (**Figure 6**). An involvement of Phospholipase C (PLC) in the Na/K-ATPase-IP3R interaction is under discussion (Yuan et al., 2005). Other studies report on an involvement of the NCX in the induction of Ca^{2+} signaling. Activation of the NCX by CTS was originally thought to arise from elevation of intracellular Na^+ upon CTS dependent inhibition of the Na/K-ATPase (Langer 1972, Blaustein et al., 1998). However, more recent studies provide evidence of a direct interaction between NCX and the Na/K-ATPase, leading to the formation of specific Ca^{2+} signaling microdomains (Song et al., 2006, reviewed in Tian and Xie, 2008).
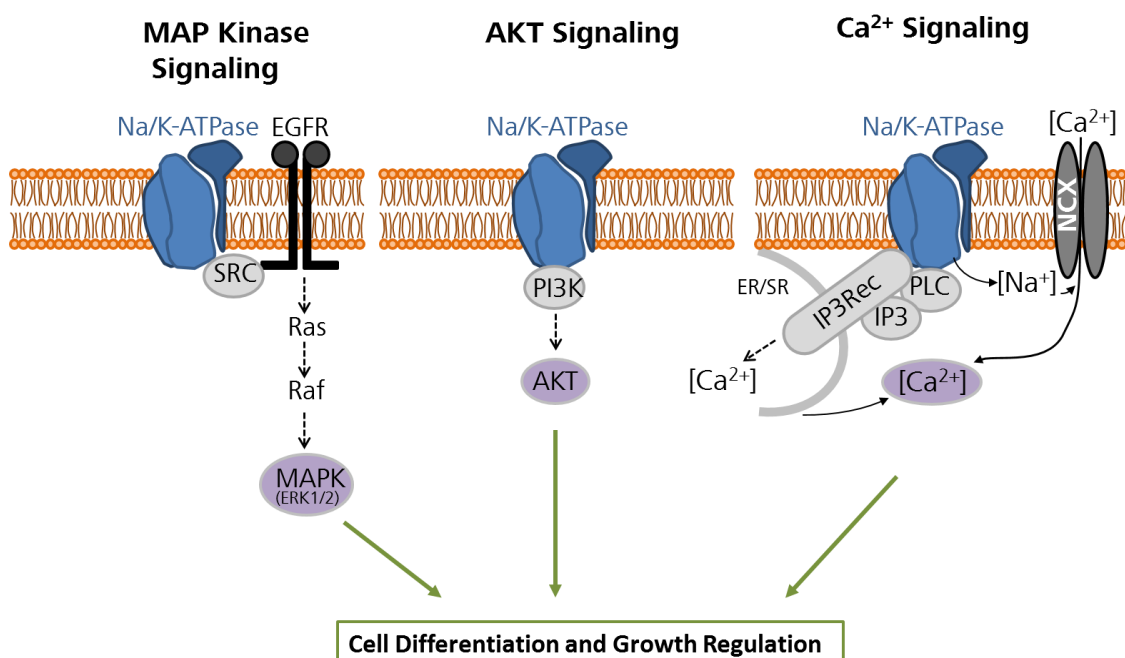
Figure 6: Schematic overview of Na/K-ATPase associated signaling cascades
CTS-bound Na/K-ATPases are implicated in the induction of three different signaling pathways. The MAPK pathway was described to be activated *via* SRC and the EGFR, the AKT pathway *via* PI3K, and Ca^{2+} dependent signaling can be activated *via* the IP3R, which can modify Ca^{2+} oscillations from the endoplasmatic/sarcoplasmatic reticulum (ER/SR) or may also be induced by the NCX (Figure modified after a figure kindly provided by Dr. Ulrike Friedrich, Institute of Human Genetics, University of Regensburg).

It is important to notice that most studies mentioned above were conducted with α1 subunit containing Na/K-ATPases. Until now, there is very little data on signaling properties of the other three α subunits. The α2 subunit was shown to be able to restore ion pumping but not α1 signaling function in a α1 knock out cell line (Xie et al., 2015), which rises the question whether α2 is capable of functioning as a signal transmitter. In contrast, the α3 subunit was shown to activate the MAPK cascade upon CTS treatment, but notably, in a mechanism independent of SRC activation (Madan et al., 2017). CTS treatment was also demonstrated to activate ERK signaling in an α4 expressing murine spermatogenic cell line, but no data on the mechanism were provided in this study (Upmanyu et al., 2016).

1.8.4 Na/K-ATPases in Intracellular Adhesion

In addition to its ion transport and signaling functions, the Na/K-ATPase further acts as a mediator of intracellular adhesion. Transdimerization of the ß1 subunit was shown to tether two cells together (Shoshani et al. 2005, Cereijido et al., 2012, Vagin et al., 2012, Tokhtaeva et al. 2016). The ß2 subunits mediates heterotypic adhesions between astrocytes and neighbouring neurons (Antonicek et al., 1987, Antonicek and Schachner, 1988, Gloor et al., 1990, Vagin et al., 2012). The mechanism underlying intracellular adhesion mediated by the ß2 subunit has not been resolved, yet. Transdimerization of two ß2 subunits was not consistent with experimental data and other factors or proteins are believed to be involved in the ß2 mediated intercellular interaction.

1.9 Aim of this Study

Despite substantial research efforts in the last 20 years, the consequences of retinoschisin deficiency and thus the initial pathomechanisms of XLRS are still not fully understood. Nevertheless, it has been shown that the Na/K-ATPase is an essential interaction partner of retinoschisin in retinal membranes (Molday 2007, Friedrich 2011). The present study focused on functional consequences and the molecular interface of this interaction.

A first project investigated an effect of retinoschisin on Na/K-ATPase levels in retinal model systems. In addition, an effect of retinoschisin on two functions of the Na/K-ATPase, namely ion transport and intracellular signal transduction, was assessed. Furthermore, the influence of retinoschisin on several cellular processes (cell volume, proliferation, viability, and apoptosis) associated with XLRS was investigated. Finally, it was sought to identify the interaction site between the Na/K-ATPase and retinoschisin.

Results of these investigations are suited to provide insight into the basic molecular pathomechanisms of XLRS, and should help to obtain a deeper understanding to initiate innovative targeted therapeutic approaches for this currently untreatable disease.

2 Material

2.1 Mouse Strains

Table 1: Mouse strains used

Mouse Strains	Source
Rs1^{tm1Web} (*Rs1h$^{-/y}$*)	Bernhard HF Weber, Institute of Human Genetics, University of Regensburg, Germany
C75BL/6	The Jackson Laboratory, Bar Harbor, Maine, USA

2.2 Escherichia coli (E.coli) Strains

Table 2: *E. coli* strain used

Strain	Source
E. coli strain DH5α	Life Technologies, Carlsbad, CA, USA

2.3 Eukaryotic Cell Lines

Table 3: Names and tissues of origin of cell lines used

Cell Line	Organism	Tissue of Origin	Source
Hek293	*Homo sapiens*	Embryonic kidney	ATCC;LGC Standards GmbH, Wesel, Germany
Hek293 +RS1	*Homo sapiens*	Embryonic kidney, cell line stably transfected with an RS1 expression vector	Institute of Human Genetics, University of Regensburg, Germany
Y-79	*Homo sapiens*	Retinoblastoma	ATCC;LGC Standards GmbH, Wesel, Germany

2.4 Oligonucleotides for PCR and Sequencing Reactions

Table 4: Names, sequences and purposes of oligonucleotides used for cloning of retinoschisin (RS1) and Na/K-ATPase expression constructs

Name	5'-3' Sequence	Purpose
RS1-HindII-F	AAG CTT TTC ATG TCA CGC AAG ATA GAA GGC TTT TTG	Expression cloning of *RS1*
RS1-XhoI-R	CTC GAG TCA GGC ACA CTT GCT GAC GCA CTC	
RS1-EcoRI-F	GAA TTC ATG TCA CGC AAG ATA GAA GGC TTT TTG	Cloning of Myc-tagged *RS1* variants
RS1-n-termMyc-R	TGA TCA ATT TCT GCT CCG ATA ATC CCA ATG TGG CTT CAT AGC CAA AGA GA	
RS1-ntermMyc-F	TGA TCA GTG AGG AAG ATC TGT CTA CCG AGG ATG AAG GCG AGG ACC CCT	
RS1-C59S-mut-F	CCA CCT CCT TGG ACA GTA TAC CAG AAT GCC	Site directed mutagenesis of *RS1*
RS1-C59S-mut-R	GGC ATT CTG GTA TAC TGT CCA AGG AGG TGG	
hATP1A2_NotI-F	GCG GCC GCA TGG GCC GTG GGG CTG GCC GTG AG	Expression cloning *ATP1A2*

21

Name	5'-3' Sequence	Purpose
hATP1A2_BamHI-R	GGA TCC TCA GTA GTA TGT CTC CTT CTC CAC	
hATP1B3-KpnI-F	GGT ACC ATG ACG AAG AAC GAG AAG AAG TCC	Expression cloning *ATP1B3*
hATP1B3-XhoI-R	CTC GAG CTA TGC ACG TGC TGT GAT TTT GAA	

Table 5: Names, sequences and purposes of oligonucleotides used for generation of ATP1B2 chimeric constructs

Name	5'-3' Sequence	Purpose
MscI-hATP1B1_OD_F	TGG CCA ACC ATC AGT GAA TTT AAG CCC AC	Expression cloning of *ATP1B1 OD*
hATP1B1-XhoI-R	CTC GAG TCA GCT CTT AAC TTC AAT TTT T	
hATP1B1-KpnI-F	GGT ACC ATG GCC CGC GGG AAA GCC AAGG	Expression cloning of *ATP1B2 OD*
MscI-hATP1B1_ID_R	TGG CCAG GGC CAC TCG GTC CTG ATA TGT GGG	
hATP1B2_I163L_Q5_F	CCG GCC TTG GGG ACT CCA CCC ACT ATG G	Site directed mutagenesis of *ATP1B2* (I163L, Patch I Region 1)
hATP1B2_I163L_Q5_R	AGC AGT TGC CCA GCT GGG TCC GGT TGA A	
hATP1B2_T119QA201T _Q5_F	TGT ACT GGG AAG CGA GAT GAA GAT GCTG	Site directed mutagenesis of *ATP1B2* (K247QL249T, Patch I Region 2)
hATP1B2_T119QA201T _Q5_R	TTG AAC ATT CAT GCT CTG GTT TGC TCC T	
hATP1B2_K247QL249T _Q5_F	TTC ACG AAT GTG ACC CCC AAC GTG GAG	Site directed mutagenesis of *ATP1B2* (T119QA201T, Patch I Region 3)
hATP1B2_K247QL249T _Q5_R	CTG CACAGC CAC CAG GGG CTG TGT GTAG	
hATP1B2-Mut214-221-F	AGT ACT TCG GCC TGG GCA ACA GCC CCA ACA TCG ACC TCA TGT ACT TCC CCT ACT AT	Insertion of *ATP1B1* Fragment into *ATP1B2* (Amplification of C-terminal part, Patch I Region 4)
hATP1B2_XhoI_R	CTC GAG GGT TTT GTT GAT GCG GAG TTT GA	
ATP1B2-Mut214-221-R	AGT ACT CCA CGT TGC CGA GAT TCT CAG CAT CTT CAT CT	Insertion of *ATP1B1* Fragment into *ATP1B2*(Amplification of N-terminal part, Patch I Region 4)
B2_KpnI_F	CCC GGT ACC ATG GTC ATC CAG AAA GAG AAG	
Region I Docking Patch II_F	CCTCAGATCGAGAACCTTGATGTCAT TGTCAATGTCAGTG	Site directed mutagenesis of *ATP1B2* (Patch II Region 1)
Region I Docking Patch II_R	AATCTGTGTCAAGCCCGGTGTGGCC AG	
hATP1B2_PatchII_Reg2 _1F	AGT TAG GTT CTT GGA GCC TTA CAA CG	Site directed mutagenesis of *ATP1B2* (Step 1 of 3 subsequent mutagenesis reactions, Patch II Region 2)
hATP1B2_PatchII_Reg2 _1R	ATGTTC AGA ACA TGC TGG TCC CAG CT	
hATP1B2_PatchII_Reg2 _2F	CAA AGA CTC TAT CCA AGC CCA AAA G	Site directed mutagenesis of *ATP1B2* (Step 2 of 3 subsequent mutagenesis reactions, Patch II Region 2)
hATP1B2_PatchII_Reg2 _2R	CAA AGA CTC TGC CCA AGC CCA AAA G	
hATP1B2_PatchII_Reg2 _3F	CAA AGA CTC TGC CCA AGC CCA AAA G	Site directed mutagenesis of *ATP1B2* (Step 3 of 3 subsequent mutagenesis reactions, Patch II Region 2)
hATP1B2_PatchII_Reg2 _3R	TAC TTC TCC AAGAAC CTA AC	

Region 3 Docking Patch II_F	AAC CGA GTC ATC AAC TTC TAT GCA G	Site directed mutagenesis of *ATP1B2* (Patch II Region 3)
Region 3 Docking Patch II_R	GAG CTT GAT GAA GAC ACA GGG CTG	
Region 4 Docking Patch II_F	CGT GAA CTA CCT GCA GCC CCT GG	Site directed mutagenesis of *ATP1B2* (Patch II Region 4)
Region 4 Docking Patch II_R	TGG AAC TTT TTG CCA TAG	

Table 6: Names, sequences and purposes of oligonucleotides used for confirmation of positive clones and Sanger sequencing

Name	5'-3' Sequence	Purpose
pTLN1_fwd	GAA TAC AAG CTT GCT TGT TCT	Vector primer for pTLN1
pTLN1_rev	CGA ATC TCTGAG GTA AGC CC	
M13F	CGC CAG GGT TTT CCC AGT CAC GAC	Vector primer for pGem®-T
M13R	AGC GGA TAA CAA TTT CAC ACA GGA	
T7_F	TAA TAC GAC TCA CTA TAG GG	Vector primer for pCDNA3.1
BGH_R	TAG AAG GCA CAG TCG AGG	
pCEP fwd	GGA CTT TCC AAA ATG TCG TAA TAA	Vector primer for pCEP4
pCEP rev	CAA ATA AAG CAA TAG CAT CAC AAA T	
hATP1A3Seq1F	ATG GGG GAC AAG AAA GAT GA	Sequencing of *ATP1A3*
hATP1A3Seq2F	CCC AGA GTG GGT CAA GTT TT	
hATP1A3Seq3F	GTG GAG ATC AAG GGT GGA GA	
hATP1A3Seq4F	GCA CTT CAT CCA GCT CAT CA	
hATP1A3Seq5F	GAC AGG GAC CCT CAC TCA GA	
hATP1A3Seq6F	TAC CAG CTC TCC ATC CAT GA	
hATP1A3Seq7F	CCT TCGACT GTG ATG ACG TG	
hATP1A3Seq8F	AGC AAATCG ACG AGATCC TG	
hATP1A3Seq9F	CCT ACA CCC TGA CCA GCA AT	
hATP1A3Seq10F	TTG GAA TGA TCC AGG CTC TC	
hATP1A3Seq1R	ATG CCA GGT ACA GGT TGTC	
hATP1A3Seq2R	GTC AGG GAG GAG TTG TCC A	
hATP1A3Seq3R	GGA AGA TGA CAG CCT CAA GC	
hATP1A3Seq4R	CAG GTG TGC GAA CTC TTG TC	
hATP1A3Seq5R	ACC AGC AGG TAT CGG TTG TC	
hATP1A3Seq6R	GGT GAC CAT GAT GAC CTT GA	
hATP1A3Seq7R	CCA CAA TGA TGA GCT TCT GC	
hATP1A3Seq8R	CAT GAT GAA CAG CAG GAA GG	
hATP1A3Seq9R	ACT GCT GCC CGT AAC TGT CT	
hATP1A3Seq10R	TCA GTA GTA GGT TTC CTT CTC CA	
hATP1B2Seq1F	ATG GTC ATC CAG AAA GAG AAG AA	Sequencing of *ATP1B2*
hATP1B2Seq2F	CCC CAA GAC TGAGAA CCT TG	
hATP1B2Seq3F	TCC ACC CAC TAT GGT TAC AGC	
hATP1B2Seq1R	TTT GGG CTT GGA TA GAG TCG	
hATP1B2Seq2R	ATG ACG AAG TTG CCG AGA TT	

hATP1B2Seq3R	TCA GGT TTT GTT GAT GCG GAGT	
hRS1-ex4-5-F	AGT CAA GGC TTT GGG TGT GCC TG	
hRS1-ex6-R	TGG CAA TGC GGA CGT GCC AG	Sequencing of *RS1*
RT-hRS1_F	TGG TAC CAA AAA GCA TGC AA	
RT-hRS1_R	CAC CCA AAG CCT TGA CTG TT	
hATP1A1/2_Seq1_F	CCT CAG CAA GCC CTT GTG AT	
hATP1A1/2_Seq1_R	GTC ATC TTC CTC ATC GGA TC	
hATp1A1/2_Seq2_F	TGG TGA TGA AGG GGC CCC A	Sequencing of *ATP1A1* and *ATP1A2*
hATp1A1/2_Seq2_R	TGG GGC CCC TTC ATC ACC A	
hATp1A1/2_Seq3_F	CTG GAT GAC AAC TTT GCC TC	

All oligonucleotides were purchased from Metabion, Planegg, Germany.

2.5 Oligonucleotides and Corresponding Probes Used for qRT-PCR

Table 7: Name, sequence and corresponding probe numbers for oligonucleotides used for qRT-PCR

Name	5'-3' Sequence	Gene	Roche Universal Probe Library #
hEGR1-qRT-F	AGC CCT ACG AGC ACC TGA C	*EGR1*	22
hEGR1-qRT-R	GGT TTG GCT GGG GTA ACT G		
hMYC-qRT-F	GCT GCT TAG ACG CTG GAT TT	*MYC*	66
hMYC-qRT-R	TAA CGT TGA GGG GCA TCG		
hBAX-qRT-F	ATG TTT TCT GAC GGC AAC TTC	*BAX*	57
hBAX-qRT-R	ATC AGT TCC GGC ACC TTG		
hHPRT-qRT-F	TGA CCT TGA TTT ATT TTG CAT ACC	*HPRT*	73
hHPRT-qRT-R	CGA GCA AGA CGT TCA GTC CT		
mEGR1-qRT-F	CCT ATG AGC ACC TGA CCA CA	*Egr1*	22
mEGR1-qRT-R	TCG TTT GGC TGG GAT AAC TC		
mMYC-qRT-F	CCT AGT GCT GCA TGA GGA GA	*Myc*	77
mMYC-qRT-R	TCC ACA GAC ACC ACA TCA ATT		
mBAX-qRT-F	GTG AGC GGC TGC TTG TCT	*Bax*	83
mBAX-qRT-R	GGT CCC GAA GTA GGA GAG GA		
mHPRT-qRT-F	TGA CAC TGG TAA AAC AAT GCA	*Hprt*	95
mHPRT-qRT-R	TCC TTT TCA CCA GCA AGC TTG		

All oligonucleotides were purchased from Metabion, Planegg, Germany and all probes from Roche, Basel, Switzerland.

2.6 Plasmids and Expression Constructs

Table 8: List of expression constructs, application and source

Vector Name	Application	Source
pCEP_RS1	Expression of RS1	Institute of Human Genetics, University of Regensburg
pCEP_RS1_C59S	Expression of RS1_C59S	Institute of Human Genetics, University of Regensburg
pCDNA3_RS1_Myc	Expression of Myc-tagged RS1	Generated during this project
pCDNA3_RS1_C59S_Myc	Expression of Myc-tagged RS1_C59S	Generated during this project
pCEP_ATP1A3_ATP1B2	Bicistronic expression of ATP1A3 and ATP1B2	Institute of Human Genetics, University of Regensburg
pCEP_ATP1A1	Expression of ATP1A1	Generated during this project
pCEP_ATP1A2	Expression of ATP1A2	Institute of Human Genetics, University of Regensburg
pCEP_ATP1A3	Expression of ATP1A3	Generated during this project
pCEP_ATP1A3_RD	Expression of ATP1A3 (ouabain insensitive)	Generated during this project
pCEP_ATP1B1	Expression of ATP1B1	Institute of Human Genetics, University of Regensburg
pCEP_ATP1B2	Expression of ATP1B2	Institute of Human Genetics, University of Regensburg
pCEP_ATP1B3	Expression of ATP1B3	Generated during this project
pCEP_ATP1B2_OD	Expression of ATP1B2 Outer Domain fused to ATP1B1 Inner Domain	Institute of Human Genetics, University of Regensburg
pCEP_ATP1B1_OD	Expression of ATP1B1 Outer Domain fused to ATP1B2 Inner Domain	Institute of Human Genetics, University of Regensburg
pCEP_ATP1B2_I163L	Expression of ATP1B2 Docking Patch mutant Patch I Region 1	Generated during this project
pCEP_ATP1B2_T199Q_A201T	Expression of ATP1B2 Docking Patch mutant Patch I Region 2	Generated during this project
pCEP_ATP1B2_K247Q_L249T	Expression of ATP1B2 Docking Patch mutant Patch I Region 3	Generated during this project
pCEP_ATP1B2_227-237_ATP1B1	Expression of ATP1B2 Docking Patch mutant Patch I Region 4	Generated during this project
pCEP_ATP1B2_MIRPKT_83-88_TQIPQI	Expression of ATP1B2 Docking Patch mutant Patch II Region 1	Generated during this project

pCEP_ATP1B2_QKLNKFLEPYNDSI 108-121_LNIVRFLEKYKDSA	Expression of ATP1B2 Docking Patch mutant Patch II Region 2	Generated during this project
pCEP_ATP1B2_KMNR181-184_KLNR	Expression of ATP1B2 Docking Patch mutant Patch II Region 3	Generated during this project
pCEP_ATP1B2_T240L	Expression of ATP1B2 Docking Patch mutant Patch II Region 4	Generated during this project
pCEP_ATP1B2_227-237_ATP1B1+I163L+T199Q_A201T	Expression of ATP1B2 Docking Patch mutant Patch I Region 1+2+4	Generated during this project
pCEP_ATP1B2_227-237_ATP1B1+I163L+K247Q_L249T	Expression of ATP1B2 Docking Patch mutant Patch I Region 1+3+4	Generated during this project
pCEP_ATP1B2_227-237_ATP1B1 +T199Q_A201T+K247Q_L249T	Expression of ATP1B2 Docking Patch mutant Patch I Region 2+3+4	Generated during this project
pCEP_ATP1B2_I163L+ T199Q_A201T+ K247Q_L249T	Expression of ATP1B2 Docking Patch mutant Patch I Region 1+2+3	Generated during this project
pCEP_ATP1B2_227-237_ATP1B1+I163L	Expression of ATP1B2 Docking Patch mutant Patch I Region 1+4	Generated during this project
pCEP_ATP1B2_227-237_ATP1B1+T199Q_A201T	Expression of ATP1B2 Docking Patch mutant Patch I Region 2+4	Generated during this project
pCEP_ATP1B2_227-237_ATP1B1+ K247Q_L249T	Expression of ATP1B2 Docking Patch mutant Patch I Region 3+4	Generated during this project
pCEP_ATP1B2_227-237_ATP1B1+I163L+ T199Q_A201T+ K247Q_L249T	Expression of ATP1B2 Docking Patch mutant Patch I Region 1+2+3+4	Generated during this project
pCEP_ATP1B2_MIRPKT_83-88_TQIPQI+ KMNR_181-184_KLNR	Expression of ATP1B2 Docking Patch mutant Patch II Region 1+3	Generated during this project
pTLN1_ATP1B2	*ATP1B2* cRNA synthesis for *X. leavis* oocyte injection	Generated during this project
pTLN1_ATP1A3_RD	*ATP1A3* (ouabain resistant) cRNA synthesis for *X. leavis* oocyte injection	Dr. Jan B. Koenderink, Department of Pharmacology and Toxicology, Nijmegen University, Netherlands
pCEP4	Expression vector	Themo Fisher Scientific, Waltham, MA, USA
pTLN1	Expression vector for *X. leavis* cDNA synthesis	Prof. Karl Kunzelmann, Insitute for Physiology, University of Regensburg, Germany
pGEM®-T	Cloning	Promega Corporation, Madison, WI, USA
pCDNA3.1	Expression vector	Themo Fisher Scientific, Waltham, MA, USA

2.7 Primary Antibodies

Table 9: Specifications on primary antibodies used

Antibody	Type	Species	Dilution	Application	Source
RS1	mAB	mouse	1:10000/ 1:1000	WB/ IHC	Professor Dr. Robert S. Molday, Department of Ophthalmology and Visual Sciences, University of British Columbia, Canada
RS1	pAB	rabbit	1:10000/ 1:1000	WB/ IHC	Professor Dr. Robert S. Molday, Department of Ophthalmology and Visual Sciences, University of British Columbia, Canada
ß-Actin (#A2228)	mAB	mouse	1:10000	WB	Sigma-Aldrich, St. Louis, MO, USA
Myc-Tag (9B11) (#2276)	mAB	mouse	1:1000	WB	Cell Signaling Technologies, Danvers, MA, USA
p-ERK (#4370)	pAB	rabbit	1:1000	WB	Cell Signaling Technologies, Danvers, MA, USA
ERK (#M5670)	pAB	rabbit	1:1000	WB	Sigma-Aldrich, St. Louis, MO, USA
p-Raf (#9427)	pAB	rabbit	1:1000	WB	Cell Signaling Technologies, Danvers, MA, USA
Raf (#9422)	pAB	rabbit	1:1000	WB	Cell Signaling Technologies, Danvers, MA, USA
p-AKT (#4060)	pAB	rabbit	1:1000	WB	Cell Signaling Technologies, Danvers, MA, USA
AKT (#4691)	pAB	rabbit	1:1000	WB	Cell Signaling Technologies, Danvers, MA, USA
p-CAMKII (#PA1-26727)	pAB	rabbit	1:1000	WB	Thermo Fisher Scientific, Waltham, MA, USA
CAMKII (#PA5-14033)	pAB	rabbit	1:1000	WB	Thermo Fisher Scientific, Waltham, MA, USA
p-SRC (#6943)	pAB	rabbit	1:1000	WB	Cell Signaling Technologies, Danvers, MA, USA
SRC (#2123)	pAB	rabbit	1:1000/ 1:250	WB/ IHC	Cell Signaling Technologies, Danvers, MA, USA
Pan-Cadherin (#ab6528)	mAB	mouse	1:1000	WB	Abcam, Cambridge, UK
IP3R (#8568)	pAB	rabbit	1:250	IHC	Cell Signaling Technologies, Danvers, MA, USA
pLCγ1 (#5690)	pAB	rabbit	1:100	IHC	Cell Signaling Technologies, Danvers, MA, USA
Caveolin (#3267)	pAB	rabbit	1:800	IHC	Cell Signaling Technologies, Danvers, MA, USA
ATP1A1 (#55187-1-AP)	pAB	rabbit	1:1000	WB	Proteintech, Rosemont, IL, USA
ATP1A2 (#16836-1-AP)	pAB	rabbit	1:1000	WB	Proteintech, Rosemont, IL, USA
ATP1A3 (#MA3-915)	mAB	mouse	1:0000/ 1:500	WB/ IHC	Thermo Fisher Scientific, Waltham, MA, USA
ATP1A3 (# ab2826)	mAB	Mouse	1:1000	WB (used in Figure 32)	Abcam, Cambridge, UK

ATP1B1 (#15192-1-AP)	pAB	rabbit	1:1000/ 1:50	WB/ FACS	Proteintech, Rosemont, IL, USA
ATP1B2 (#PA5-26279)	pAB	rabbit	1:1000/ 1:250/ 1:50	WB/ IHC/ FACS	Thermo Fisher Scientific, Waltham, MA, USA
ATP1B3 (MAB1723)	pAB	mouse	1:1000/ 1:50	WB/ FACS	Abnova, Taipeh, Tawain
Rho 1D4	mAB	mouse	1:1000	IHC	Professor Dr. Robert S. Molday, Department of Ophthalmology and Visual Sciences, University of British Columbia, Canada

pAB: polyclonal antibody, mAB: monoclonal antibody, WB: Western blot, IHC immunohistochemistry; FACS: fluorescence activated cell sorting; indicated in brackets (#) are manufacturer's product identification numbers where available

2.8 Secondary Antibodies

Table 10: Specifications on primary antibodies

Antibody	Dilution	Application	Source
Goat Anti-Mouse IgG, Peroxidase Conjugated	1:10000	WB	(Calbiochem) Merck Chemicals GmbH, Schwalbach, Germany
Goat Anti-Rabbit IgG, Peroxidase Conjugated	1:10000	WB	(Calbiochem) Merck Chemicals GmbH, Schwalbach, Germany
Goat Anti-Mouse IgG, Alexa Fluor ® 488	1:1000	IHC/FACS	Life Technologies, Carlsbad, CA, USA
Goat Anti-Mouse IgG, Alexa Fluor ® 549	1:1000	IHC	Life Technologies, Carlsbad, CA, USA
Goat Anti-Rabbit IgG, Alexa Fluor ® 488	1:1000	IHC/FACS	Life Technologies, Carlsbad, CA, USA
Goat Anti-Rabbit IgG, Alexa Fluor ® 549	1:1000	IHC	Life Technologies, Carlsbad, CA, USA

WB: Western blot, IHC: immunohistochemistry; FACS: fluorescence activated cell sorting

2.9 Molecular Weight Standards

Table 11: List of molecular weight standards

Standard	Purpose	Source
GeneRuler™ DNA Ladder Mix	Size standard for agarose gel electrophoresis of DNA fragments	Thermo Fisher Scientific, Waltham, MA, USA
PageRuler™ Prestained Protein Ladder	Molecular weight standard for protein analysis *via* SDS PAGE	Thermo Fisher Scientific, Waltham, MA, USA
Color-coded Prestained Protein Marker, High Range (43-315 kDa)	Molecular weight standard for protein analysis *via* non-reducing SDS PAGE	Cell Signaling Technologies, Danvers, MA, USA

2.10 Enzymes

Table 12: Enzymes used

Enzyme	Source
BamHI-HF	New England Biolabs, Ipswich, MA, USA
GoTaq® DNA Polymerase	Promega Corporation, Madison, WI, USA
HindIII	New England Biolabs, Ipswich, MA, USA
KpnI-HF	New England Biolabs, Ipswich, MA, USA
NcoI	New England Biolabs, Ipswich, MA, USA
NotI-HF	New England Biolabs, Ipswich, MA, USA
Pfu DNA Polymerase	Life Technologies, Carlsbad, CA, USA
PfuUltra II Fusion HotStart DNA Polymerase	Agilent Technologies, Santa Klara, CA, USA
RevertAid™ Reverse Transcriptase	(Fermentas) Thermo Fisher Scientific, Waltham, MA, USA
T4 DNA Ligase	New England Biolabs, Ipswich, MA, USA
XhoI-HF	New England Biolabs, Ipswich, MA, USA
House Taq DNA Polymerase	Institute of Human Genetics, University of Regensburg, Germany

2.11 Kit Systems

Table 13: List of kit systems used

Kit	Source
BigDye Terminator v1.1, v3.1 Cycle Sequencing Kit	Life Technologies, Carlsbad, CA, USA
Clarity Max™ Western Blotting Substrate	Bio-Rad Laboratories GmbH, Munich, Germany
Clarity ™ Western Blotting Substrate	Bio-Rad Laboratories GmbH, Munich, Germany
DC™ Protein Assay	Bio-Rad Laboratories GmbH, Munich, Germany
EnzChek™ Caspase-3 Assay Kit #2	Thermo Fisher Scientific, Waltham, MA, USA
GoTaq® Long Expand PCR Master Mix	Promega Corporation, Madison, WI, USA
mMESSAGE mMACHINE™ SP6 Transcription Kit	Thermo Fisher Scientific, Waltham, MA, USA
NucleoBond® XtraMidi	MACHEREY-NAGEL GmbH & Co. KG, Düren, Germany
NucleoSpin® Gel and PCR Clean-up	MACHEREY-NAGEL GmbH & Co. KG, Düren, Germany
NucleoSpin® Plasmid	MACHEREY-NAGEL GmbH & Co. KG, Düren, Germany
pGEM®-T Vector	Promega Corporation, Madison, WI, USA
Pierce™ Anti-c-Myc Agarose	Thermo Fisher Scientific, Waltham, MA, USA
Pierce™ Cell Surface Protein Isolation Kit	Thermo Fisher Scientific, Waltham, MA, USA
PureLink™ RNA Micro Kit	Invitrogen, Carlsbad, CA, USA
Q5®Site-Directed Mutagenesis Kit	New England Biolabs, Ipswich, MA, USA
RevertAid™ H Minus First Strand cDNA Synthesis Kit	Thermo Fisher Scientific, Waltham, MA, USA
RNeasy Micro Kit	QIAGEN, Venlo, Netherlands
TransIT® -LTI Transfectionreagent	Mirus Bio LLC, Madison, WI, USA

2.12 Chemicals and Ready Made Solutions

Table 14: List of chemicals used

Chemical/Reagent	Source
2-(4-(2-Hydroxyethyl)-1-piperazinyl)-ethansulfonicacid, $C_8H_{18}N_2O_4S$ (HEPES)	Merck Chemicals GmbH, Schwalbach, Germany
25 % Glutaraldhyde	Carl Roth GmbH + Co. KG, Karlsruhe, Germany
3-(4,5-Dimethylthiazol-2-yl)-2,5-diphenyltetrazoliumbromide (MTT)	Sigma-Aldrich, St. Louis, MO, USA
37 % Formaldehyde	Merck Chemicals GmbH, Schwalbach, Germany
4',6-Diamidin-2-phenylindol (DAPI)	Life Technologies, Carlsbad, CA, USA
5-Bromo-4-chloro-3-indolyl β-D-galactopyranoside, $C_{14}H_{15}BrClNO_6$ (X-Gal)	AppliChem GmbH, Darmstadt, Germany
Acetic acid (100%), $C_2H_4O_2$	Merck Chemicals GmbH, Schwalbach, Germany
Adenosinetriphosphate potassium salt	Sigma-Aldrich, St. Louis, MO, USA
Adenosinetriphosphate sodium salt	Sigma-Aldrich, St. Louis, MO, USA
Agarose (Biozym LE)	Biozym Scientific GmbH, Hessisch Oldendorf, Germany
Alexa Fluor ™488-conjugated peanut agglutinin	Thermo Fisher Scientific, Waltham, MA, USA
Ammoniumperoxodisulfat, $(NH_4)_2S_2O_8$ (APS)	AppliChem GmbH, Darmstadt, Germany
Ampicillin sodium salt, $C_{16}H_{18}N_3NaO_4S$	Carl Roth GmbH + Co. KG, Karlsruhe, Germany
Bacto Agar	BD Bioscience, Heidelberg, Germany
Bacto Yeast Extract	BD Bioscience, Heidelberg, Germany
Boric acid H_3BO_3	Merck Chemicals GmbH, Schwalbach, Germany
Bovine Serum Albumin (BSA)	New England Biolabs, Ipswich, MA, USA
Bromphenolblue sodium salt, $C_{19}H_9Br_4O_5SNa$	Sigma-Aldrich, St. Louis, MO, USA
Calcium chloride, $CaCl_2$	Carl Roth GmbH + Co. KG, Karlsruhe, Germany
Chloroquine, $C_{18}H_{26}ClN_3$	Merck Chemicals GmbH, Schwalbach, Germany
Citric acid, $C_6H_8O_7$	Merck Chemicals GmbH, Schwalbach, Germany
Coomassie Brilliant Blue R-250, (sodium salt) $C_{45}H_{44}N_3NaO_7S_2$	VWR International Germany GmbH, Darmstadt, Germany
Dako Fluorescence Mounting Medium	Agilent, Santa Clara, CA, USA
Dimethylformamid, C_3H_7NO	Carl Roth GmbH + Co. KG, Karlsruhe, Germany
Dimethylsulfoxid, C_2H_6OS (DMSO)	AppliChem GmbH, Darmstadt, Germany
dNTPs (dATP, dGTP, dCTP, dTTP)	Genaxxon Bioscience, Ulm, Germany
Ethanol ≥99,8 p.a, C_2H_6O	Carl Roth GmbH + Co. KG, Karlsruhe, Germany
Ethidiumbromide, $C_{21}H_{20}BrN_3$ in H_2O	AppliChem GmbH, Darmstadt, Germany
Ethylendiamintetraacetat disodium dihydrate salt $C_{10}H_{14}N_2Na_2O_8 \cdot 2H_2O$ (EDTA)	Merck Chemicals GmbH, Schwalbach, Germany

Galactose, $C_6H_{12}O_6$	Merck Chemicals GmbH, Schwalbach, Germany
Glucose, $C_6H_{12}O_6$	Merck Chemicals GmbH, Schwalbach, Germany
Glycerol 87%, $C_3H_8O_3$	University of Regensburg, Chemical Supplies
Glycine, $C_2H_5NO_2$	Merck Chemicals GmbH, Schwalbach, Germany
HiDi™ Formamide, CH_3NO	Thermo Fisher Scientific, Waltham, MA, USA
Hydrochloric acid 1M, HCl	Merck Chemicals GmbH, Schwalbach, Germany
Hydrochloric acid fuming 37%, HCl	Merck Chemicals GmbH, Schwalbach, Germany
Isopropaonol, C_3H_8O	Merck Chemicals GmbH, Schwalbach, Germany
Isopropyl β-D-1-thiogalactopyranoside, $C_9H_{18}O_5S$ (IPTG)	AppliChem GmbH, Darmstadt, Germany
Magnesiumsulfate heptahydrate, $MgSO_4 \cdot 7H_2O$	Merck Chemicals GmbH, Schwalbach, Germany
Malachit Green, $C_{46}H_{50}N_4 \cdot 2HC_2O_4 \cdot C_2H_2O_4$	Sigma-Aldrich, St. Louis, MO, USA
Mannose, $C_6H_{12}O_6$	Merck Chemicals GmbH, Schwalbach, Germany
Methanol, CH_4O	Merck Chemicals GmbH, Schwalbach, Germany
NEG 50™ Frozen Section Medium	Thermo Fisher Scientific, Waltham, MA, USA
Odyssey Blocking Buffer (TBS)	LI-COR Biosciences, Lincoln, NE, USA
Ouabain Octahydrate, $C_{29}H_{44}O_{12} \cdot 8H_2O$	Sigma-Aldrich, St. Louis, MO, USA
Paraformyaldehyde, $(CH_2O)_n$ (PFA)	AppliChem GmbH, Darmstadt, Germany
Pepton	Carl Roth GmbH + Co. KG, Karlsruhe, Germany
Phenylmethansulfonylfluoride, $C_7H_7FO_2S$ (PMSF)	Merck Chemicals GmbH, Schwalbach, Germany
PhosSTOP™ Phosphatase inhibitor	Sigma-Aldrich, St. Louis, MO, USA
Potassium chloride, KCl	Merck Chemicals GmbH, Schwalbach, Germany
Potassium dihydrogen phosphate, KH_2PO_4	Merck Chemicals GmbH, Schwalbach, Germany
Roti ®Quant	Carl Roth GmbH + Co. KG, Karlsruhe, Germany
Rotiphorese Gel 40% Acrylamide/ Bisacrylamide	Carl Roth GmbH + Co. KG, Karlsruhe, Germany
Saccharose, $C_{12}H_{22}O_{11}$	Merck Chemicals GmbH, Schwalbach, Germany
Silver nitrate, $AgNO_3$	Carl Roth GmbH + Co. KG, Karlsruhe, Germany
Skimmed Milk Powder	Carl Roth GmbH + Co. KG, Karlsruhe, Germany
Sodium chloride, $NaCl$	VWR International Germany GmbH, Darmstadt, Germany
Sodium dodecyl sulfate ≥99%, $C_{12}H_{25}NaO_4S$ (SDS)	Merck Chemicals GmbH, Schwalbach, Germany
Sodium hydroxide, $NaOH$	Merck Chemicals GmbH, Schwalbach, Germany

Sodium thiosulfate pentahydrate, $Na_2S_2O_3 \cdot 5H_2O$	Merck Chemicals GmbH, Schwalbach, Germany	
Sodiumacetate trihydrate, $CH_3COONa \cdot H_2O$	Merck Chemicals GmbH, Schwalbach, Deutschland	
Sodiumcarbonate, Na_2CO_3	Merck Chemicals GmbH, Schwalbach, Germany	
ß-Mercaptoethanol, $HSCH_2CH_2OH$	Sigma-Aldrich, St. Louis, MO, USA	
Tetramethylethylendiamin (TEMED), $(CH_3)_2NCH_2CH_2N(CH_3)_2$	Merck Chemicals GmbH, Schwalbach, Germany	
Tris(hydroxymethyl)-aminomethan, $NH_2C(CH_2OH)_3$ (Tris)	Affymetrix, Santa Clara, CA, USA	
Triton® X-100	AppliChem GmbH, Darmstadt, Germany	

2.13 Buffers and Solutions

Table 15: Composition of buffers and solutions used

Buffer/Solutions	Composition	Amounts
0.1 M HCl in Isopropanol	Isopropanol 1 M HCl	90 % (v/v) 10 % (v/v)
2x HBS	NaCl KCl Na_2HPO_4 HEPES H_2O dest.	280 mM 10 mM 1.5 mM 50 mM
5x Laemmli Buffer	Bromphenolblue Tris-HCl pH 6.8 β-Mercaptoethanol SDS Glycerol H_2O dest.	0.01 % 60 mM 5 % (v/v) 2 % (w/v) 10 % (v/v)
Ammoniummolybdate Solution	Ammoniummolybdate Hydrochloric acid	4.2 % (w/v) 4 M
Antibody Solution for Immunohistochemistry	Goat serum TritonX-100 PB	2.5 % (v/v) 0.1 % (v/v)
Antibody Solution for Western Blot	1x TBS-T Skimmed Milk Powder	 5 % (w/v)
ATP Stock Solution	ATP H_2O dest.	300 mM
ATPase Testbuffer	Tris-HCl, pH 7,4 NaCl KCl $MgCl_2$ H_2O dest.	100 mM 130 mM 20 mM 3 mM
ATPase Testbuffer w/o K^+	Tris-HCl, pH 7,4 NaCl $MgCl_2$ H_2O dest.	100 mM 130 mM 3 mM
ATPase Testbuffer w/o Na^+	Tris-HCl, pH 7,4 KCl $MgCl_2$ H_2O dest.	100 mM 20 mM 3 mM
Blocking Solution for Immunohistochemistry	Goat serum	10 % (v/v)

	TritonX-100	0.3 % (v/v)
	PB	
Blocking Solution for Western Blot	1x TBS-T	
	Skimmed Milk Powder	5 % (w/v)
Bromphenolblue Loading Buffer	Bromphenolblue	0.01 % (w/v)
	Glycerol 87%	40 % (v/v)
	H_2O dest.	
Coomassie Destaining Solution	Methanol	30 % (v/v)
	H_2O dest I	60 % (v/v)
Coomassie Staining Solution	Methanol	30 % (v/v)
	Acetic acid	10 % (v/v)
	Coomassie Brilliant Blue	0.10 % (w/v)
	H_2O dest.	
House Taq DNA Polymerase 10 x Buffer	KCl	500 mM
	Tris, pH 9.0	100 mM
	$MgCl_2$	15 mM
	Triton X	1 % (v/v)
IPTG Solution	IPTG	0.1 M
	H_2O	
LB Agar	Trypton	1 % (w/v)
	Yeast extract	0.5 % (w/v)
	NaCl	1 % (w/v)
	Bacto-Agar	15 % (w/v)
	H_2O dest.	
Lysogeny Broth (LB) medium	Pepton	1 % (w/v)
	Yeast extract	0.5 % (w/v)
	NaCl	1 % (w/v)
	H_2O dest.	
Malachitgreen Solution	Malachitgreen	0.05 % (w/v)
	H_2O dest.	
MTT Solution	MTT	0.05 % (w/v)
	1x PBS	
PB, pH 7.2	Na_2HPO_4	78 mM
	NaH_2PO_4	26 mM
	H_2O dest.	
PBS, pH 7.4	NaCl	137 mM
	KCl	0,27 mM
	Na_2HPO_4	10 mM
	KH_2PO_4	1.8 mM
	H_2O dest.	
PFA Solution	PFA	4 % (w/v)
	PBS	
Phosphate Reagent	Ammoniummolybdate Solution	25 % v(/v)
	Malachitgreen Solution	75 % (v/v)
SDS Running Buffer, pH 8.6	Tris-HCl	0.25 mM
	Glycin	0.2 M
	SDS	1 % (w/v)
	H_2O dest.	
Silver Staining Solution A	Acetic Acid	10 % (v/v)
	Ethanol	30 % (v/v)
	H_2O dest.	60 % (v/v)
Silver Staining Solution B	Sodiumacetate	6.8 % (w/v)
	$Na_2S_2O_3 \cdot 5H_2O$	0.2 % (w/v)
	25 % Glutaraldehyde	5 % (v/v)

	Ethanol	30 % (v/v)
	H_2O dest.	
Silver Staining Solution C	$AgNO_3$	0.2 % (w/v)
	H_2O dest.	
Silver Staining Solution E	Glycine	1 % (w/v)
	H_2O dest.	
Silver Staining Solution D	Na_2CO_3	2.5 % (w/v)
	H_2O dest.	
SOC Medium	Tryptone	2 % (w/v)
	Yeast extract	0.5 % (w/v)
	NaCl	10 mM
	KCl	2.5 mM
	$MgCl_2$	10 mM
	Glucose	20 mM
TBE, pH 8.0	Tris	100 mM
	Boric acid	100 mM
	EDTA	1 mM
	H_2O dest.	
TBS, pH 7.5	Tris	50 mM
	NaCl	150 mM
	H_2O dest.	
TBS-T	Tween® 20	0.1 % (v/v)
	TBS	
Towbin	Glycine	190 mM
	Tris	0.25 mM
	Methanol	20 % (v/v)
	H_2O dest.	
X-Gal Solution	X-Gal	0.04 % (w/v)
	Dimethyformamid	

2.14 Cell Culture Media and Supplements

Table 16: List of cell culture media and supplements/additives used

Component	Source
Antibiotic-Antimycotic (100X)	Sigma-Aldrich, St. Louis, MO, USA
DMEM Hams F12 Medium	Thermo Fisher Scientific, Waltham, MA, USA
DMEM High Glucose Medium (4,5 g/L)	Thermo Fisher Scientific, Waltham, MA, USA
Dulbecco's PBS (DPBS)	Thermo Fisher Scientific, Waltham, MA, USA
Fetal Bovine Serum Gold (FBS)	Thermo Fisher Scientific, Waltham, MA, USA
G418 Sulfate solution, $C_{20}H_{40}N_4O_{10} \cdot 2H_2SO_4$	Thermo Fisher Scientific, Waltham, MA, USA
Gentamicin (50 mg/ml)	Thermo Fisher Scientific, Waltham, MA, USA
Hygromycin B	Thermo Fisher Scientific, Waltham, MA, USA
Insulin (27 USP-units/mg)	Thermo Fisher Scientific, Waltham, MA, USA
L-Glutamin 200 mM (100x)	Thermo Fisher Scientific, Waltham, MA, USA
OptiMEM™ Medium	Thermo Fisher Scientific, Waltham, MA, USA
Penicillin (10.000 Units)/Streptomycin (10 mg/ml), (Pen/Strep)	Thermo Fisher Scientific, Waltham, MA, USA
Poly-L-Lysin Hydrobromide (0.1 mg/ml)	Sigma-Aldrich, St. Louis, MO, USA
RPMI Medium 1640	Thermo Fisher Scientific, Waltham, MA, USA

2.15 Consumables

Table 17: List of consumables used

Consumable	Source
12-well tissue culture plate	Corning Incorporated, Corning, NY, USA
24-well tissue culture plate	Life Technologies, Carlsbad, CA, USA
5 ml Polystyrene Round-Bottom Tube	BD Falcon, Franklin Lakes, NJ, USA
6-well tissue culture plate	Corning Incorporated, Corning, NY, USA
Cell scrapers	Orange Scientific, Braine-l'Alleud, Belgium
CryoPure tube 1.6 ml	Sarstedt AG & Co., Nümbrecht, Germany
Cuvettes	Sarstedt AG & Co., Nümbrecht, Germany
Eppendorf tube pistills	Hartenstein GmbH, Würzburg, Germany
Eppendorf tube 0.5 ml	Sarstedt AG & Co., Nümbrecht, Germany
Eppendorf tube 1.5 ml	Sarstedt AG & Co., Nümbrecht, Germany
Eppendorf tube 2 ml	Sarstedt AG & Co., Nümbrecht, Germany
Falcontube 15 ml	Sarstedt AG & Co., Nümbrecht, Germany
Falcontube 50 ml	Sarstedt AG & Co., Nümbrecht, Germany
Flat bottom 96-well assay plate	GreinerBio-One GmbH,Kremsmünster, Austria
Matrix Pipet tips	Thermo Fisher Scientific, Waltham, MA, USA
MicroAmp™ Optical 384-well plate	Life Technologies, Carlsbad, CA, USA
MicroAmp™ Optical Adhesive Film	Life Technologies, Carlsbad, CA, USA
Nitril gloves	VWR International Germany GmbH, Darmstadt, Germany
Pasteur pipet 3 ml	VWR International Germany GmbH, Darmstadt, Germany
PCR-Cups 0.5 ml	Biozym Scientific GmbH, Hessisch Oldendorf, Germany
Petri dishes (10 cm)	Sarstedt AG & Co., Nümbrecht, Germany
Pipet tips 10 µl	VWR International Germany GmbH, Darmstadt, Germany
Pipet tips 100 µl	VWR International Germany GmbH, Darmstadt, Deutschland
Pipet tips 1000 µl	VWR International Germany GmbH, Darmstadt, Deutschland
Pipet tips, sterile, with filter	Nerbe Plus GmbH, Winsen, Germany
Plastic pipets 5/10/20 ml	Sarstedt AG & Co., Nümbrecht, Germany
PVDF membrane	Merck Chemicals GmbH, Schwalbach, Germany
Slide-A-Lyzer™ MINI Dialysis Device, 10K MWCO	Thermo Fisher Scientific, Waltham, MA, USA
Tissue culture dish 10 cm	Sarstedt AG & Co., Nümbrecht, Germany
Tissue culture flask T25 vent. Cap	Sarstedt AG & Co., Nümbrecht, Germany
Whatman paper 3 mm	Carl Roth GmbH + Co. KG, Karlsruhe, Germany

2.16 Instruments

Table 18: List of instruments used

Instrument	Source
Accu-jet Pipet Controller	Brand, Wertheim, Germany
Autoclave „Autoklav V-150"	Systec GmbH, Wettenberg, Germany
Bunsen burner Gasprofi1	WLD Tec, Göttingen, Germany
CASY TT Cell Counter	Innovatis Roche AG, Bielefeld, Germany
Centrifuge Biofuge fresco (table top for Eppendorf tubes)	Heraeus Holding GmbH, Hanau, Germany
Centrifuge Megafuge 1.0R (Falcon tubes)	Heraeus Holding GmbH, Hanau, Germany
Centrifuge Megafuge 3L (Falcontubes	Heraeus Holding GmbH, Hanau, Germany
Cold microtom Leica CM1850	Leica, Solmis, Deutschland
Duomax 1030 Rocking Platform Shaker	Heidolph Instruments GmbH & Co.KG, Schwabach, Germany
FACSCanto-II flow cytometer	BD Biosciences, San Jose, CA, USA
Fine scales „Feinwaage Explorer"	OHAUS, Nänikon, Switzerland
FLUOstar OPTIMA Microplate Reader	BMG Labtech, Allmendgruen, Germany
Gelelectrophoresis chamber Blue Marine200	SERVA Electrophoresis GmbH, Heidelberg, Germany
Gelelectrophoresis chamber Mini PROTEAN®	Bio-Rad Laboratories GmbH, Munich, Germany
Icemachine AF 100	Scotsman, VerNicht Hills, IL, USA
Incubator for bacteria 37°C	Memmert GmbH, Schwabach, Germany
Incubator Hera Cell 150	Thermo Fisher Scientific, Waltham, MA, USA
Matrix Equalizer Pipet	Thermo Fisher Scientific, Waltham, MA, USA
Microwave KOR-6D07	Daewoo, Seoul, Korea
Milli-Q-Synthesis Water Purification System	Merck Chemicals GmbH, Schwalbach, Germany
NanoDrop® ND1000 Spectrophotometer	NanoDrop, Wilmington, DE, USA
Odyssey FC Imager	LI-COR Biosciences, Lincoln, NE, USA
pH Meter Lab 850	SI Analytics GmbH, Mainz, Germany
Power Pack Blue Power 500	SERVA Electrophoresis GmbH, Heidelberg, Germany
Power Pack Blue Power Plus	SERVA Electrophoresis GmbH, Heidelberg, Germany
QuantStudio ® 5 Real-Time PCR System	Life Technologies, Carlsbad, CA, USA
RM5 Roller	(Assistent®) Glaswarenfabrik Karl Hecht GmbH & Co KG, Sondheim/Rhön, Germany
Rotator RS-24	Biosan, Riga, Lettland
Scales	SCALTEC Instruments GmbH, Heiligenstadt, Germany
Shaking incubator 37°C Ceromat R	B. Braun Biotech International GmbH, Melsungen, Germany
Short Plates Mini PROTEAN®	Bio-Rad Laboratories GmbH, Munich, Germany
Spacer Plates Mini PROTEAN® 0.75 mm	Bio-Rad Laboratories GmbH, Munich, Germany

Spacer Plates Mini PROTEAN® 1.5 mm	Bio-Rad Laboratories GmbH, Munich, Germany
Spectralphotometer Ultraspec 2100 pro	Amersham Biosciences, Life Technologies, Carlsbad, CA, USA
Sterile work bench	Heraeus Holding GmbH, Hanau, Germany
Thermocycler T3	Biometra GmbH, Göttingen, Germany
Thermocyler Peqstar 2x gradient	VWR International Germany GmbH, Darmstadt, Germany
Thermomixer compact	Eppendorf AG, Hamburg, Germany
Trans-Blot® Turbo™ Transfer System	Bio-Rad Laboratories GmbH, Munich, Germany
Transferpipette ® 10 µl	Brand, Wertheim, Germany
Transferpipette ® 100 µl	Brand, Wertheim, Germany
Transferpipette ® 1000 µl	Brand, Wertheim, Germany
Transilluminator UST-30_M-8R	BioView Ltd., Billerica, MA, USA
Vacuumpump MZ 2 C	Vacuubrand GmbH, Wertheim, Germany
Vibra Cell VCX400 Ultrasound device	Sonics& Materials, Newtown, CT,USA
VisiScope CSU-X1 Confocal System Microscope	Visitron Systems, Puchheim, Germany
Vortex Genie2	Scientific Industries, Bohemia, NY, USA
Water destiller	GFL GmbH, Burgwedel, Germany
Waterbath W12	Labortechnik Medingen, Arnsdorf, Germany
Workbench Heraguard	Heraeus Holding GmbH, Hanau, Germany

2.17 Software

Table 19: List of softwares used

Software	Source
ApE - A Plasmid Editor	M.Wayne Davis, Department of Biology, University of Utah
AxioVision LE 4.8	Zeiss, Oberkochen, Germany
Corel Draw	Corel Corporation, Ottawa, Canada
Diva Ver 7.0	BD Biosciences, San Jose, CA, USA
Image Studio	LI-COR Biosciences GmbH, Lincoln, NE, USA
ImageJ	Wayne Rasband, National Institutes of Health, USA
Microsoft Office	Microsoft Cooperation, Redmond, WA, USA
Photoshop Elements	Adobe Systems GmbH, Munich, Germany
SigmaPlot Version12.5	Systat Software, San Jose, CA, USA

3 Methods

3.1 Cloning of Expression Constructs

3.1.1 RNA Isolation

RNA isolation from cells was carried out using the Qiagen RNeasy Mini Kit according to the manufacturer's instructions. RNA was eluted in RNase-free water and RNA concentration was determined using a NanoDrop® ND1000 Spectrophotometer. RNA was stored at -80 °C until further use.

3.1.2 cDNA Synthesis

For cDNA synthesis, 1 µl of poly(dT) primer (30 nmol) was added to 1 µg of RNA and the final reaction volume was adjusted to 12.5 µl using RNase-free H_2O. This mixture was incubated for 5 min at 65 °C (step 1 in **Table 21**). After incubation, samples were immediately put on ice and 7.5 µl of the cDNA synthesis reaction mix given in **Table 20** were added. Subsequently, cDNA synthesis was carried out in a thermocycler with the program given in **Table 21** (step 2).

Table 20: Composition of cDNA synthesis reaction mix

Component	Volume
RNase-free H_2O	0.5 µl
5x Reaction Buffer for RevertAid™ Reverse Transcriptase	4 µl
dNTPs (1.25 mM)	2 µl
RevertAid™ Reverse Transcriptase	1 µl

Table 21: Thermocycler program for cDNA synthesis

Reactionstep	Temperature	Duration
Step 1: Annealing	65 °C	5 min
Step 2: cDNA synthesis and heat-inactivation	25 °C	10 min
	42 °C	60 min
	70 °C	10 min

3.1.3 PCR Amplification of Coding Sequences

Coding sequences of genes to be cloned into expression vectors were amplified from cDNA or plasmid DNA using a mixture of 7 parts GoTaq® DNA polymerase and 1 part Pfu DNA polymerase. The PCR reaction mix is given in **Table 22** and the thermocycler program in

Table 23. PCR conditions were adjusted to the requested coding sequence by changing annealing temperature (primers given in **Table 4**, respective annealing temperatures were determined with ApE – a plasmid editor) and elongation time (1 min/1000 bp).

Table 22: PCR reaction mix

Component	Volume
5X Green GoTaq® Reaction Buffer	5 µl
Primer forward (10 µM)	0.8 µl
Primer reverse (10 µM)	0.8 µl
dNTPs (1.25 mM)	1 µl
cDNA (25 ng/µl) /Plasmid DNA (25 ng/µl)	2 µl
GoTaq® DNA polymerase +Pfu DNA polymerase	0.5 µl
H_2O (Millipore)	14.9 µl

Table 23: Thermocycler program for PCR amplification

Reactionstep	Temperature	Duration	Cycles
Initial denaturation	95 °C	3 min	
Denaturation	94 °C	30 s	
Annealing	x °C	30 s	30
Elongation	72 °C	x min	
Final elongation	72 °C	5 min	
Pause	4 °C	∞ min	

x indicates variable temperature and time, adjusted for each sequence to be amplified

3.1.4 Agarose Gel Electrophoresis

PCR products were run on agarose gels to check for correct size and purity of the amplification products. Agarose gels were prepared by heating 1 % (w/v) agarose in TBE buffer until the agarose had melted completely, cooling the solution down to <45 °C and adding 4 drops of a 0.003 % ethidiumbromide solution.

Bromphenolblue loading buffer (5x solution) was added to DNA samples before loading them onto the gel. 3 µl GeneRuler™ DNA Ladder Mix were used as a size standard and gels were run at 190 V for 20 min.

3.1.5 Purification of PCR Products from Agarose Gels

PCR products of the correct size were excised from agarose gels and purified using the NucleoSpin® Gel and PCR Clean-up kit according to the manufacturer's instructions. DNA was eluted from columns in 25 µl of Millipore H_2O and stored at -20 °C until further use.

3.1.6 Ligation into pGEM®-T

Successfully amplified PCR products were ligated into the pGEM®-T vector using the ligation protocol given in **Table 24** and ligase supplied with the pGEM®-T vector kit. Ligation mixtures were incubated at 4 °C over night.

Table 24: pGEM®-T vector ligation mix

Component	Volume
pGEM®-T vector	1 µl
PCR fragment	2 µl
T4 DNA Ligase Puffer (2x)	5 µl
T4 DNA Ligase	1 µl
H_2O (Millipore)	1 µl

3.1.7 Heat Shock Transformation of *E. coli*

E. coli strain DH5α cells were transformed with plasmid DNA *via* a heat shock procedure. 100 µl aliquots of competent *E. coli* cells were thawed on ice before the complete ligation mixture was added to the cells. DNA and cells were mixed by flicking the tube and then incubated on ice for 30 min. Cells were then heat shocked at 42 °C for 45 s and put back on ice for 10 min. 400 µl of SOC medium were added and cells were incubated at 37 °C for 45 min before plating them on LB plates containing 100 µg/ml ampicillin. When transforming *E. coli* with pGEM®-T, LB plates were pre-treated with a mixture of 10 µl IPTG and 50 µl X-Gal solutions as this vector is suitable for blue/white screening. IPTG/X-Gal treatment was omitted when plating *E. coli* cells transformed with any other vector.

3.1.8 Plasmid DNA Miniprep

Single clones were picked from LB plates and transferred into 5 ml of LB medium containing 100 µg/ml ampicillin. After incubation at 37 °C over night, DNA isolation was carried out using the NucleoSpin® Plasmid kit according to the manufacturer's instructions. Plasmid DNA was eluted from columns in 25 µl of Millipore H_2O and the concentration was determined using a NanoDrop® ND1000 Spectrophotometer.

3.1.9 Sanger Sequencing

Sanger sequencing of full length inserts was performed to verify that DNA fragments cloned into pGEM®-T were correct. For sequencing, the BigDye® Terminator v1.1, v3.1 Cycle Sequencing Kit was used. Reaction mix and thermocycler program are given in **Table 25** and **Table 26**.

Table 25: Reaction mix for Sanger sequencing

Component	Volume
Plasmid DNA (25 ng/µl)	2 µl
BigDye® Terminator Reaction Mix	0.3 µl
5x BigDye® Terminator Sequencing Buffer	2 µl
Primer (10 µM)	1 µl
H_2O (Millipore)	4.7 µl

Table 26: Thermocycler program for Sanger sequencing

Reactionstep	Temperature	Duration	Cycles
Initial denaturation	94 °C	2 min	
Denaturation	94 °C	30 s	
Annealing	58 °C	30 s	27
Elongation	60 °C	3 min	
Final elongation	60 °C	5 min	
Pause	4 °C	∞ min	

For DNA precipation, 2 µl 3 M sodium acetate and 25 µl 100 % ethanol were added to each sample. Samples were vortexed and then centrifuged for 45 min at 4000 rpm (Megafuge 1.0R/3L by Heraeus) at 4 °C. The supernatant was discarded and pellets were washed in 100 µl of 70 % ethanol (4000 rpm, 20 min, 15°C). The supernatant was discarded again and pellets were resuspended in 15 µl of HiDi™ formamide before transferring them into a 96-well plate to be run on a Abi3130x1 Genetic Analyser. Obtained sequences were analysed using ApE - A Plasmid Editor.

3.1.10 Restriction Digestion

After confirming the correct sequence, inserts were transferred from pGEM®-T into eukaryotic expression vectors pCEP4 or pCDNA3.1. Inserts were excised from pGEM®-T using restriction sites which were added to PCR products by the amplification primers. Restriction digestion mixtures were pepared according to **Table 27** and incubated over night at 37 °C. For inserts to be excised from pGEM®-T, 3 µg of DNA were digested, while 500 ng of target expression vector was digested with the same enzymes.

Digested DNA was run on agarose gels, DNA fragments of the correct size were excised from

the gel and purified as described in 3.1.4 and 3.1.5. DNA concentrations were determined using a NanoDrop® ND1000 Spectrophotometer.

Table 27: Reaction mix for restriction digestion of plasmid DNA

Component	Volume
Plasmid DNA	3 µg or 500 ng, respectively
Enzyme 1	1 µl
Enzyme 2	1 µl
10x NEB Endonuclease Buffer	2 µl
H_2O (Millipore)	ad. 20 µl

3.1.11 Ligation into Expression Vectors

Inserts and expression vectors were ligated in a 3:1 molar ratio using T4 DNA ligase according to **Table 28**. Ligations were incubated at 4 °C over night and subsequently transformed into *E. coli*.

Table 28: Reaction mix for ligation of inserts into expression vectors

Component	Volume
Vector DNA	10-20 ng
Insert DNA	x µl
T4 DNA Ligase Puffer (10x)	1 µl
T4 DNA Ligase	1 µl
H_2O (Millipore)	ad. 10 µl

3.1.12 Colony PCR

Colony PCR was performed to pre-select positively transformed *E. coli* clones. Single clones were picked from selection plates, transferred into 20 µl LB medium containing 100 µg/ml ampicillin and incubated at 37 °C for 2 h. This culture was then used as DNA template in the subsequent PCR reaction described in **Table 29** and **Table 30**. Vector primers given in **Table 4** were used for amplifying insert fragments.

Table 29: Reaction mix for colony PCR

Component	Volume
E. coli culture	3 µl
Primer forward (10 µM)	0.8 µl
Primer reverse (10 µM)	0.8 µl
dNTPs (1.25 mM)	0.5 µl
House Taq DNA polymerase	0.4 µl
Buffer 10x (15 mM $MgCl_2$)	2.5 µl
H_2O (Millipore)	17 µl

Table 30: Thermocycler program for colony PCR

Reactionstep	Temperature	Duration	Cycles
Initial denaturation	94 °C	10 min	
Denaturation	94 °C	30 s	
Annealing	58 °C	30 s	27
Elongation	72 °C	1 min/1000 bp	
Final elongation	72 °C	5 min	
Pause	10 °C	∞ min	

3.1.13 Plasmid DNA "Midi" Preparation

Expression constructs were isolated from 100 ml over night *E. coli* cultures using the NucleoBond® XtraMidi according to the manufacturer's instructions. Elution was done with 100 µl of Millipore H_2O. DNA concentration was determined using a NanoDrop® ND1000 Spectrophotometer and adjusted to 1 µg/µl. Plasmid DNA was stored at -20 °C.

3.1.14 Preparation of Glycerolstocks for Long Term Storage

For long term storage of bacterial cultures, 825 µl of fresh over night culture were mixed with 175 µl sterile 87 % glycerol and immediately frozen at -80 °C. Specifications about plasmid constructs were entered into the Institute of Human Genetics' database for glycerol cultures.

3.2   Generating Myc-tagged *RS1* Variants

To generate N-terminally Myc-tagged retinoschisin, a Myc-tag was inserted in between the signal peptide and the RS1 specific domain of retinoschisin. For this, the N-terminal part of the RS1 coding sequence from nucleotide positions 1 to 69 (aa 1–23) was fused to the N-terminal half of the Myc-tag sequence *via* PCR. The N-terminal half of the Myc-tag was added by the applied reverse primer in this amplification step. The C-terminal part of the RS1 coding sequence (nucleotide position 70 to stop codon) was fused to the C-terminal half of the Myc-tag sequence. The C-terminal half of the Myc-tag was added by the applied forward primer in this amplification step. pCEP_RS1 (**Table 8)** was used as a template, primers are given in **Table 4**. The full sequence was then fused together and ligated into a pCDNA3.1™ expression vector *via* HindIII and XhoI restriction sites, as described in 3.1.10 and 3.1.11.

3.3   Generating RS1-C59C Expression Constructs

The RS1-C59S expression constructs pCEP_RS1_C59S and pCDNA_RS1_C59S_Myc were generated by site directed mutagenesis using PfuUltra II Fusion HotStart DNA Polymerase and the reaction mixture and thermocycler program given in **Table 31** and **Table 32**. pCEP_RS1 and pCDNA_RS1_Myc were used as templates (**Table 8**) and mutagenesis

primers are given in **Table 5**.

After PCR amplification, the reaction mix was subjected to a DpnI digestion to specifically remove methylated template DNA. The digestion mix given in **Table 33** was incubated for 2 h at 37 °C and then used to transform *E. coli* as described in 3.1.7. Mutagenesis was controlled by sequencing of single clones as described in 3.1.9. Successfully mutagenized sequences were then cloned into pCEP4 using EcoRI and XhoI restriction sites, and into pcDNA3.1 using HindIII and XhoI restriction sites, as described in 3.1.10 and 3.1.11.

Table 31: Reaction mix for site directed mutagenesis using PfuUltra II Fusion HotStart DNA Polymerase

Component	Volume
Template DNA (20 ng/µl)	2 µl
Primer forward (10 µM)	2 µl
Primer reverse (10 µM)	2 µl
dNTPs (1.25 mM)	4 µl
PfuUltra II Fusion HotStart DNA Polymerase	0.2 µl
Reaction Buffer 10x	2.5 µl
H$_2$O (Millipore)	12.3 µl

Table 32: Thermocycler program for site directed mutagenesis using PfuUltra II Fusion HotStart DNA Polymerase

Reactionstep	Temperature	Duration	Cycles
Initial denaturation	94 °C	10 min	
Denaturation	94 °C	1 min	
Annealing	55 °C	1 min	18x
Elongation	72 °C	1min/1000 bp	
Final elongation	72 °C	5 min	
Pause	10 °C	∞ min	

Table 33: Reaction mix for DpnI digestion

Component	Volume
PCR product	20 µl
DpnI	1 µl
10x Endonuclease Reaction Buffer	3 µl
H$_2$O (Millipore)	7 µl

3.4   Generating Expression Constructs for ATP1B2-ATP1B1 Chimeras

Expression constructs for the ATP1B2-ATP1B1 chimeras ATP1B2_I163L, ATP1B2_T199Q_A201T, and ATP1B2_K247Q_L249T (ATP1B2 mutated in Patch I Regions 1, 2 or 3) as well as for ATP1B2_MIRPKT_83-88_TQIPQI, ATP1B2_KMNR181-184_KLNR, and ATP1B2_T240L (ATP1B2 mutated in Patch II Regions 1, 3 or 4) were generated with the Q5® Site Directed Mutagenesis Kit using the pTLN1_ATP1B2 vector (**Table 8)** as template. Primers (see **Table 5**) were designed using the NEBaseChanger v1.2.6 tool available at

http://nebasechanger.neb.com/. All further steps were carried out according to the manufacturer's protocol.

The ATP1B2-ATP1B1 chimera ATP1B2_QKLNKFLEPYNDSI108_121_LNIVRFLEKYKDSA (ATP1B2 mutated in Patch II Region 2) was also generated with the Q5® Site Directed Mutagenesis Kit and pTLN1_ATP1B2 vector (**Table 8**) as first template. However, three subsequent mutagenesis reaction with three different sets of primers were required to introduce all required nucleotide exchanges as there were too many to be mutagenized at once. Primers for the subsequent reactions are given in **Table 5**.

To generate the ATP1B2-ATP1B1 chimera ATP1B2_227-237_ATP1B1, a different approach was used. This construct contains 8 aa exchanges and two additional aa compared to the normal ATP1B2 sequence. PCR primers given in **Table 5** and were used to amplify the N-terminal and the C-terminal part of ATP1B2 with overhangs for the additional aa and a ScaI restriction site. Both fragments were sub-cloned in pGEM®-T and then fused together *via* their ScaI restriction site.

Mutagenesis of ATP1B2 was confirmed *via* Sanger sequencing (described in 3.1.9) of single clones. Successfully mutagenized sequences were cloned into pCEP expression vector using KpnI and XhoI restriction sites as described in 3.1.10 and 3.1.11.

3.5 Cell Culture

All cell lines were kept in a Hera Cell 150 incubator at a constant temperature of 37 °C and a 5 % CO_2 atmosphere. Cells were passaged under sterile conditions. All cell culture media and supplies were stored at 4 °C unless indicated differently by the manufacturer and pre-warmed to 37 °C before use. Current condition and confluency of cells was checked under a microscope each time they were passaged or before used in experiments.

3.5.1 Cultivation of Hek293 Cells

Human embryonic kidney (Hek293) cells were cultivated in 10 cm dishes in 10 ml DMEM High Glucose Medium (4.5 g/L) to which 10 % FCS, 1 % Penicillin/Streptomycin (5000 units/ml Penicillin and 5000 µg/ml Streptomycin) as well as 1 % Geneticin™ Selective Antibiotic (G418 Sulfate) had been added. Hek293 cells were passaged when they reached about 90 % confluency. Old medium was removed and cells were washed off the dish with fresh medium. Hek293 cells were sub-cultured at a 1:10 ratio twice a week for maintenance.

For cultivation of Hek293 cells stably transfected with an retinoschisin expression vector (see Friedrich et al., 2011), the medium was additionally supplemented with 1500 µg/ml Hygromycin B. To obtain retinoschisin containing supernatant from this cell line, the cells were kept in

OptiMEM™ containing 1% Penicillin/Streptomycin (5000 units/ml Penicillin and 5000 µg/ml Streptomycin) and 1500 µg/ml Hygromycin B for 72 h and the supernatant was harvested afterwards.

3.5.2 Cultivation of Y-79 Cells

The human retinoblastoma cell line Y-79 was cultured in RPMI 1640 medium supplemented with 10 % FCS and 1 % Penicillin/Streptomycin (5000 units/ml Penicillin and 5000 µg/ml Streptomycin). Y-79 cells are suspension cells and were grown in T25 tissue culture flasks with ventilated caps in 10 ml medium. Cells were subcultured in a 1:3 ratio when they reached a concentration of 4 -5 x 10^5 cells/ml. Only cells passaged less than ten times were used for signaling pathway experiments.

3.5.3 Transfection of Hek293 Cells – TransIT® -LTI Transfection Reagent

For transfection of Hek293 cells in 6-Wells, the TransIT® -LTI Transfection reagent was used according to the manufacturer's instructions. Cells used for transfection were seeded the day before so they reached 70 % confluency when being transfected (1:18 of total cells from a 100 % confluent 10 cm dish, in 3 ml of medium).

3.5.4 Transfection of Hek293 cells – Calcium-Phosphate Method

For generation of large volumes of supernatants containing (Myc-tagged) retinoschisin variants, the Calcium Phosphate method was used for transfection of Hek293 cells. Cells were seeded on Poly-L-Lysine coated 10 cm dishes the day before transfection so they reached 70 % confluency the next day (1:3 of total cells from a 100 % confluent 10 cm dish, ad 10 ml with medium). On the day of transfection, the culture medium was changed to DMEM High Glucose Medium (4.5 g/L) containing 10 % FCS, 1 % Penicillin/Streptomycin (5000 units/ml Penicillin and 5000 µg/ml Streptomycin) and 1 µM Chloroquine. After one hour of incubation, the medium was changed back to DMEM High Glucose Medium (4.5 g/L) with 10 % FCS, 1 % Penicillin/Streptomycin (5000 units/ml Penicillin and 5000 µg/ml Streptomycin) as well as 1 % Geneticin™ Selective Antibiotic (G418 Sulfate). The transfection mix was prepared according to **Table 34** by first mixing DNA with H_2O followed by adding $CaCl_2$ and then gently adding 2x HBS dropwise. The mixture was aerated using a 1 ml pipet before dropwise adding it to cells. 7 h after transfection the medium was changed to OptiMEM™ containing 1 % Penicillin/Streptomycin (5000 units/ml Penicillin and 5000 µg/ml Streptomycin) and cells were grown for 72 h.

Table 34: Transfection mix for Calcium Phosphate transfection

Component	Volume/Amount
Plasmid DNA	20 µg
H_2O (Millipore)	ad. 438 µl
$CaCl_2$	62 µl
2x HBS	500 µl

3.6 Purification of Myc-tagged Retinoschisin Variants

N-terminally Myc-tagged retinoschisin variants were purified from supernatant of transiently transfected Hek293 cells by immunoprecipitation using Pierce™ Anti-c-Myc Agarose and an adapted version of the manufacturer's protocol. 100 µl of Agarose beads were transferred into a 1.5 ml Eppendorf tube, centrifuged for 30 s at 12000 rpm (Biofuge fresco by Heraeus) and the supernatant was discarded. Beads were washed once in 100 µl TBS (30 s, 12000 rpm) and then incubated with 4 ml cell culture supernatant over night at 4 °C on a rotator. After over night incubation, beads were spun down (3 min, 4000 rpm, 4 °C) and washed three times in TBS-T (3 min, 4000 rpm, 4 °C). Bound proteins were eluted by applying 100 µl 0.25 mg/ml c-Myc peptide and incubating the beads at room temperature for 15 min before collecting the eluate. Elution was repeated once and both eluates were pooled for further analysis and experiments. Purified retinoschisin variants were stored in 100 µl aliquots at -20 °C until further use. A control eluate was obtained by transfecting Hek293 cells with an empty pCDNA3.1 expression vector and subjecting the supernatant from those cells to the procedure described above. This control eluate served as negative control in any experiments conducted with purified retinoschisin variants.

3.7 Dialysis of Purified Retinoschisin Variants

Retinoschisin variants to be used in a Na/K-ATPase activity assay were dialysed against the respective test buffers. 100 µl of purified protein were put into a Slide-A-Lyzer™ MINI Dialysis Device (10K MWCO) and the device was put in a glass beaker containing 500 ml of the dialysis buffer. Dialysis was carried out at 4 °C for 18 h and the dialysis buffer was exchanged for fresh buffer after 5 h.

3.8 Sodiumdodecylsulfate Polyacrylamide Gel Electrophoresis (SDS PAGE)

3.8.1 Reducing SDS PAGE

Unless stated otherwise, proteins analysed in Western blot experiments or *via* Coomassie or silver staining were separated by reducing SDS PAGE on 12.5 % acrylamide gels. The gels were cast according to **Table 35** and **Table 36** using Bio-Rad MiniPROTEAN® equipment.

Samples to be run on SDS gels were prepared by sonicating for 10 s at 40 % intensity before adding 5x Laemmli buffer and heating samples at 95 °C for 10 min. 3.5 µl of PageRuler™ Prestained Protein Ladder were used as a size standard. Gels were run in SDS running buffer at 50 V until samples had entered the resolving gel and then at 150 V for 1 h to 1.5 h depending of the size of the proteins to be analysed.

Table 35: Composition of 12.5% acrylamide resolving gels

Component	Volume
1 M Tris-HCl pH 8.8	3.38 ml
H_2O dest.	2.42 ml
Polyacrylamide (40 %)	3.75 ml
SDS (20 %)	100 µl
APS (10 %)	100 µl
TEMED	10 µl

Table 36: Composition of 3% acrylamide stacking gels

Component	Volume
1 M Tris-HCl pH 6,8	2.76 ml
H_2O dest.	1.69 ml
Polyacrylamide (40 %)	0.55 ml
SDS (20 %)	50 µl
APS (10 %)	50 µl
TEMED	5 µl

3.8.2 Non-reducing SDS PAGE

For analysis of retinoschisin multimers the SDS PAGE protocol was changed by using a non-reducing sample loading buffer (4x Loading Protein Loading Buffer by LI-COR Biosciences) and pre-cast 4-20% Mini-PROTEAN® TGX® gradient gels by Bio-Rad. The size standard used was the Color-coded Prestained Protein Marker, High Range by Cell Signaling Technologies (20 µl per lane). Gradient gels were run in SDS running buffer at 40 V and 4 °C for 8 h. The SDS running buffer was replaced by fresh buffer after 4 h.

3.9 Western Blot

3.9.1 Semi-Dry Blot

After reducing SDS PAGE, proteins were transferred onto Polyvinyldiflouride (PVDF) membranes by semi-dry blotting using the Bio-Rad Transblot Transfer System. Membranes were activated in methanol for 30 s, transferred into Towbin buffer and equilibrated for 5 min. Two 3 mm Whatman papers as well as the SDS gels were also equilibrated in Towbin buffer. Protein transfer from gels to membranes was performed at 24 V for 40 min. For Western blot

analysis of retinoschisin, blotting time was reduced to 35 min. After blotting, membranes were submerged in blocking solution for 1 h at room temperature and then incubated with primary antibodies over night at 4 °C. Before incubation with secondary antibodies, membranes were washed three times for 5 min in TBS-T at room temperature. Incubation with secondary antibodies was carried out at room temperature for 1 h. After washing membranes again (3 x 5 min in TBS-T), protein bands were visualized using Clarity™ ECL Western Blotting Substrate (Bio-Rad) according to the manufacturer's instructions and an Odyssey FC imager. For protein targets with weak signals, Clarity Max™ Western Blotting Substrate was used to increase signal intensity.

3.9.2 Wet Blot

Wet blot protein transfer was used for analysis of retinoschisin multimers. After running a non-reducing SDS PAGE as described in 3.8.2, proteins were blotted onto PVDF membranes at 30 V for 14 h at 4 °C. Pre-cooled Towbin buffer was used for this experiment. After blotting, membranes were blocked and subjected to antibody staining as described in 3.9.1.

3.10 Coomassie Staining

For Coomassie staining of proteins in SDS gels, the gels were transferred into Coomassie staining solution directly after protein separation as described in 3.8.1. After 2 h of staining the gels were destained using Coomassie destaining solution which was changed for several times until the background was clear. The staining and destaining procedure was carried out under gentle agitation on a shaker.

3.11 Silver Staining

For silver staining of proteins in SDS gels, gels were fixed in silver staining solution A for 30 min, subsequently transferred into silver staining solution B and incubated over night. 2 µl of 37 % formaldehyde were added to 10 ml of solution C right before use and gels were washed 3 times in H_2O dest., before they were submerged in silver staining solution C for 20 min. Silver staining solution D was prepared by adding 1 µl 37 % formaldehyde to 10 ml solution right before use. Solution C was replaced by solution D and gels were incubated until staining of proteins bands became visible. Solution D was discarded once protein bands had reached the desired intensity and replaced by silver staining solution E. All silver staining solutions were prepared freshly and incubation steps were carried out at room temperature with gently agitation.

3.12 Bradford Assay

For protein quantification a Bradford assay was performed using Roti® Quant. 800 µl H_2O (Millipore) were mixed with 200 µl of Roti® Quant solution and 5-50 µl of the protein sample to be measured were added. After 20 min of incubation at room temperature, absorbance at 595 nm was measured using a photometer. Defined amounts of bovine serum albumin were used to generate a calibration curve.

3.13 Cell Surface Biotinylation Assay

Isolation of cell surface proteins was performed to address membrane expression of different Na/K-ATPase subunits and ATP1B2-ATP1B1 chimeras. Hek293 cells were transfected with expression constructs for the different Na/K-ATPase subunits in a 6-well format. 48 h after transfection, cell surface proteins were biotinylated and isolated using the Pierce™ Cell Surface Protein Isolation Kit according to the manufacturer's instructions. Purified membrane proteins were analysed by Western blotting.

3.14 Fluorescence Activated Cell Sorting (FACS) Analysis

FACS analyses were performed to additionally investigate cell surface localization of different Na/K-ATPase subunits and ATP1B2-ATP1B1 chimeras. $3x10^5$ transfected Hek293 cells were harvested, washed twice in 300 µl PBS +1% FCS (5 min, 300xg, 4°C) and then incubated in primary antibodies against Na/K-ATPase ß-subunits ATP1B2, ATP1B2 and ATP1B3 for 25 min. After two washing steps in 300 µl PBS +1% FCS (5 min, 300xg, 4°C), cells were incubated in secondary antibody solution (Alexa-Fluor 488 conjugated anti-mouse or anti-rabbit, 1:100 in PBS +1% FCS) for 25 min and subsequently washed again twice. Cell pellets were resuspended in 100 µl PBS + 1 % FCS and transferred to 5 ml polystyrene round-bottom tubes. During the whole antibody staining procedure, cells were kept on ice, centrifugation steps were carried out at 4 °C and all solutions used were pre-cooled. FACS analysis were performed using a FACSCanto-II flow cytometer which was run by Diva software (Ver. 7.0). FACS experiments were done in cooperation with Dr. Jens Wild, Institute of Clinical Microbiology, University of Regensburg.

3.15 Quantitative Real-Time PCR

For quantitative real-time PCR (qRT PCR) all primers were designed using the "Universal Probe Library" by Hoffmann-La Roche. The qRT PCR experiments were run on a QuantStudio™ 5 Real-Time PCR System utilizing a comparative experimental approach. All samples were analysed in triplicates on 384-well plates. Reaction mixture and amplification

conditions for qRT PCR are given in **Table 37** and **Table 38**.

Data was analysed using the ΔΔCt-approach and statistical significance of results obtained was evaluated with Student's t-test.

Table 37: Reaction mix for qRT PCR analysis

Component	Volume
cDNA (20 ng/µl)	2.5 µl
2x TaqMan Gene Expression Master Mix	5 µl
Primer forward (50 µM)	1 µl
Primer reverse (50 µM)	1 µl
Probe	0.125 µl
H_2O (Millipore)	0.375 µl

Table 38: qRT PCR cycling conditions

Reactionstep	Temperature	Duration	Cycles
Denaturation	95°C	40 s	
Annealing	60°C	60 s	
Elongation	72°C	2 min	40

3.16 Animal Model

The *Rs1h*$^{-/Y}$ mouse was generated as described earlier (Weber et al., 2002) and kept on a C57BL/6 background. Mice were housed under specific pathogen-free barrier conditions at the Central Animal Facility of the University of Regensburg and maintained under conditions established by the institution for their use, in strict compliance with European Union and German legal guidelines. Mice were killed 10, 14, 16 or 18 days after birth (postnatal day 10, 14, 16, or 18, p10, p14, p16, or p16) by decapitation or cervical dislocation, respectively.

3.17 Retina Preparation

Rs1h$^{-/Y}$ mice were killed at p10, p14, p16 or p18, eyes were enucleated and transferred into 1x PBS. Using scissors and cutting along the Ora Serrata, cornea, lens and vitreous body were separated from retina, choroid and sclera. The lens, cornea and vitreous body were carefully removed and the retina was gently released from the retinal pigment epithelium. Retinae were either stored at -80 °C or used immediately.

3.18 Immunohistochemistry on Retinal Cryosections

Retinal explants were briefly rinsed in PBS and subsequently submerged in 4 % (w/v) paraformaldehyde for 1 h at room temperature. Retinae were then washed in PBS twice before they were put into 30 % (w/v) sucrose over night. Single retinae were embedded in Richard-

Allan Scientific™ Neg-50™ Frozen Section Medium and fast frozen on dry ice. 10 μm cryosections were cut and stained with different antibodies as described in Friedrich et al., 2011. In brief, cryosections were allowed to thaw and covered in 1x PB, which was then replaced by blocking solution and sections were incubated for 30 min at room temperature. The blocking solution was removed and sections were covered in antibody solution and incubated at 4°C over night. Cryosections were washed 3 times for 5 min in 1x PB the next day before they were incubated in secondary antibody solution for 30 min at room temperature. The antibody solution was removed, sections were washed 3 times for 5 min with 1x PB and then a small droplet of Dako fluorescence mounting medium was put on each section and covered with a cover slip. Cone visualization was performed with Alexa Fluor™ 488-conjugated peanut agglutinin. All sections were counterstained with 4′,6-diamidino-2-phenylindol (DAPI, 1:1000). Images were taken with custom-made VisiScope CSU-X1 Confocal System (Visitron Systems, Puchheim, Germany) equipped with high-resolution sCMOS camera (PCO AG, Kelheim, Germany).

3.19 Retinoschisin Binding Assay

3.19.1 Retinoschisin Binding to Hek293 Cells Transfected with Different Na/K-ATPase Subunit Combinations

Analysis of retinoschisin binding to Hek293 cells transiently transfected with Na/K-ATPase subunits was performed as described by Friedrich et al., 2011, with minor modifications. Hek293 cells were grown in 6-well plates and transfected with different Na/K-ATPase subunits. 48 h after transfection, the medium was replaced by 1 ml of retinoschisin containing cell culture supernatant (obtained from Hek293 cells stably transfected with a retinoschisin expression vector, "Input" in later analysis). Cells were incubated with retinoschisin for 1 h at 37 °C and then harvested by centrifugation (3 min, 1000 rpm, Biofuge fresco by Heraeus). The supernatant was removed and collected as "Flowthrough" fraction for later analysis. The cell pellet was resuspended in 400 μl of PBS and centrifuged for 3 min at 4600 rpm. This washing step was repeated three times and the supernatant of the last washing step ("Wash" fraction) was collected for later analysis. The pellet was resuspended in 200 μl of PBS and processed for Western blot analysis.

3.19.2 Binding of Retinoschisin Variants to Y-79 cells

For comparing binding affinities of retinoschisin and RS1-C59S to Y-79, 4×10^6 Y-79 cells were incubated in 5 ml medium containing 1 μg of purified (Myc-tagged) retinoschisin or RS1-C59S at 37 °C for 10 min, 30 min or 1 h. Subsequent steps were performed as described in 3.19.1.

3.19.3 Binding of Retinoschisin Variants to Retinal Explants

For comparing binding affinities of retinoschisin and RS1-C59S to $Rs1h^{-/Y}$ murine retinal membranes, homogenized tissue of 2 retinae (from mice aged 14 to 18 days) were incubated with 1 µg of purified (Myc-tagged) retinoschisin or RS1-C59S in 800 µl RPMI medium at 37 °C for 10 min, 30 min or 1 h. After that, 3 washing steps in 200 µl PBS followed by centrifugation at 4600 rpm for 15 min at 4°C (Biofuge fresco by Heraeus) were performed. Homogenization was achieved with an Eppendorf tube pistil. Fractions for Western blot analysis were collected as described for Hek293 cells.

For localization of bound recombinant RS1 variants on $Rs1h^{-/Y}$ murine retinae, $Rs1h^{-/Y}$ murine retinal explants from postnatal day 10 were incubated with 1 µg RS1, RS1-C59S or control eluate in 800 µl pre-warmed DMEM-Hams F12 with 10% FCS, 100 U/ml penicillin/streptomycin, 2 mM L-glutamine, and 2 µg/ml insulin. After 30 min of incubation, the retinal tissue was washed with PBS once before immunolabelling of retinal cryosections (3.18) was performed.

3.20 Investigations on the Effect of Retinoschisin on Signaling Pathways in Retinal Model Systems

For analysing an effect of retinoschisin on signaling pathway activity, Y-79 cells or $Rs1h^{-/Y}$ murine retinal explants were treated with retinoschisin, RS1-C59S or control eluate for 10 or 30 min. Activation of signaling pathways was followed by Western blot analysis or qRT-PCR for marker proteins or target genes, respectively.

Y-79 cells were grown to a concentration of 4-5 x 10^5 cells/ml in 10 ml medium. The experiment was started by adding 1 µg of purified retinoschisin, RS1-C59S, or equal volume of control eluate. After 10 or 30 min of incubation at 37 °C, cells were harvested by centrifugation (3 min, 1000 rpm, Biofuge fresco by Heraeus). For Western blotting, cells were resuspended in 200 µl of pre-cooled PBS with PhosSTOP™ and lysed by sonication (10 sec, 40 % intensity). For RNA isolation, cells were washed once with pre-cooled PBS before they were subjected to RNA isolation as described in 3.1.1.

Retinal explants from $Rs1h^{-/Y}$ mice at postnatal day 10 were dissected as prepared and described in 3.17. Immediately after preparation, explants were transferred into 2 ml Eppendorf tubes containing 800 µl pre-warmed DMEM-Hams F12 with 10 % FCS, 100 U/ml penicillin/streptomycin, 2 mM L-glutamine, and 2 µg/ml insulin), to which 1 µg purified retinoschisin or RS1-C59S, or equal volumes of control eluate had been added. After 10 or 30 min of incubation at 37 °C, retinal explants were removed from medium and transferred to 200 µl of pre-cooled PBS containing PhosSTOP™ phosphatase inhibitor. For Western blot analysis, retinal explants were sonicated for 10 sec at 40 % intensity. For RNA isolation, retinal

explants were immediately transferred into lysis buffer of the PureLink™ RNA Micro Kit and RNA isolation was done with PureLink™ RNA Micro Kit according to the manufacturer's protocol.

3.21 Investigations on the Effect of Retinoschisin on Cellular Processes in Y-79 Cells

3.21.1 MTT Assay to Assess Cell Viability

MTT ((3-(4,5-dimethylthiazol-2-yl)-2,5-diphenyltetrazolium bromide) assays were performed to determine viability and proliferation of Y-79 cells after treatment with retinoschisin. For treatment with increasing amounts of retinoschisin, 900000 cells/well were seeded on Poly-L-Lysine coated 24 well plates and incubated with 0.015, 0.03, 0.75, 0.15 or 0.3 µg of retinoschisin or equal volumes of control eluate in 0.5 ml RPMI medium with 5000 units/ml Penicillin and 5000 µg/ml Streptomycin but without FCS. Proliferation was assessed after 24 h. For analysis of cell viability after treatment with H_2O_2 and retinoschisin, 900000 cells/well were seeded onto Poly-L-Lysine coated 24 well plates and allowed to adhere over night. After over night incubation, 0.1 µg of purified retinoschisin or RS1-C59S, or equal volumes of control eluate were added to each well. After 1 h, the culture medium was changed to 1 ml RPMI (containing retinoschisin variants or control eluate as before) and 0.2 mM or 0.5 mM H_2O_2 to induce apoptosis or 0 mM H_2O_2 as control. After 2 h, the medium was replaced again by 0.5 RPMI containing retinoschisin variants or control eluate as before. Cells were allowed to recover for 18 h before they were subjected the MTT assay procedure. To start the MTT assay, the culture medium was removed and cells were washed twice with pre-warmed PBS before 500 µl of fresh medium were added. 50 µl of MTT solution were added to the medium and cells were incubated for 30 min, until violet crystals were visible. The medium was removed, cells were washed twice in PBS, and finally, 200 µl of 0.1 M HCl in isopropanol were added to each well to dissolve the violet crystals. After ten minutes of gentle agitation, all the crystals had dissolved and samples were transferred into 1.5 ml Eppendorf tubes and centrifuged for 5 min at 10000 rpm (Biofuge fresco by Heraeus). The supernatant was transferred into 96-well flat-bottom assay plates and absorbance at 540 nm was measured using a FLUOstar™ OPTIMA Microplate Reader.

3.21.2 CASY TT Cell Analyzer to Assess Cell Number and Diameter

A CASY TT Cell Analyzer was used to determine cell numbers and mean cell diameters of Y-79 cells after treatment with retinoschisin. Y-79 cells were seeded at a starting concentration of 200000 cells/well in 24 well plates and 0.1 µg of recombinant retinoschisin or control eluate were added. Cells were then incubated for 24, 72, and 96 h, and measurements were

performed on 60 μl of the cell suspensions after each time point. All measurements were carried out according to the manufacturer's directions using a 1:100 dilution of cells in 6 ml of CASY-Ton solution.

3.21.3 Caspase-3 Assay to Assess Apoptosis

Y-79 cells were seeded onto Poly-L-Lysine coated 24 well plates at a concentration of 2×10^6 cells/well and allowed to adhere over night. After over night incubation, 0.1 μg of purified retinoschisin or RS1-C59S, or equal volumes of control eluate were added to each well. After 1 h, the culture medium was changed to 1 ml RPMI (containing retinoschisin variants or control eluate as before) and 0.2 mM H_2O_2 to induce apoptosis or 0 mM H_2O_2 as control. After 2 h, the medium was replaced again by 1 ml RPMI containing retinoschisin variants or control eluate as before. Cells were allowed to recover for 18 h before they were subjected to analysis of caspase activity using the EnzChek® Caspase-3 Assay Kit #2 according to the manufacturer's directions.

3.22 Investigations on the Effect of Retinoschisin on the Na/K-ATPase Activity

3.22.1 Na/K-ATPase Catalyzed ATP Hydrolysis in Murine Retinal Explants

A plasma membrane-enriched fraction was collected from retinae of $Rs1h^{-/Y}$ mice at postnatal day 16 as described before (Friedrich *et al.*, 2011) and solubilized in TBS or Na^+ free ATPase test buffer (the latter only for Na^+ affinity experiments). Protein concentrations of enriched membrane fractions were determined using a Bradford assay as described in 3.12.

For testing the effect of recombinant retinoschisin on Na/K-ATPase catalysed ATP hydrolysis, $Rs1h^{-/Y}$ retinal membrane fractions were incubated for 30 min with or without recombinant retinoschisin (1.25 μg/ml) before starting the experiment. ATP hydrolysis reactions were performed at 37 °C for 60 min in a buffer system containing 100 mM Tris/HCl, pH 7.4, 120 mM NaCl, 20 mM KCl, 3 mM ATP, and 3 mM $MgCl_2$, with and without 0.1 mM ouabain. 10 μl of each sample were transferred into a 96-well flat-bottom assay plate at 0 and 60 min, and kept on ice.

Pi release (Jones et al., 2005) was measured colourimetrically (Howard and Ridley, 1990). To start the colorimetric reaction, 300 μl of phosphate reagent (freshly prepared during the 1 h incubation step, Triton-X added right before use) were added to each sample and the reaction was stopped after 3 min by adding 60 μl of 34 % citric acid. A calibration curve containing defined amounts of phosphate (1 nM, 2 nM, 3 nM, 4 nM, 5 nM, 6 nM, and 7 nM) was included. The photometric measurement at 630 nm was performed on a FLUOstar™ OPTIMA Microplate Reader.

To test whether the addition of retinoschisin influences Na/K-ATPase affinity towards its substrates the Na/K-ATPase activity was carried out as described above, but with varying concentrations of Na^+ (0-130 mM), K^+ (0–25 mM) or ATP (0-3 mM). All other test parameters remained unchanged.

The amount of phosphate generated in presence of ouabain was accounted as background P_i release by enzymes other than the Na/K-ATPase and subtracted from the overall free phosphate measured.

Less than 5 % of the ATP was hydrolysed during the assay. Data were analysed by nonlinear regression using Sigma Plot Graph System 12.5 (Jandel Scientific). Activation curves were fitted according to the Hill model for ligand binding. Michaelis-Menten constants (K_m values) were derived from the Michaelis-Menten equation.

Binding of recombinant retinoschisin to murine $Rs1h^{-/Y}$ retinal membranes under the different buffer conditions was investigated in binding assays as described in 3.19.3, with following modifications: recombinant retinoschisin (1 µg/ml), which had previously been dialysed against the respective test buffers was applied and the different Na/K-ATPase test buffers were used for incubation and wash steps.

3.22.2 Na/K-ATPase Pump Function in *Xenopus leavis* Oocytes

All experiments on *X. leavis* oocytes were conducted by the laboratory of Prof. Thomas Friedrich, Institute of Chemistry, Technical University of Berlin, Germany.

The cRNAs for ouabain insensitive ATP1A3 (ATP1A3_RD, expression vector kindly provided by Dr. Jan B. Koenderink, Department of Pharmacology and Toxicology, Nijmegen University, Netherlands) and ATP1B2 were transcribed *in vitro* using the mMESSAGE mMACHINE™ SP6 Transcription Kit. Oocyte isolation, cRNA injection, heterologous Na/K-ATPase expression in oocytes, as well as Rb^+ uptake experiments were performed as described in (Dürr et al., 2013). All assay were conducted in the presence of 10 µM ouabain to inhibit endogenous Na/K-ATPase activity. Rb^+ uptake was assessed with an AAnalyst 800 utilizing the THGA Furnace System and evaluated as described in (Dürr et al., 2013). Oocytes were incubated for 1 h with or without recombinant retinoschisin (1 or 8 µg/ml) before starting the experiment.

3.23 Investigations on the Effect of Retinoschisin on Na/K-ATPase Stability

To analyse a potential influence of retinoschisin on Na/K-ATPase protein stability and turnover, murine $Rs1h^{-/Y}$ retinal explants and transiently transfected Hek293 cells were treated with retinoschisin or control eluate and the amounts of Na/K-ATPase subunit proteins were analysed after different time points.

For experiments with heterologously expressed Na/K-ATPase, Hek293 cells were transiently

transfected with pCEP_ATP1A3+ATP1B2 vector (enabling bicistronic expression of ATP1A3 and ATP1B2) in a 12-well format and the experiment was started 72 h later. 0.5 µg of recombinant retinoschisin or equal volume of control eluate was added to each well and cells were incubated at 37 °C for 0, 4, 8, or 24 h before they were harvested. Cell pellets were resuspended in 150 µl PBS and immediately frozen until further analysis.

As an alternative approach, retinae were isolated from $Rs1h^{-/Y}$ at p14 and transferred into 500 µl pre-warmed DMEM-Hams F12 with 10 % FCS, 100 U/ml penicillin/streptomycin, 2 mM L-glutamine, and 2 µg/ml insulin. 0.5 µg of purified retinoschisin or equal volume of control eluate were added to the medium. Retinae were incubated at 37 °C for 0, 4, 8, or 24 h before they transferred were into 150 µl PBS and immediately frozen until further analysis.

Collected Hek293 cells and retinae were finally sonicated at 40 % intensity for 30 s and 50 µl of the lysate was saved for later analysis (total fraction). 100 µl of PBS were added to the remaining sample and a membrane enrichment was carried out as described in Friedrich et al., 2011. The enriched membranes were resuspended in 100 µl and analysed *via* Western blot.

4 Results

4.1 Cloning and Characterization of Recombinant Myc-tagged Retinoschisin Variants

4.1.1 Cloning of N-terminal Myc-tagged Retinoschisin and RS1-C59S

Functional properties of retinoschisin were analysed conducting experiments with heterologously expressed, purified retinoschisin (NM_000330.3) and an XLRS-associated variant harbouring an aa exchange from Cysteine to Serine at aa position 59, termed RS1-C59S (NM_000330.3(RS1): c.175T>A [p.Cys59Ser]). RS1-C59S is one of the rare XLRS variants which are not subjected to co- or posttranslational degradation, but instead are translated and secreted from cells, although, in case of RS1-C59S not as a stable octamer but as a dimer (Wu et al., 2003. Wu et al., 2005).

To enable enrichment and purification of the recombinant proteins, non-mutant retinoschisin and RS1-C59S were fused to an N-terminal Myc-tag. N-terminal Myc-tagged retinoschisin had previously been used by another group and was shown to be stable and oligomerize into octamers (Dyka and Molday, 2007). Due to cleavage of the signal peptide upon secretion, the tag was inserted between the signal peptide and the RS1 domain (**Figure 7**). The coding sequences of Myc-tagged retinoschisin and RS1-C59S were introduced into a pCDNA3.1 expression vector.
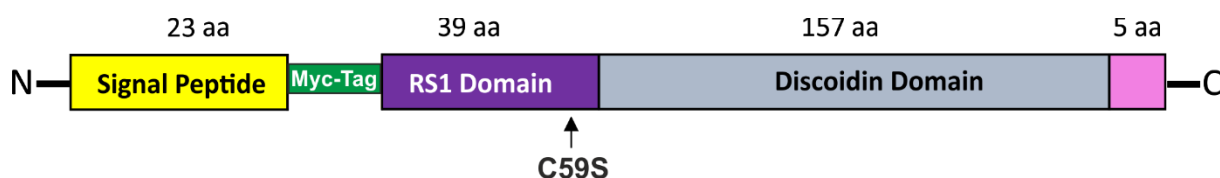
Figure 7: Schematic representation of N-terminal Myc-tagged retinoschisin
To obtain an N-terminal tagged protein after secretion the Myc-tag peptide sequence (green) was inserted between the signal peptide (yellow) and the RS1 domain (purple). The position of the pathogenic aa exchange at aa position 59, C59S, is marked by the black arrow.

4.1.2 Purification of Recombinant Retinoschisin Variants

An immunoprecipitation protocol was applied to purify retinoschisin and RS1-C59S from supernatant of Hek293 cells transiently transfected with the generated expression vectors for Myc-tagged retinoschisin or RS1-C59S (pCDNA3_RS1_Myc or pCDNA3_RS1_C59S_Myc). As an additional control, the same protocol was applied on supernatant of Hek293 cells transfected with an empty pCDNA3.1 expression vector. Purity and enrichment of the purified retinoschisin variants was analysed by Coomassie staining, silver staining and Western blotting (**Figure 8**).

Coomassie and silver staining revealed prominent protein bands of 55 to 100 kDa in the

unpurified supernatants of all samples. In the supernatants of retinoschisin or RS1-C59S expressing Hek293 cells, weak signals at 25 kDa, the expected size for retinoschisin monomers, were additionally observed. After purification, a distinct band of 25 kDa was visible in the eluates of retinoschisin and RS1-C59S containing supernatants, but not in the control. No other bands were detected in the stained gels after purification (**Figure 8 A** and **B**). Western blot analyses with antibodies against retinoschisin and the Myc-tag (**Figure 8 C**) showed signals at around 25 kDa in the samples with unpurified and purified retinoschisin variants, but not in the control. The detected signals of tagged retinoschisin variants showed a slightly increased molecular weight compared to untagged retinoschisin, in consistence with increased molecular weight due to the fused Myc-tag. Signal intensity of Myc-tagged retinoschisin in the purified protein fractions was stronger than in the applied supernatant.

Together, these data indicate successful enrichment and purification of the recombinant proteins.
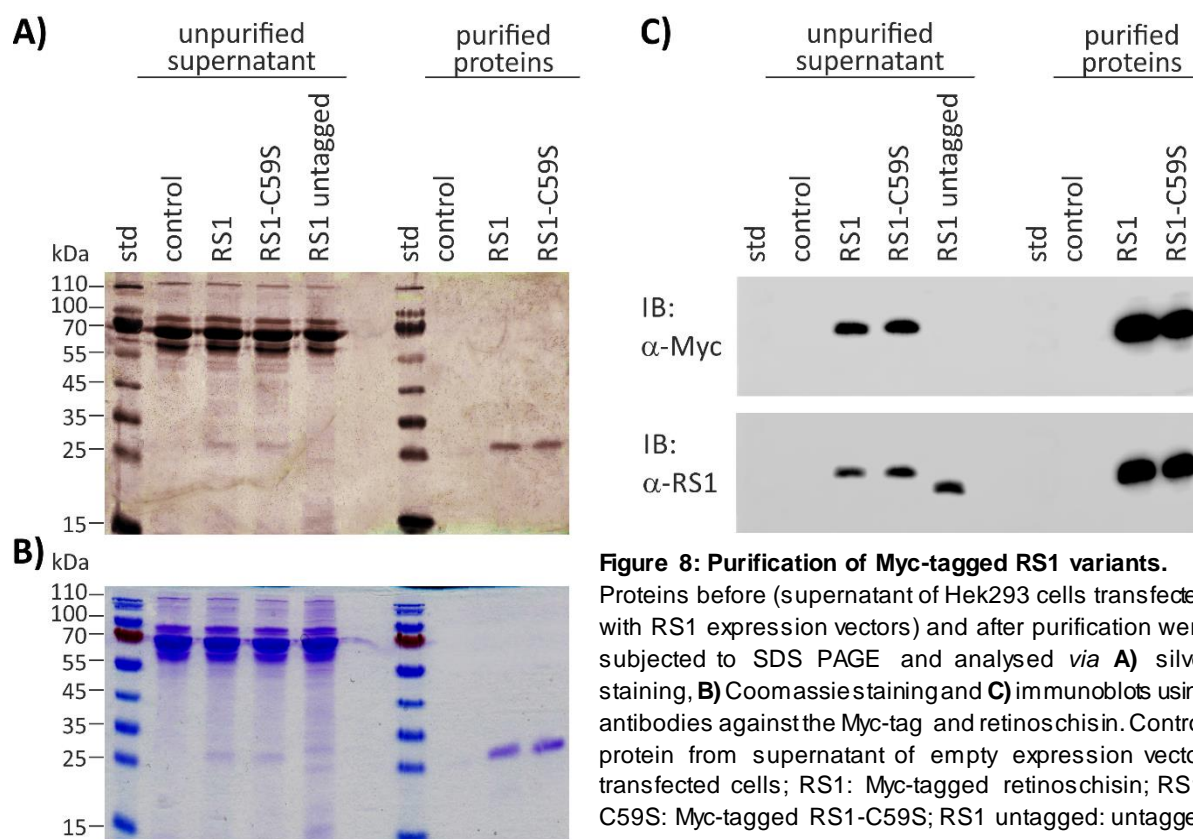
Figure 8: Purification of Myc-tagged RS1 variants. Proteins before (supernatant of Hek293 cells transfected with RS1 expression vectors) and after purification were subjected to SDS PAGE and analysed *via* **A)** silver staining, **B)** Coomassie staining and **C)** immunoblots using antibodies against the Myc-tag and retinoschisin. Control: protein from supernatant of empty expression vector transfected cells; RS1: Myc-tagged retinoschisin; RS1-C59S: Myc-tagged RS1-C59S; RS1 untagged: untagged retinoschisin. (Figure modified from Plössl et al., 2017a)

To check for correct oligomerization of the recombinant retinoschisin variants, unpurified and purified proteins were further subjected to a non-reducing SDS page and subsequent Western blot analysis (**Figure 9**). Unpurified as well as purified normal retinoschisin migrated at the expected size for retinoschisin octamers of around 200 kDa. RS1-C59S (unpurified and purified) migrated as a single band of about 50 kDa in size, consistent with previously described oligomerization properties of this variant (Wu et al., 2003, Wu et al., 2005, **Figure 9**, left panel). The same samples separated *via* SDS-PAGE under reducing conditions migrated as distinct single bands at 25 kDa, the expected size for retinoschisin monomers (**Figure 9**, right panel).

This shows that addition of the Myc-tag and the purification process do not alter the oligomerization properties of the Myc-tagged retinoschisin variants.
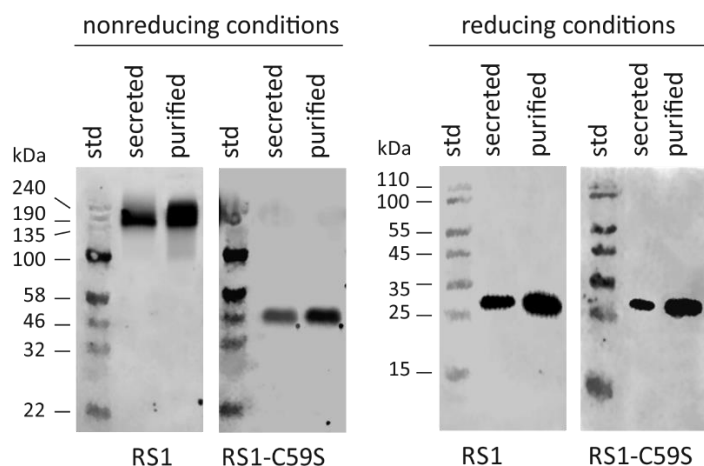
Figure 9: Oligomerization of Myc-tagged retinoschisin variants
Proteins before (supernatant of Hek293 cells transfected with RS1 expression vectors) and after purification were subjected to SDS PAGE under non-reducing and reducing conditions, followed by Western blot analyses using an anti-retinoschisin antibody. RS1: Myc-tagged retinoschisin; RS1-C59S: Myc-tagged RS1-C59S. (Figure modified from Plössl et al., 2017a)

4.1.3 Binding of Retinoschisin Variants to Retinal Membranes

Previous studies showed that retinoschisin binds to retinal membranes *via* its interaction with the retinal Na/K-ATPase, consisting of the two subunits ATP1A3 and ATP1B2 (Molday et al., 2007, Friedrich et al., 2011). To investigate binding properties as well as functionality of Myc-tagged retinoschisin variants, their affinity to retinal membranes was analysed. Retinoschisin binding was tested on murine retinal membranes from $Rs1h^{-/Y}$ mice as well as on membranes of the human retinoblastoma cell line Y-79. Previous studies at the Institute of Human Genetics, University of Regensburg, showed that this cell line also endogenously expresses ATP1A3 and ATP1B2 (published in Plössl et al., 2017a).

Y-79 cells and $Rs1h^{-/Y}$ retinal explants exposed to purified retinoschisin for 10, 30, and 60 min stably bound the externally added retinoschisin, even after only 10 min of incubation (**Figure 10**). In comparison, RS1-C59S exhibited a strongly reduced binding affinity to Y-79 cells and $Rs1h^{-/Y}$ retinal explants (**Figure 10**).

In a next step, immunohistochemical analyses were applied to test for correct localization of bound recombinant retinoschisin on retinal membranes. *Rs1h*[-/Y] retinal explants incubated with recombinant retinoschisin for 30 min showed an intense retinoschisin staining in the inner segments, colocalizing with the endogenously expressed retinal Na/K-ATPase of the murine retina (**Figure 11**). Similar staining patterns were obtained for retinoschisin and the Na/K-ATPase at the photoreceptor inner segments of wildtype retinae (Molday et al., 2007, Friedrich et al., 2011). However, in contrast to wildtype retinae, no recombinant retinoschisin was detected in the plexiform layers of the retinal explants. This could be a result of limited diffusion of the externally added retinoschisin through the retinal layers. No retinoschisin signals were obtained when *Rs1h*[-/Y] retinal explants were incubated with RS1-C59S or control eluate (**Figure 11**).
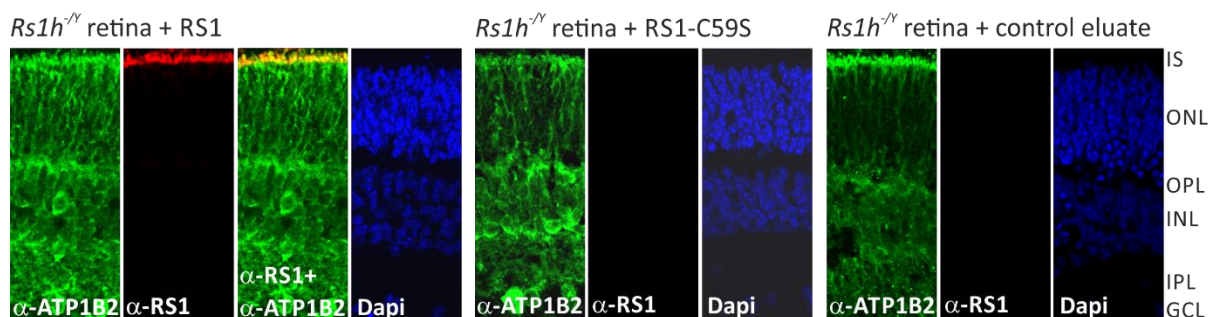
Figure 11: Localization of recombinant retinoschisin variants on retinal membranes
Rs1h[-/Y] retinal explants (P10) were incubated for 30 min with retinoschisin, RS1-C59S, or control protein. After washing and embedding, cryosections of these explants were subjected to immunohistochemical analyses using antibodies against ATP1B2 and retinoschisin. DAPI staining shows the nuclei of the different retinal layers. IS, inner segments; ONL, outer nuclear layer; OPL, outer plexiform layer; INL, inner nuclear layer; IPL, inner plexiform layer; GCL, ganglion cell layer (Figure modified from Plössl et al., 2017a)

4.2   Influence of Retinoschisin on Na/K-ATPase Stability and Turnover

Na/K-ATPase binding members of the FXYD family were reported to stabilise Na/K-ATPases in membranes, thus exerting an important effect of regulating Na/K-ATPase activity (Mishra et al., 2011). Likewise, retinoschisin could also affect stability of the retinal Na/K-ATPase in retinal membranes, or influence Na/K-ATPase levels at other stages like protein expression or export. An effect of retinoschisin on Na/K-ATPase levels was thus assessed in $Rs1h^{-/Y}$ retinal explants or Hek293 cells heterologously expressing ATP1A3 and ATP1B2. These were incubated with recombinant retinoschisin or control eluate. Retinal Na/K-ATPase expression was analysed after various time points (0, 4, 8, and 24 h) by Western blot, applying antibodies against ATP1A3 and ATP1B2. To distinguish between total Na/K-ATPase and Na/K-ATPase levels at plasma membranes, total cell lysate and a plasma membrane enriched membrane fraction of the treated Hek293 cells or retinal explants were included in the study.

Hek293 cells were transiently transfected with a bicistronic expression vector for ATP1A3 and ATP1B2 and incubated for 72 h before addition of recombinant retinoschisin or control eluate. Western blot analyses (**Figure 12**) detected bound recombinant retinoschisin in total cell lysates as well as in enriched membrane fractions of the retinoschisin treated Hek293 cells (except for the 0 h control sample). Na/K-ATPase subunits ATP1B2 and ATP1A3 were present in all fractions and their signal intensities were evaluated by densitometry. ATP1B2 and ATP1A3 expression was not affected by retinoschisin treatment at any time point, neither in total cell lysates nor in enriched membrane fractions (**Figure 12**).

A)

IB: α-ACTB

IB: α-RS1

IB: α-ATP1A3

IB: α-ATP1B2

RS1 - +   - +   - +   - +
     0 h   4 h   8 h   24 h

B)

IB: α-CAD

IB: α-RS1

IB: α-ATP1A3

IB: α-ATP1B2

RS1 - +   - +   - +   - +
     0 h   4 h   8 h   24 h
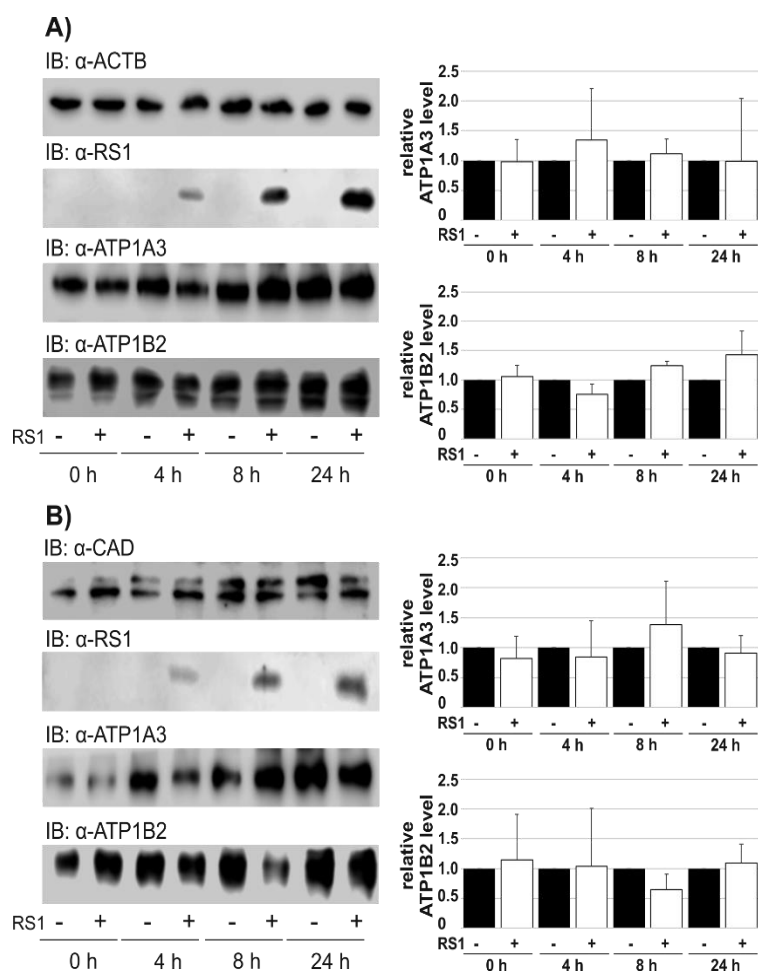
Figure 12: Effect of retinoschisin on retinal Na/K-ATPase levels after heterologous Na/K-ATPase expression in Hek293 cells
Hek293 cells were transfected with a bicistronic expression vector for ATP1A3 and ATP1B2. 72 h after transfection, they were treated with recombinant retinoschisin (+) or control eluate (-). After 0, 4, 8, and 24 h of incubation samples from **A)** total cell lysates as well as **B)** enriched membrane fractions were subjected to Western blot analyses with antibodies against retinoschisin, ATP1B2, ATP1A3 and retinoschisin. ACTB and pan-Cadherin (CAD) served as loading controls. Densitometric quantification was done with ImageJ. Signals for ATP1A3 and ATP1B2 (only the 55 kDa mature protein band) in total cell lysates were normalized against ACTB and calibrated against the control. Signals for ATP1B2 and ATP1A3 in enriched membrane fractions were normalized against Cadherin and calibrated against the control. Data given are means + SD (n=3).

Murine *Rs1h*^{-/Y} retinal explants also showed binding of recombinant retinoschisin. Both total cell lysates as well as enriched membrane fractions showed specific 25 kDa bands in samples exposed to recombinant retinoschisin (**Figure 13**). The anti-retinoschisin staining also gave unspecific signals with a size slightly smaller than for retinoschisin in all samples. Densitometric evaluation of ATP1B2 and ATP1A3 in total tissue lysates failed to reveal any differences between control or retinoschisin treated samples at any time point (**Figure 13 A**). Signal intensities of ATP1A3 and pan-Cadherin in enriched membrane fractions of murine *Rs1h*^{-/Y} retinal explants were too faint to be evaluated. ATP1B2 signals in enriched membrane fractions in contrast were clearly visible, but their densitometric evaluation showed no effect due to retinoschisin treatment (**Figure 13 B**).
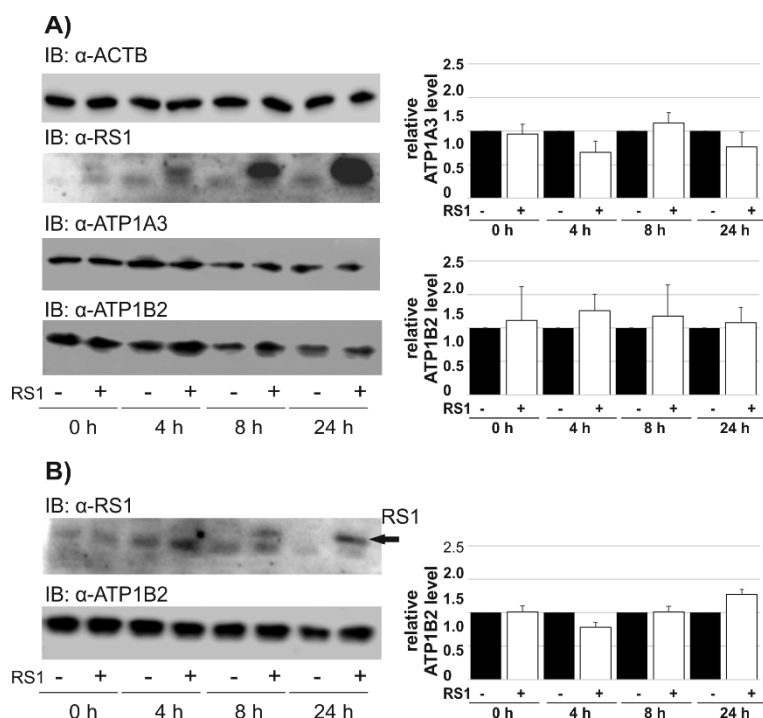
Figure 13: Effect of retinoschisin on retinal Na/K-ATPase protein stability in murine *Rs1h$^{-/Y}$* retinal explants

Murine retinal explants were treated with recombinant retinoschisin (+) or control eluate (-). After 0, 4, 8, and 24 h of incubation samples from **A)** total cell lysates as well as **B)** enriched membrane fractions were subjected to Western blot analyses with antibodies against retinoschisin, ATP1B2, ATP1A3, and retinoschisin. ACTB served as loading controls. Densitometric quantification was done with ImageJ. In total cell lysates signals for ATP1B2 (only the 55 kDa mature protein band) and ATP1A3 were normalized against ACTB and calibrated against the control. Signals for ATP1B2 in enriched membrane fractions were calibrated against the control. Data given are means + SD (n=3).

4.3 Influence of Retinoschisin on Na/K-ATPase Ion Pump Activity

4.3.1 Effect of Retinoschisin on Na/K-ATPase Mediated ATP Hydrolysis and Substrate Affinity in Retinal Membranes

Na/K-ATPase binding proteins such as the extracellular fragment of amyotrophic lateral sclerosis associated glycoprotein non-metastatic melanoma protein B (GNMPB) (Ono et al., 2016) or FXYD family members (Béguin et al.,1997, Arystarkhova et al., 1999, Therien et al., 1999, Pu et al., 2001, Jones et al., 2005, Geerig, 2006) were reported to affect Na/K-ATPase ion transport activity. Likewise, retinoschisin could also affect the active ion pump function of the retinal Na/K-ATPase. The following experiments were performed to assess an effect of recombinant retinoschisin on retinal Na/K-ATPase mediated ATP hydrolysis and cation transport.

Enriched *Rs1h$^{-/Y}$* retinal membranes were pre-incubated with recombinant retinoschisin for 30 min before the enzymatic assay was started. A colorimetric assay was used to determine free phosphate generated by ATP hydrolysis after 1 h of incubation. Ouabain sensitive ATP hydrolysis in *Rs1h$^{-/Y}$* retinal explants was 5.6 ± 1.3 nmol Pi /(µg protein*h) and did not change in the presence of recombinant retinoschisin (5.5 nmol ± 1.1 nmol Pi /[µg protein*h]; P=0.76, n=11).

Binding of FDXY2 to the Na/K-ATPase was reported to influence its substrate affinity but not its activity under optimal test conditions (Jones *et al.*, 2005). Substrate affinity of the murine retinal Na/K-ATPase in presence or absence of retinoschisin was thus additionally addressed

via the ouabain sensitive ATP hydrolysis assay. For this approach, Na/K-ATPase activity was measured as a function of Na$^+$ (0-130 mM), K$^+$ (0-25 mM) or ATP (0-3 mM). Addition of recombinant retinoschisin did not affect Na/K-ATPase affinities for either Na$^+$, K$^+$ or ATP (**Figure 14**).
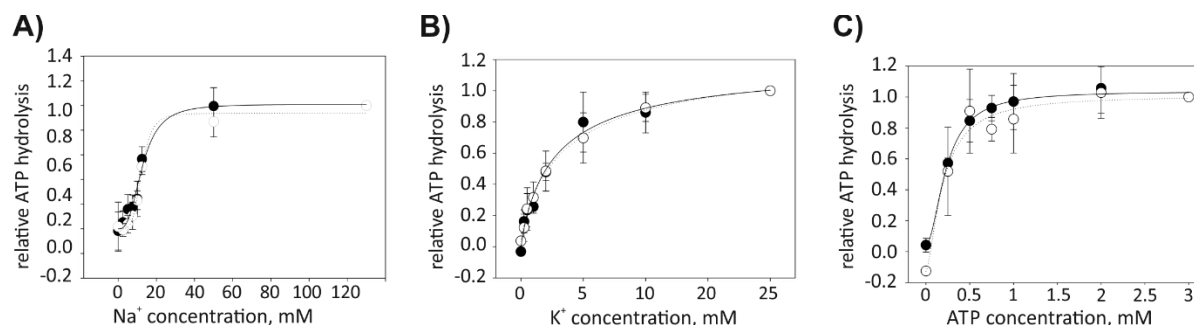
**Figure 14: Influence of retinoschisin on substrate affinity of the retinal Na/K-ATPase**
Rs1h$^{-/Y}$ retinal membrane fractions were pre-incubated for 30 min with (open circles) or without (closed circles) retinoschisin (1.25 µg/ml). Subsequently, Na/K-ATPase catalysed ATP hydrolysis was measured as a function of Na$^+$ (A, n=4), K$^+$ (B, n=4), and ATP (C, n=3). Data are given as means + SD. (Figure modified from Plössl et al., 2017b)

The corresponding Michaelis-Menten constants for Na$^+$, K$^+$, and ATP were derived from the Michaelis-Menten equation and reveal no statistically significant differences (**Table 39**).

Table 39: Michaelis-Menten constants (Km) for Na/K-ATPase from murine *Rs1h$^{-/Y}$* retinal membranes incubated with or without recombinant retinoschisin (RS1). (Table modified from Plössl et al., 2017b)

	Rs1h$^{-/Y}$ +RS1	wildtype	*P*
K$_m$ (Na$^+$), mM	12.32 ± 0.42	12.17 ± 0.60	0.6975
K$_m$ (K$^+$), mM	2.20 ± 0.16	2.20 ± 0.45	1.000
K$_m$ (ATP), mM	0.29 ± 0.06	0.29 ± 0.06	0.956

Recombinant retinoschisin was dialysed against the different Na/K-ATPase test buffers before its application to the enzymatic assays. In addition, the utilized Na/K-ATPase test buffers were different to the buffers usually applied in retinoschisin binding assays. To confirm binding of recombinant retinoschisin to the retinal membranes under these experimental conditions, binding assasys were performed using dialyzed retinoschisin and the different Na/K-ATPase test buffers. As shown in **Figure 15** the altered conditions did not affect retinoschisin binding to retinal membranes of *Rs1h$^{-/Y}$* mice.
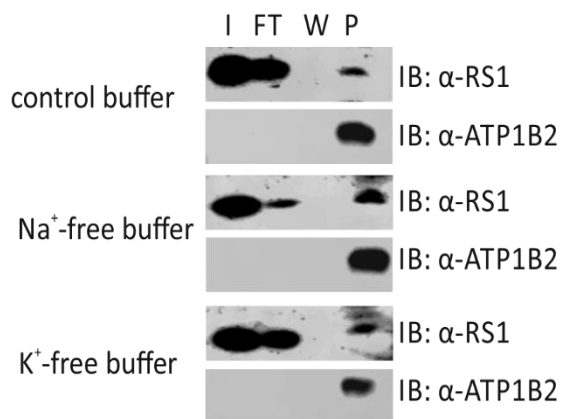
Figure 15: Binding of recombinant retinoschisin to retinal Na/K-ATPases under different Na/K-ATPase test buffer conditions.
Rs1h$^{-/Y}$ retinal membrane fractions were incubated with 1.25 µg/ml retinoschisin dialysed against different Na/K-ATPase test buffers (control buffer, Na$^+$-free buffer and K$^+$-free buffer) in the respective test buffer for 1 h. I = input, respective buffer + dialysed retinoschisin; FT = flowthrough; W = last wash with respective buffer, P = pellet, final murine retinal membrane fraction. (Figure modified from Plössl et al., 2017b)

An identical set of experiments comparing Na/K-ATPase activity and substrate affinities in *Rs1h$^{-/Y}$* retina versus wildtype retina was carried out by Melanie Royer as part of her master thesis which she conducted at the Institute of Human Genetics, University of Regensburg from March to September 2016. Similar results were obtained for Na/K-ATPase activities and Michaelis-Menten constants for Na$^+$, K$^+$, and ATP and showed no statistical significant differences between samples *Rs1h$^{-/Y}$* and wildtype retina (published in Plössl et al., 2017b).

4.3.2 Effect of Retinoschisin on Rb$^+$ Import into X. leavis Oocytes Mediated by Heterologously Expressed Retinal Na/K-ATPase

A putative influence of retinoschisin on Na/K-ATPase pump function was further addressed using *X. leavis* oocytes heterologously expressing both subunits (ATP1A3 and ATP1B2) of the retinal Na/K-ATPase as a model system. All experiments on *X. leavis* oocytes were performed by the group of Prof. Thomas Friedrich at the Technical University of Berlin.

For analysis of ion pump function in oocytes a mutated, ouabain insensitive version of the ATP1A3 subunit was used. Two aa exchanges (Q108R and N119D) were introduced into the coding sequence of ATP1A3 which leads to a reduced ouabain affinity of this mutated enzyme with half-maximal inhibitory concentration (IC$_{50}$) in the millimolar range (Price and Lingrel, 1988; Dürr et al., 2013). This allows for distinction between heterologously expressed pumps and endogenous *X. leavis* Na/K-ATPases, which can be inhibited by 10 µM ouabain (Dürr et al., 2013).

To confirm that retinoschisin is also capable of binding to the ouabain insensitive Na/K-ATPase, a binding assay was performed in Hek293 cells heterologously co-expressing ATP1B2 and the ouabain insensitive ATP1A3 subunit. Like to the normal retinal ATP1A3 subunit, retinoschisin efficiently bound to the ouabain-insensitive ATP1A3 variant (**Figure 16 A**).

Atomic Absorption Spectroscopy (AAS) determined the import of Rb$^+$ ions, which act as a congener of K$^+$, into ATP1A3 and ATP1B2 expressing oocytes. Upon heterologous expression

of the retinal Na/K-ATPase, Rb$^+$ uptake by oocytes increased about 6 fold compared to untransfected oocytes (**Figure 16**). The average uptake was 7 ng Rb$^+$ per transfected oocyte in 3 min (corresponding to 7899 nC), which is in line with published results for Na/K-ATPase activity in transfected oocytes (Dürr et al., 2013). 10 mM ouabain lead to an inhibition of the heterologously expressed Na/K-ATPase by around 80 % (**Figure 16 B** and **C**). The addition of 1 µg/ml retinoschisin had no effect on ion pumping activity of the Na/K-ATPase (**Figure 16 B**). An increase to 8 µg/ml retinoschisin also revealed no effects (**Figure 16 C**).
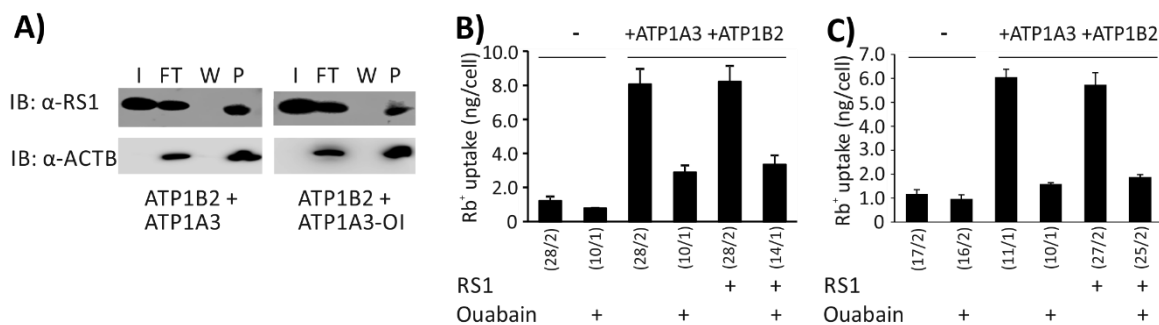
Figure 16: Analysis of Na/K-ATPase pump function in *X. leavis* oocytes
A) Hek293 cells were transfected with an expression vector for ATP1A3 or ouabain insensitive ATP1A3 (ATP1A3-OI) in combination with an expression vector for ATP1B2. 72 h after transfection, cells were incubated for 60 min with retinoschisin containing cell culture supernatant (input). After intensive washing, retinoschisin binding was assessed by subjecting cell pellets to Western blot analyses with antibodies against retinoschisin. The ACTB immunoblot was performed as loading control. I = input; FT = flowthrough; W = last wash, P = final Hek293 cell pellet. **B)** and **C)** Oocytes were injected with cRNAs for human ATP1A3 and ATP1B2 and incubated for 3 days. Rb$^+$ uptake was determined with or without ouabain (10 mM) at pH 5.5 in a solution containing 5 mM Rb$^+$. Oocytes were preincubated for 1 h with or without 1 (B) or 8 (C) µg/ml retinoschisin. The number of replicates (number of cells/number of independent cell batches) is given in brackets. Data are presented as means + SEM. (Figure modified from Plössl et al., 2017b)

4.4 Influence of Retinoschisin on Intracellular Signaling

Protein and mRNA expression profiling revealed an upregulation of MAPK signaling, in particular of the ERK pathway, in *Rs1h$^{-/Y}$* mice compared to wildtype littermates at different postnatal stages (Gehrig et al., 2007). Yet, whether these differences are a primary consequence of retinoschisin deficiency or a secondary effect due to retinal degeneration, remained unresolved. Subsequently, two different retinal model systems, P10 *Rs1h$^{-/Y-}$* retinal explants and Y-79 cells, were used to address this question and analyse a possible role for retinoschisin in the direct regulation of the ERK pathway, potentially *via* its effect on the Na/K-ATPase. In addition, an involvement of two more Na/K-ATPase associated signaling pathways, IP3/AKT signaling and Ca^{2+} signaling, was also addressed in this study.

4.4.1 Effect of Retinoschisin on the ERK Pathway Activity in Retinal Model Systems

To assess an effect of retinoschisin on ERK signaling, Y-79 cells or retinal explants were treated with recombinant retinoschisin, RS1-C59S, or equal volumes of control eluate and incubated for 10 or 30 min. Phosphorylation and hence activation of ERK signaling constituents was then followed by Western blotting. In specific, these analyses addressed phosphorylation of extracellular-signal-regulated kinases 1 and 2 (ERK1/2) and C-RAF, a central constituent of the ERK pathway, the activation of which precedes and is required for Erk1/2 phosphorylation (Roskoski, 2012).

In Y-79 cells a downregulation of phosphorylated C-RAF (77.6 ± 9.7 %) was observed after 10 min of treatment with recombinant retinoschisin, but not upon treatment with RS1-C59S. Differences in phosphorylated C-RAF levels between retinoschisin treatment and control or RS1-C59S-treatment were statistically significant. ($P < 0.05$). After 30 min of treatment with retinoschisin, the effect of retinoschisin on C-RAF phosphorylation was still evident, with a reduction of phosphorylated C-RAF activation to 78.4 ± 17.0 % (**Figure 17 A**). In contrast to its effect on C-RAF, 10 min of incubation with retinoschisin failed to show an effect on ERK1/2 phosphorylation. However, 30 min of retinoschisin treatment reduced ERK activation to around 69.6 ± 5.3 % in Y-79 cells ($P < 0.05$ compared to control protein or RS1-C59S) (**Figure 17 B**). No alterations in total C-RAF and total ERK1/2 protein levels were seen after 10 or 30 min, excluding an effect of retinoschisin on expression or stability of the two proteins (**Figure 17**).
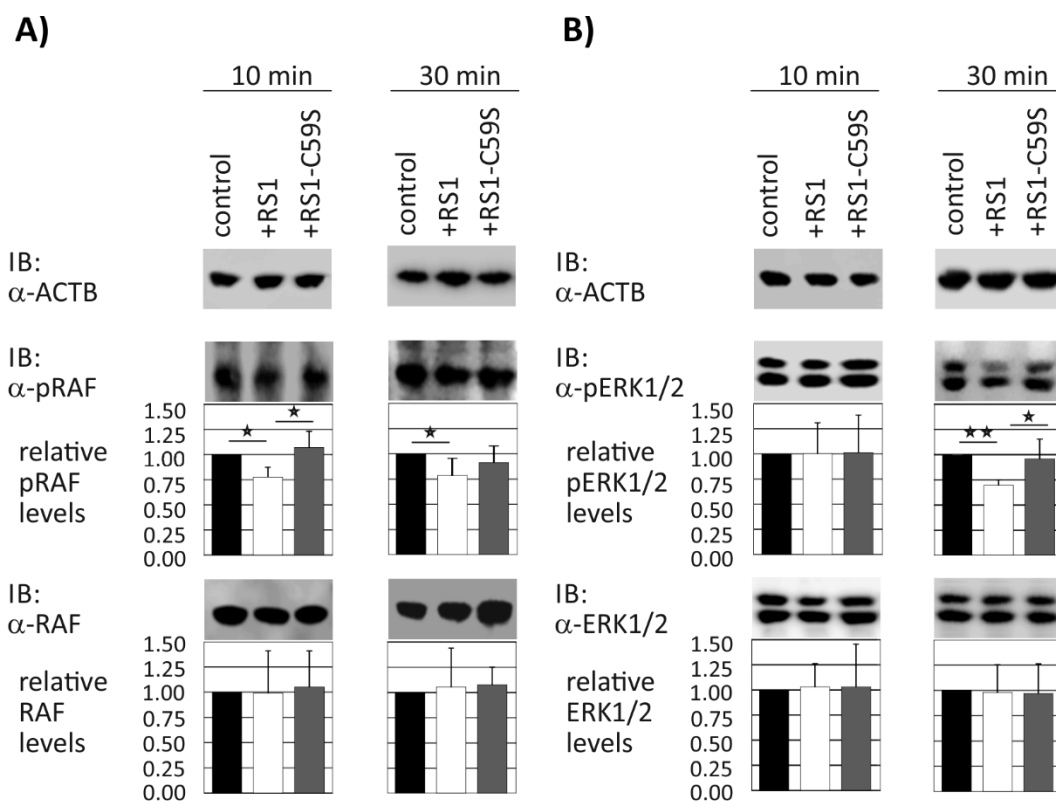
Figure 17: Influence of retinoschisin on the ERK pathway in Y-79 cells.
Y-79 cells were treated for 10 min or 30 min with 1 µg/ml retinoschisin, RS1-C59S, or equal volumes of control eluate. Cell lysates were subjected to Western blot analyses with antibodies against **A)** phosphorylated c-Raf (pRaf) and total c-Raf (Raf), or **B)** phosphorylated Erk1/2 (pErk1/2), or total Erk1/2 (Erk1/2). ActB served as a loading control. Densitometric quantification was done with ImageJ. Signals for pRaf, Raf, pErk1/2 and Erk1/2 were normalized against ActB and calibrated against the control. Data given are means + SD (n=5). Asterisks mark statistically significant (*P < 0.05) and highly significant (**P < 0.01) differences. (Figure modified from Plössl et al., 2017a)

A comparable effect of retinoschisin on ERK signaling was also observed in murine $Rs1h^{-/Y}$ retinal explants. After 10 min of incubation with retinoschisin, phosphorylated c-Raf levels were reduced to 73.4 ± 16.3 %, while RS1-C59S treatment had no effect on c-Raf phosphorylation. The differences in phosphorylated c-Raf were statistically significant (P < 0.05) between retinoschisin and control or RS1-C59S treatment. The reduction of c-Raf phosphorylation by retinoschisin treatment was still observable after 30 min of retinoschisin treatment, with a decrease in c-Raf phosphorylation to 81.4 ± 14.1 %, compared to control (**Figure 18 A**). Likewise to the effects seen in Y-79 cells, Erk1/2 phosphorylation murine $Rs1h^{-/Y}$ retinal explants was not affected after 10 min of treatment with recombinant retinoschisin. A clear reduction of phosphorylated Erk1/2 (68.7 ± 18.2 % compared to control) was observed after 30 min of treatment with retinoschisin (P < 0.05 compared to control or RS1-C59S treatment). RS1-C59S did not decrease Erk1/2 phosphorylation after 10 or 30 min (**Figure 18 B**). Total c-Raf and total Erk1/2 protein levels in retinal explants were unaffected by the different treatments (**Figure 18**).
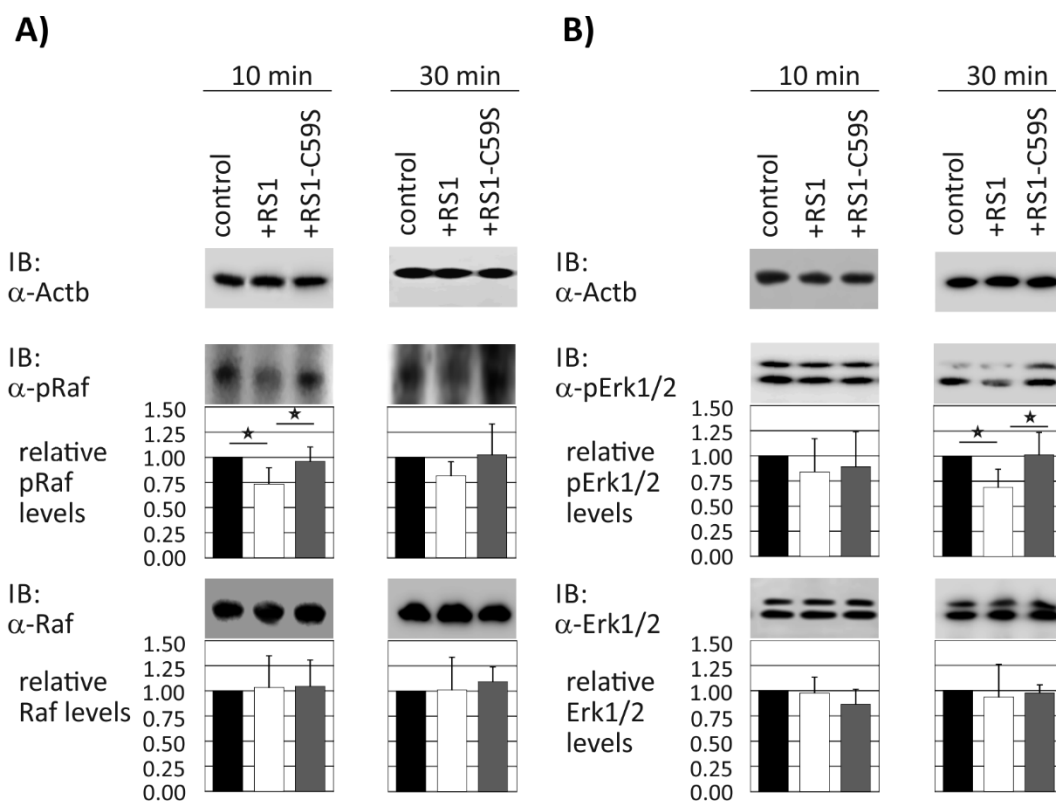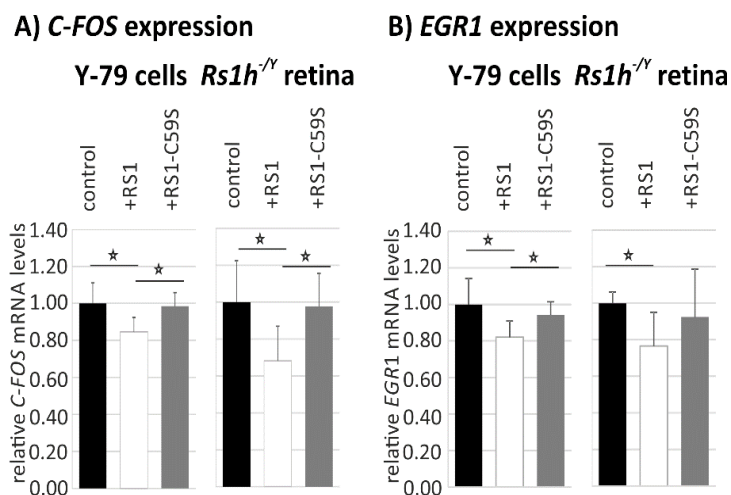
Figure 18: Influence of retinoschisin on the ERK pathway in murine *Rs1h^-/Y* retinal explants.
P10 *Rs1h^-/Y* retinal explants were treated for 10 min or 30 min with 1 µg/ml retinoschisin, RS1-C59S, or equal volume of control eluate. Subsequently, lysates were subjected to Western blot analyses with antibodies against **A)** phosphorylated c-Raf (pRaf) and total c-Raf (Raf), or **B)** phosphorylated Erk1/2 (pErk1/2) and total Erk1/2 (Erk1/2). ActB served as a loading control. Densitometric quantification was done with ImageJ. Signals for pRaf, Raf, pErk1/2 and Erk1/2 were normalized against ActB and calibrated against the control. Data given are means + SD (n=5). Asterisks mark statistically significant differences (*P < 0.05). (Figure modified from Plössl et al., 2017a)

In a next step, the effect of retinoschisin on the expression of two MAPK target genes, early growth response protein 1 (EGR1) and FBJ murine osteosarcoma viral oncogene homolog gene (C-FOS) (Whitmarsh and Davis, 1996, Hazzalin and Mahadevan, 2002, Hess et al., 2004, Murphy and Blenis, 2006, Whitmarsh, 2007) were also addressed *via* qRT-PCR in both model systems.

Upon treatment with recombinant retinoschisin, *C-FOS* mRNA in Y-79 cells was decreased to 84.6 ± 7.7 % in Y-79 cells and to 68.1 ±18.9 % in *Rs1h^-/Y* murine retinal explants (P < 0.05). RS1-C59S treatment, in contrast, had no prominent effect on *C-FOS* transcripts levels. The differences between the retinoschisin and control or RS1-C59S treatment were statistically significant (P < 0.05) in both model systems (**Figure 19 A**).

Similarly, retinoschisin treatment also caused a marked decrease in *EGR1* expression (**Figure 19 B**). *EGR1* transcript levels were reduced to 82.0 ± 8.8 % in Y-79 cells and to 76.6 ±18.8 % in *Rs1h^-/Y* murine retinal explants (P < 0.05) when compared to control treatment. No prominent decrease of *EGR1* mRNA levels was found after treatment with RS1-C59S compared to retinoschisin treatment.

A) *C-FOS* expression

Y-79 cells *Rs1h$^{-/Y}$* retina

B) *EGR1* expression

Y-79 cells *Rs1h$^{-/Y}$* retina

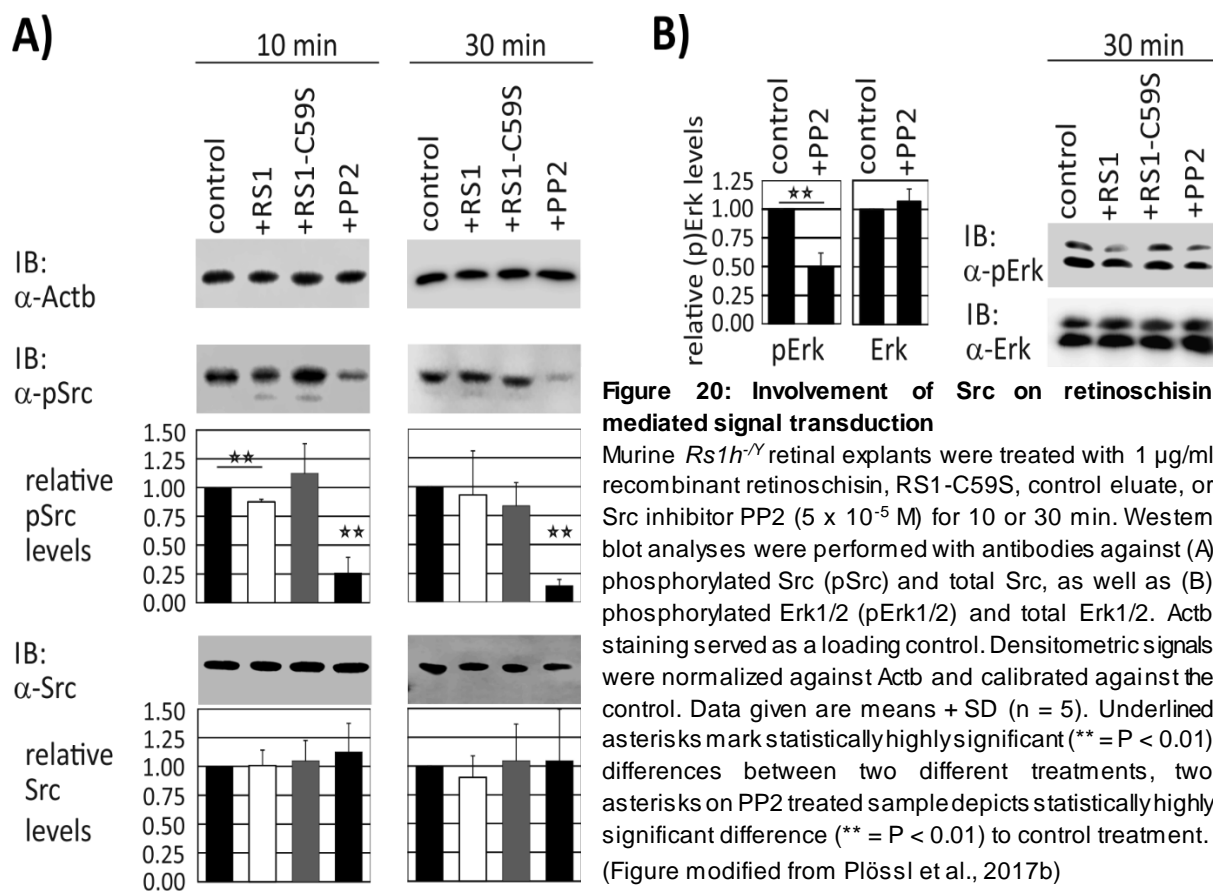**Figure 19: Influence of retinoschisin on expression of ERK1/2 pathway target genes**
A) Y-79 cells or **B)** *Rs1h$^{-/Y}$* retinal explants were treated with recombinant retinoschisin, RS1-C59S or control eluate for 2 h (Y-79 cells) and 30 min (murine retinal explants). C-FOS and EGR1 mRNA expression was determined *via* qRT-PCR. Results were normalized to HPRT transcript levels and calibrated against the control. Data given are means + SD (n=5). Asterisks mark statistically significant differences (*P < 0.05). (Plössl et al., 2017a)

4.4.2 Role of SRC in the Retinoschisin Induced Inhibition of ERK Singaling

For further studies on the mechanism of signaling regulation by retinoschisin, a focus was set on the retinal explant model system.

Activation of the non-receptor tyrosine-protein kinase SRC was described as an initial step in ERK1/2 activation by Na/K-ATPases (Haas et al., 2002; Tian et al., 2005; Quintas et al., 2010; Reinhard et al., 2013; Banerjee et al., 2015; Yosef et al., 2016). A possible influence of retinoschisin on Src phosphorylation was hence addressed by incubating retinal explants with retinoschisin or controls. Src activation was followed by Western blot analyses against phosphorylated and thus activated Src. To assess an involvement of Src in Erk1/2 activation, additional assays were performed in the presence of the specific Src kinase inhibitor PP2 (4-amino-5-(4-chlorophenyl)-7-(dimethylethyl)pyrazolo[3,4-*d*]pyrimidine).

Murine *Rs1h$^{-/Y}$* retinal explants were treated for 10 and 30 min with recombinant retinoschisin, RS1-C59S, control eluate, or PP2. 10 min of retinoschisin treatment slightly reduced Src phosphorylation to 86.8 ± 2.9 % compared to control treatment, (P < 0.01). Src activity was not decreased by RS1-C59S treatment (110.9 ± 23.8 %, compared to control). The reduction of Src activity was no longer visible after 30 min of incubation with retinoschisin (**Figure 20 A**). Treatment with PP2 lead to an almost complete de-phosphorylation of Src (pSrc levels about 25 % at 10 min, 10 % at 30 min). Total Src levels were not affected by any of the treatments, which excludes an effect on overall Src protein stability or expression levels. Addition of the Src inhibitor PP2 to retinal explants resulted in a strong and statistically highly significant downregulation of Erk1/2 phosphorylation after 30 min of incubation (50.0 ± 11.8 %, P < 0.01 compared to control treatment). Total Erk1/2 protein levels were not affected by PP2, excluding an effect on expression or stability of Erk1/2 (**Figure 20 B**).

A)

B)

Figure 20: Involvement of Src on retinoschisin mediated signal transduction

Murine *Rs1h⁻/Y* retinal explants were treated with 1 µg/ml recombinant retinoschisin, RS1-C59S, control eluate, or Src inhibitor PP2 (5×10^{-5} M) for 10 or 30 min. Western blot analyses were performed with antibodies against (A) phosphorylated Src (pSrc) and total Src, as well as (B) phosphorylated Erk1/2 (pErk1/2) and total Erk1/2. Actb staining served as a loading control. Densitometric signals were normalized against Actb and calibrated against the control. Data given are means + SD (n = 5). Underlined asterisks mark statistically highly significant (** = $P < 0.01$) differences between two different treatments, two asterisks on PP2 treated sample depicts statistically highly significant difference (** = $P < 0.01$) to control treatment. (Figure modified from Plössl et al., 2017b)

4.4.3 Effect of Retinoschisin on PI3K/AKT and Ca²⁺ Signaling

An influence of retinoschisin on PI3K/AKT signaling was investigated by following phosphorylation of its central signaling constituent Akt (Tang et al., 2017) in *Rs1h⁻/Y* murine retinal explants. However, no differences in Akt activation could be seen in retinoschisin treated explants compared to control treatments, neither after 10 nor after 30 min of incubation. Total Akt levels were also not affected by any of the treatments (**Figure 21 A**).

A potential influence of retinoschisin on Ca²⁺ signaling was tested using Ca²⁺/calmodulin-dependent protein kinase II (Camk2) phosphorylation as a marker (Illario et al., 2003). Camk2 activation was not affected by 10 min of treatment with retinoschisin or RS1-C59S. In contrast, after 30 min of incubation with retinoschisin, but not with RS1-C59S, phosphorylated Camk2 levels were significantly reduced (61.4 ± 15.5 % compared to control eluate treatment ($P < 0.05$) or to explants treated with RS1-C59S (107.2 ± 32.3 %, $P < 0.05$). Total Camk2 protein levels were not affected by the treatments (**Figure 21 B**).
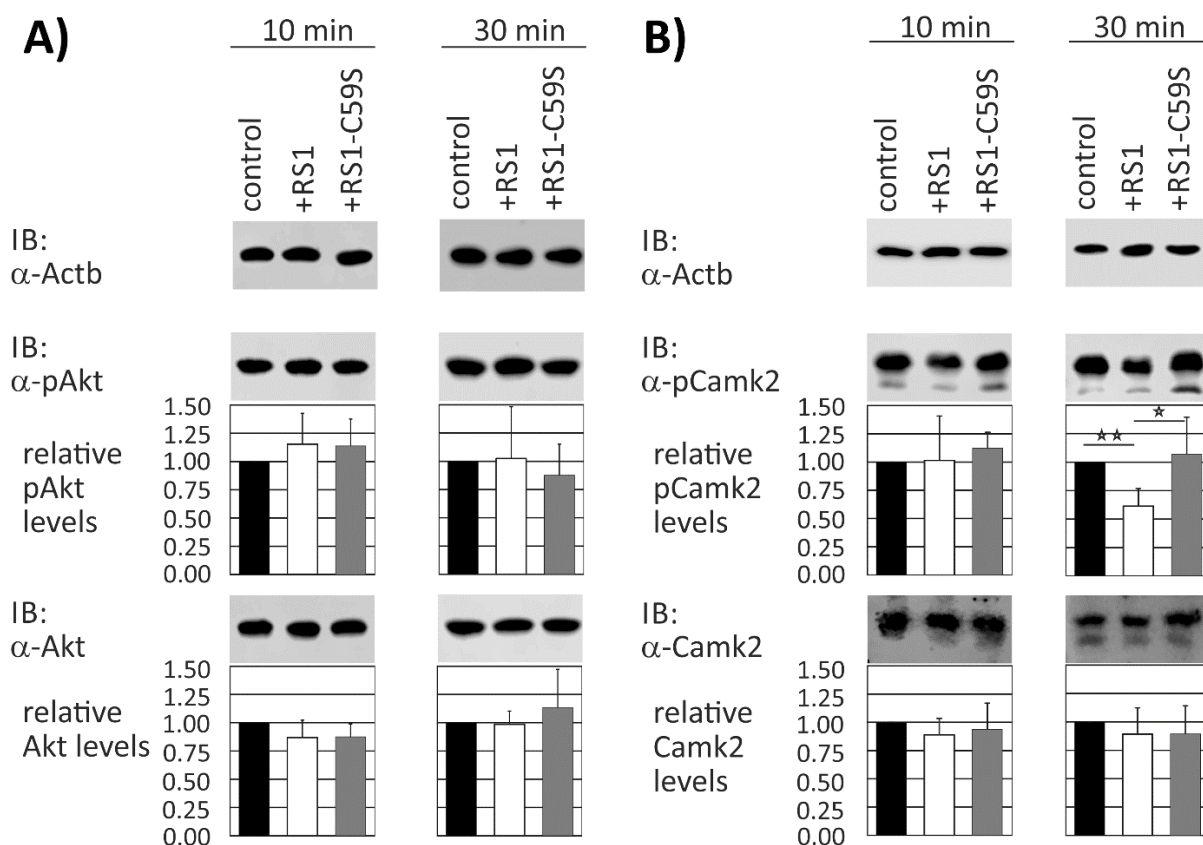
Figure 21: Effect of retinoschisin on PI3K/AKT-signaling and Ca²⁺ signaling

A) and **B)** *Rs1h⁻/ʸ* retinal explants were treated with retinoschisin, RS1-C59S, or control eluate for 10 and 30 min. Subsequently, Western blot analyses with antibodies against phosphorylated Akt (pAkt), total Akt, phosphorylated Camk2 (pCamk2), and total Camk2, as well as Actb as control were performed. *Rs1h⁻/ʸ* retinal explants were treated with Ca²⁺ signaling inhibitor 2-APB for 30 min. Subsequently, they were subjected to Western blot analyses with antibodies against phosphorylated Erk1/2 (pErk1/2), total Erk1/2 (Erk1/2), as well as Actb as control.
Signals for pAkt, Akt, pCamk2, Camk2, pErk1/2 and Erk1/2 were normalized against Actb and calibrated against the control. Data are given as means + SD (n=5). Underlined asterisks mark statistically significant (* = P < 0.05) and statistically highly significant (** = P < 0.01) differences. (Figure modified from Plössl et al., 2017b)

Since Ca²⁺ signaling can also influence ERK activation (e.g. Illario et al., 2003; Rusciano et al., 2010), the effect of the Ca²⁺ signaling inhibitor 2-APB (2-Aminoethoxydiphenyl borate, inhibits IP3R function) on phosphorylation of Erk1/2 was also tested in *Rs1h⁻/ʸ* murine retinal explants. A marked decrease in phosphorylated Erk1/2 levels was seen after 30 min of incubation with 2-APB (36.0 ± 9.6 %, P < 0.05). Total Erk1/2 protein levels were not affected (**Figure 22**).
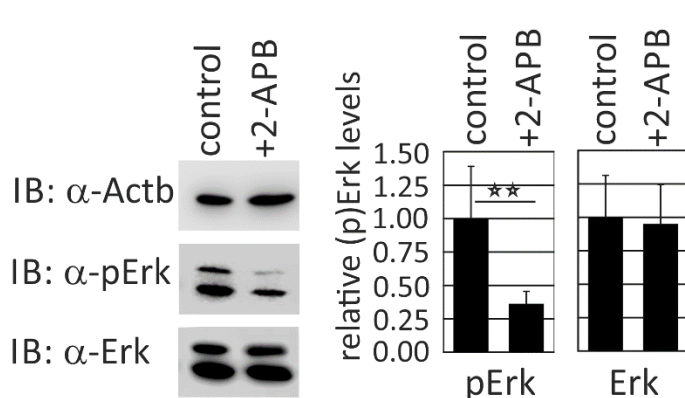
Figure 22: Influence of Ca²⁺ signaling inhibitor 2-APB on Erk1/2 activation in murine retina

Rs1h⁻/Y retinal explants were treated with Ca²⁺ signaling inhibitor 2-APB for 30 min. Subsequently, they were subjected to Western blot analyses with antibodies against phosphorylated Erk1/2 (pErk1/2), total Erk1/2 (Erk1/2), as well as Actb as control. Signals for pAkt, Akt, pCamk2, Camk2, pErk1/2 and Erk1/2 were normalized against Actb and calibrated against the control. Data are given are means + SD (n=5). Underlined asterisks mark statistically highly significant (** = P < 0.01) differences. (Figure modified from Plössl et al., 2017b)

4.4.4 Colocalization of the Retinoschisin-Na/K-ATPase Complex with Signaling Constituents in the Murine Retina

To date, there are different hypotheses about how Na/K-ATPases actually transduce signals from outside a cell onwards to intracellular signaling cascades. Scaffolding proteins like ankyrin or caveolin have been suggested to anchor and concentrate Na/K-ATPases to special signaling membrane microdomains (Liu et al., 2003, Wang et al., 2004, Liang et al., 2007). In addition, a direct interaction or close proximity of the Na/K-ATPase to intracellular signal transmitters was described to be essential for mediating Na/K-ATPase signaling (Wang et al., 2004; Liang et al., 2007; Liu et al., 2008; Quintas et al., 2010; Bai et al., 2016). Colocalization of the retinoschisin-Na/K-ATPase complex with scaffolding proteins and intracellular Na/K-ATPase associated signal transmitters was thus assessed in 10 day old murine wildtype retinae. A focus on the retinoschisin containing retinal layers (inner segments, outer nuclear layer and outer plexiform layer) revealed colocalization between retinoschisin and the Na/K-ATPase subunits Atp1a3 (**Figure 23 A**) and Atp1b2 (**Figure 23 B**). Computational analysis of signal overlaps resulted in Pearson's coefficients above 0.5 and overlap coefficients above 0.9 (**Table 40**).

The scaffolding protein ankyrin-B and the retinal Na/K-ATPase have been shown to perfectly colocalize in murine and other vertebrate retinae (Kizhatil et al., 2009). A putative colocalization with the scaffolding protein caveolin-1 was now additionally investigated. Caveolin-1 is responsible for concentrating Na/K-ATPases in so called "caveolae" in cardiac myocytes, cardiac ventricles, kidney cell lines, and kidney outer medulla (Liu et al., 2003, Wang et al., 2004, Zhang et al., 2008). This process is supposed to play an important role in the regulation of Na/K-ATPase mediated signaling in these tissues (Wang et al., 2004; Liang et al., 2007; Quintas et al., 2010; Bai et al., 2016). Strong caveolin-1 signals were detected in the outer plexiform layer and in a horizontal line between inner segments and outer nuclear layer.

Additional signals were found in the outer nuclear layer and weak caveolin-1 staining was seen in the inner segments. This pattern is consistent with previous publications, where caveolin-1 was described to be expressed predominantly in Müller cells (Li et al., 2012; Gu et al., 2014), but also weakly in photoreceptor inner segments (Berta et al., 2011; Li et al., 2012). An overlap between retinoschisin and caveolin-1 staining was seen in inner segments and outer nuclear layer. However, retinoschisin did not overlap with the prominent caveolin-1 staining from Müller cells (the horizontal line between inner segments and outer nuclear layer) (**Figure 23 C**). This cellular distribution makes quantification by Pearson's coefficient's unsuitable (Dunn et al., 2011), but overlap coefficients depicted high values (**Table 40**).

The localization of intracellular signal transmitters playing a role in the mediation of ERK and Ca^{2+} signaling by the Na/K-ATPase (Src, Plc, and IP3R, see **Figure 23**) were also analysed *via* IHC. The non-receptor tyrosine kinase Src shows a retinal staining pattern similar to caveolin-1, with additional signals in the outer segments (**Figure 23 D**), as published before (Berta et al., 2011). Overlap coefficients of around 0.9 were obtained for Src and retinoschisin (**Table 40**).

Signals for IP3R were particularly strong in inner segments and outer plexiform layers, and weaker signals were obtained in the outer nuclear layer, in agreement with previous results (Day et al., 1993). A partial overlap between retinoschisin and the IP3R was seen in inner segments, outer nuclear layer, and outer plexiform layer with Pearson's values around 0.5 and overlap coefficients of around 0.9 (**Figure 23 E, Table 40**). The localization of Plc is similar to the one seen for the IP3R. A partial overlap between retinoschisin and Plc can be seen in inner segments (**Figure 23 F**). Overlap coefficients were around 0.9, but Pearson's coefficients were rather low (around 0.2, **Table 40**).
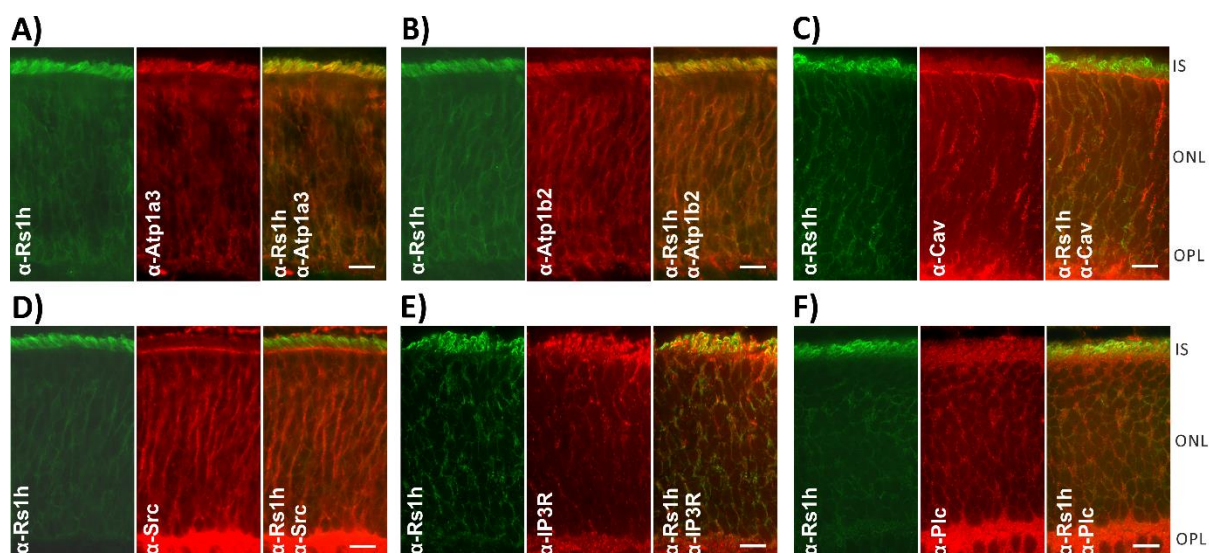
Figure 23: Localization of retinoschisin, the Na/K-ATPase and Na/K-ATPase associated signaling mediators in murine retinae

Retinal cryosections from wildtype mice at postnatal day 10 were labelled with antibodies against retinoschisin (Rs1h) and Atp1a3 (A) Atp1b2 (B) caveolin-1 (cav, C), Src (D), Plc (E) or IP3R (F). Confocal microscope images were taken under 100x magnification. Retinal layers are indicated on the right; IS, inner segment; ONL, outer nuclear layer; OPL, outer plexiform layer. Scale bar, 10 μm. (Figure modified from Plössl et al., 2017b)

Table 40: Evaluation of colocalization between retinoschisin (RS1) and the retinal Na/K-ATPase subunits Atp1a3 and Atp1b2, as well as between retinoschisin (RS1) and caveolin-1 (Cav), Src, IP3R, and Plc.

Colocalization was assessed in the entire retinal sections from Figure 25. Pearson's coefficient (linear correlation between retinoschisin and tested protein X) normal and with Costes' randomization. Overlap coefficient (size of the intersection divided by the smaller of the size of the two sets) are given with automatically and manually set thresholds. Mander's colocalization coefficients M1 and M2 are given applying manually set thresholds and thresholds set by Costes' method (Pearson's correlation coefficient as a tool for setting the thresholds). (Plössl et al., 2017b)

X	Pearson's coefficient		overlap coefficient		M1 (RS1 overlap X)		M2 (X overlap RS1)	
		Costes' randomi-zation		manual threshold	manual threshold	Costes' threshold	manual threshold	Costes' threshold
ATP1 A3	0.648	0.557, P = 1.0	0.967	0.974	0.773	0.939	0.69	0.885
ATP1 B2	0.585	0.529, P = 1.0	0.958	0.983	0.867	0.998	0.396	0.852
Cav	0.182	-0.061, P = 1.0	0.882	0.904	0.515	0.999	0.223	0.757
Src	-0.098	0.0, P = 0.0	0.899	0.928	0.816	0.0	0.098	0.0
IP3R	0.555	0.489, P = 1.0	0.914	0.897	0.639	0.999	0.418	0.871
Plc	0.218	0.128, P = 1.0	0.915	0.858	0.56	0.999	0.158	0.708

4.5   Influence of Retinoschisin on Cellular Integrity and Homeostasis

Na/K-ATPases are involved in the regulation of a variety of cellular processes like apoptosis, proliferation, neuronal development, or regulation of cellular osmolality (reviewed in Clausen et al., 2017), all processes involved in XLRS pathogenesis (reviewed in Molday et al., 2012). To investigate whether retinoschisin binding to the Na/K-ATPase could directly influence cellular integrity, several of these processes were addressed in a set of experiments using Y-79 cells or murine retinal explants as a model system.

4.5.1   Influence of Retinoschisin on Proliferation and Cell Size of Y-79 Cells

Firstly, the influence of retinoschisin on proliferation and cell size (as a measure for regulation of osmolality) was assessed. Y-79 cells (2 million cells/ml) were cultivated in the presence of 0.1 µg recombinant retinoschisin or equal volumes of control eluate and their growth and cell size were analysed with the CASY® TT Cell Counter and Analyzer after 48, 72 and 96 h. The total cell number increased over time and had doubled after 72 h. The addition of retinoschisin had no influence on the growth rate (Figure 24 **A**). The mean diameter of the cells was also recorded, and slightly increased from 1.0 to 1.2 µm, but it was not influenced by recombinant retinoschisin (Figure 24 **B**).
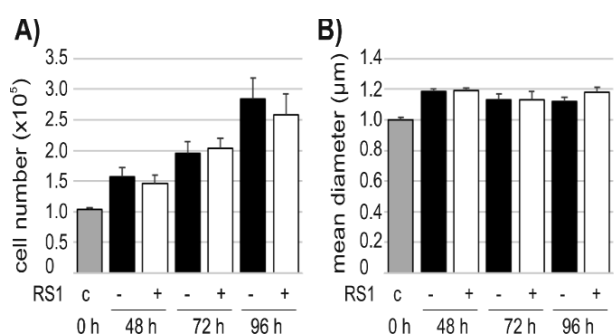
Figure 24: Influence of retinoschisin on proliferation and cell size of Y-79 cells
Y-79 cells were treated with 0.1 µg recombinant retinoschisin (+) or control eluate (-) cell growth **A)** as well as cell diameter **B)** were evaluated with a CASY® TT Cell Counter and Analyzer after 48, 72, and 96 h. Measurements were calibrated against the number/diameter of cells with which the experiment was started (control, c). Data are given are means + SD (n=8).

4.5.2   Influence of Retinoschisin on Viability of Y-79 Cells

The effect of retinoschisin on cell viability was investigated in dependence of increasing retinoschisin concentrations as well as after oxidative stress. The MTT assay was applied to assess NAD(P)H-dependent cellular oxidoreductase dependent reduction of MTT to its insoluble form formazan. This assay is frequently used to determine metabolic activity and hence viability of cells (Riss et al., 2013).

Increasing retinoschisin concentrations had no effect on cellular viability of Y-79 cells after 24 h of treatment (**Figure 25 A**). Treatment with 0.2 mM H_2O_2 for 2 h reduced cell viability to about 80% and treatment with 0.5 mM H_2O_2 resulted in only 40 % viability. However, survival rates were not altered in the presence of recombinant retinoschisin (**Figure 25 B**).

A)

B)
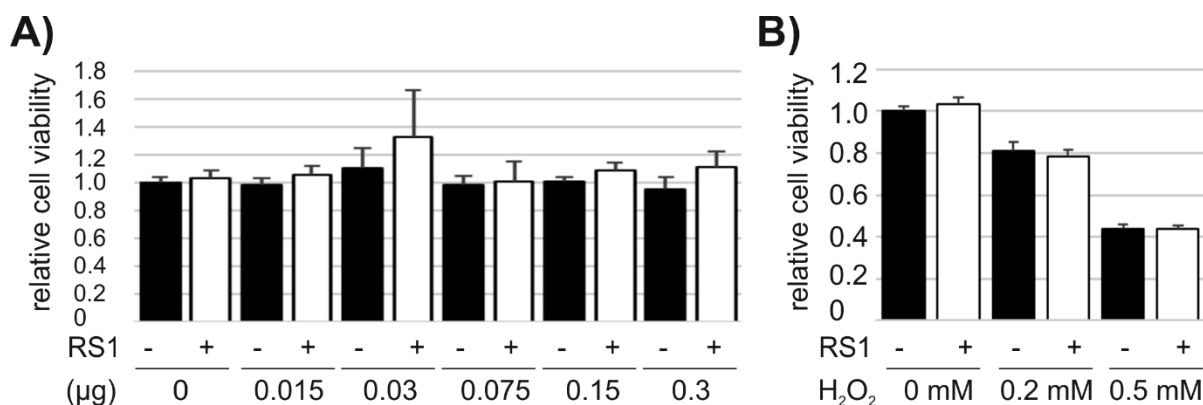
Figure 25: Influence of retinoschisin on cell viability of Y-79 cells
A) Y-79 cells were treated with increasing amounts of recombinant retinoschisin (0 to 0.3 µg) or equal volumes of control eluate (-). 24 h later, cell viability was measured using a MTT assay. Results were calibrated against the control (cells treated with 0 µg control eluate). **B)** Y-79 cells were treated with H_2O_2 for 2 h in the presence of 0.1 µg recombinant retinoschisin (+) or control eluate (-). 24 h after subsequent cultivation in the presence of recombinant retinoschisin (+) or control eluate (-), cell viability was determined by MTT assay. Results were calibrated against the control (cells treated with 0 mM H_2O_2 and control eluate). Data given are means + SD (n=4).

4.5.3 Retinoschisin Impairs Apoptosis in Retinal Model Systems

It has been shown earlier, that apoptotic activity is increased in $Rs1h^{-/Y}$ retinal tissue compared to wildtype (Gehrig et al., 2006). Therefore, a possible influence of retinoschisin on apoptosis was addressed in Y-79 cells and $Rs1h^{-/Y}$ retinal explants.

Firstly, an influence of retinoschisin on the expression of apoptosis marker *BAX* was analysed. Short time exposure to retinoschisin did not change *BAX* transcript levels in Y-79 cells (data not shown). 20 h of incubation with retinoschisin, however, significantly reduced *BAX* transcription (77.6 ± 14.0%) compared to control ($P < 0.05$) or RS1-C59S treatment ($P < 0.01$, **Figure 26 A**). In $Rs1h^{-/Y}$ retinal explants, relative *BAX* transcription was reduced to 85.4 ± 9.3 % after 30 min of incubation with retinoschisin ($P < 0.01$ compared with control and RS1-C59S-treated retinae, **Figure 26 A**). Incubation with RS1-C59S had no significant effect on *BAX* expression in Y-79 cells or retinal explants.

In an independent approach, an enzymatic assay was applied to analyse Caspase-3 activity as a marker for apoptosis. H_2O_2 treatment of Y-79 cells caused an about 2.5 fold increase in caspase-3 activity compared to unstimulated cells (**Figure 26 B**) Retinoschisin treatment of H_2O_2 stimulated cells strongly decreased caspase-3 activation (67.6 ± 9.9%) compared to control eluate or RS1-C59S ($P < 0.01$). RS1-C59S led to a slight reduction of caspase-3 activity (87.6 ± 9.1 %, $P = 0.59$) in H_2O_2 treated cells, which, however, was not statistically significant (**Figure 26 B**).

Photoreceptor cell death in $Rs1h^{-/Y}$ mice is initiated by apoptotic events around 14 days after birth (P14) (Gehrig et al., 2006). The effect of retinoschisin on photoreceptor survival was thus assessed in murine $Rs1h^{-/Y}$ retinae explanted at 18 days after birth (P18, after the apoptotic

burst at P14). *Rs1h$^{-/Y}$* retinal explants were cultured in the presence of retinoschisin, RS1-C59S or control eluate for 7 days. After incubation, cryosections were cut and stained against markers for cone as well as rod photoreceptors.

One week of cultivation resulted in a strong degeneration of retinal explants, shown by a markedly decreased thickness of the central retina and a significant reduction in photoreceptor cells (**Figure 26 C-F**). Compared to untreated, freshly explanted retinae which were not cultured for one week, 7 day cultivation reduced the number of cones to around 25 % in control and RS1-C59S treated explants (25.6 ± 8.5 % for control and 24.8 ± 8.9 % for RS1-C59S treatment (**Figure 26 C** and **D**). Noteworthy, in explants treated with retinoschisin, cone number was decreased to only about 50 % (50.3 ± 7.3 % compared to untreated retinae). The difference between retinoschisin treatment and control as well as RS1-C59S treated explants was statistically highly significant (P < 0.01).

Comparable results were also seen for rod photoreceptors. After one week of cultivation, rhodopsin signals decreased to around 24.8 ± 9.3 % for control treated, and to 28.9 ± 4.7 % for RS1-C59S treated explants. In contrast, in retinal explants treated with retinoschisin, rhodopsin signals only decreased to 59.3 ± 7.6 % compared to untreated retinae. Differences between retinoschisin and control or RS1-C59S treated explants were again statistically highly significant (P < 0.01) (**Figure 26 E** and **F**).
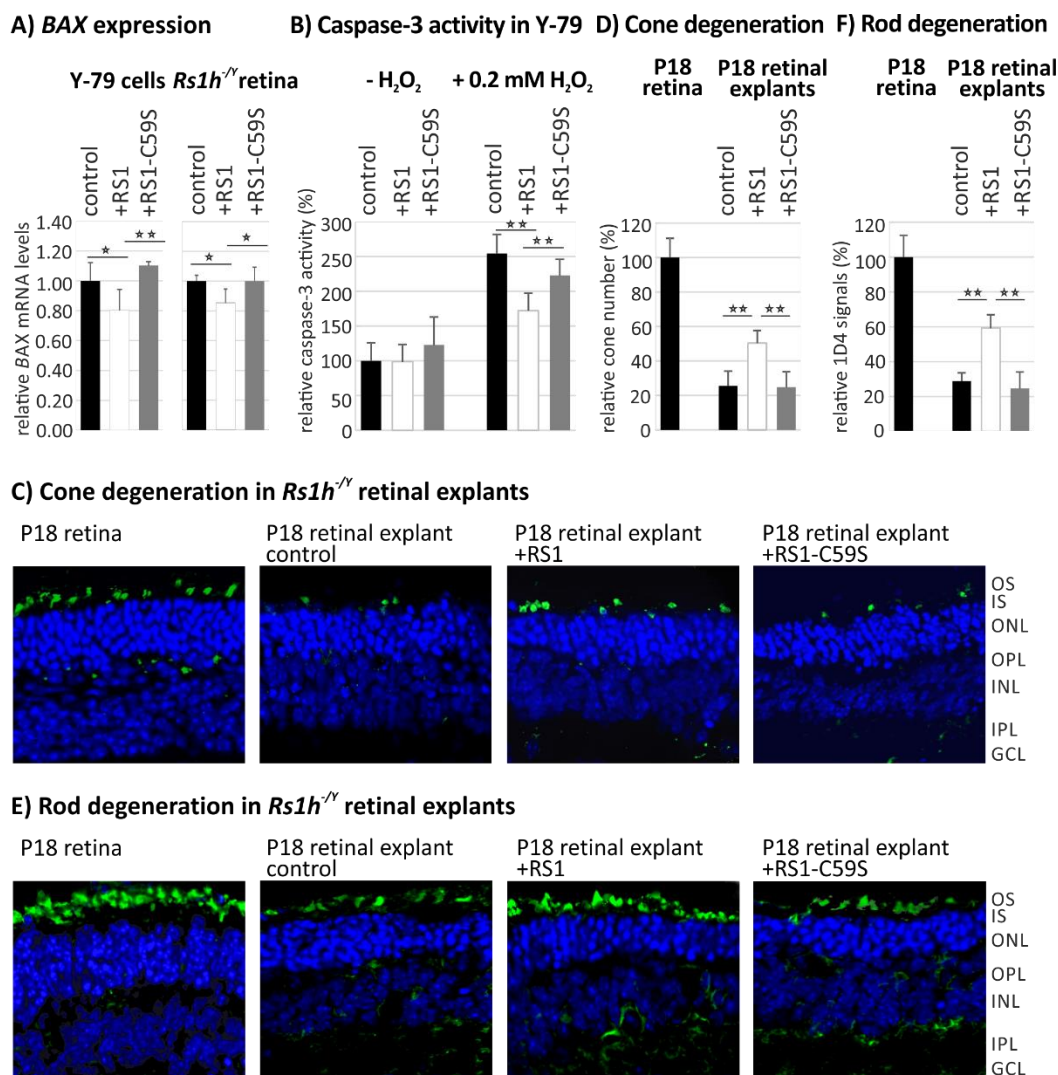
Figure 26: Influence of Retinoschisin on Apoptosis
A). Y-79 cells or retinal explants were treated with retinoschisin, RS1-C59S, or control protein for 20 h or 30 min, respectively. *BAX* mRNA expression was determined *via* qRT-PCR. Results were normalized to HPRT transcript levels and calibrated against the control. Data given are means + SD (n=5). **B)** Y-79 cells, exposed to retinoschisin, RS1-C59S, or control protein were treated with 0.2 mM H_2O_2 for 2 h. 18 h later, apoptosis was assayed by following caspase-3 specific proteolytic activity. Data given are means + SD (n=6). **C) - F)** P18 retinal explants were cultured for 1 week in medium containing retinoschisin, RS1-C59S, or control eluate. After washing and embedding, cryosections of these explants were subjected to staining for nuclei, cones and rods. OS, outer segments; IS, inner segments; ONL, outer nuclear layer; OPL, outer plexiform layer; INL, inner nuclear layer; IPL, inner plexiform layer; GCL, ganglion cell layer. DAPI staining shows the nuclei of the different retinal layers. **C)** Alexa488-conjugated peanut agglutinin (PNA) staining was applied to visualize cones. **D)** The total number of cones per analysed section was counted after staining with PNA. **E)** Anti-Rho-1D4 antibody staining was applied to visualize rod specific Rhodopsin. **F)** Rhodopsin signals per analysed section were measured using ImageJ. Data given are means + SD (n=5). Asterisks mark statistically significant (*P < 0.05) and highly significant (**P < 0.01) differences. (Plössl et al., 2017a)

4.6 Identification of the Retinoschisin-Interaction Site on the Na/K-ATPase

Previous studies revealed that retinoschisin can be co-immunoprecipitated with the retinal Na/K-ATPase subunits α3 (ATP1A3) and β2 (ATP1B2) and that expression of these subunits is required for anchorage of retinoschisin to plasma membranes (Molday et al., 2007, Friedrich et al., 2011). However, it remained unclear, whether retinoschisin binding requires the complex of both subunits or if retinoschisin specifically interacts with either ATP1A3 or ATP1B2. This project aimed to define the interface of the Na/K-ATPase binding to retinoschisin.

4.6.1 ATP1B2 is Responsible for Retinoschisin Binding

Nine different Na/K-ATPase subunit isozyme combinations (α1-β1, α1-β2, α1-β3, α2-β1, α2-β2, α2-β3, α3-β1, α3-β2, or α3-β3) were heterologously expressed in Hek293 cells and assessed for their retinoschisin binding capacity. The ATP1A4 subunit was omitted in this analysis as it was shown to be exclusively expressed in testis (Hlivko et al., 2006) and hence no physiological relevance of an interaction between this isoform and retinoschisin is to be expected.

Retinoschisin efficiently bound to Na/K-ATPases containing the ATP1B2 subunit, independent of the co-expressed α-subunit. Quantification of the binding efficiency in three independent experiments showed increased retinoschisin binding to α1-β2 expressing Hek293 cells (1.50 ± 0.33 compared to α3-β2, $P = 0.12$) (**Figure 27 A**). Whether this increase is caused by increased membrane expression or increased retinoschisin affinity of α1-β2 Na/K-ATPases was not determined in this study. No retinoschisin binding was observed to Na/K-ATPase complexes containing ATP1B1 or ATP1B3 (**Figure 27 A**). Chimeric ß subunits were generated to further narrow down the retinoschisin interaction site on ATP1B2. Two different chimeras were constructed, one consisting of the inner- and transmembrane domain of ATP1B2 (aa 1 to 79) fused to the outer domain of ATP1B1 (aa 74 to 303), termed "ATP1B1-OD", and another one consisting of the inner- and transmembrane domain of ATP1B1 (aa 1 to 71) fused to the outer domain of ATP1B2 (aa 77 to 291), termed "ATP1B2-OD". In three independent experiments, efficient retinoschisin binding was seen to ATP1B2-OD, but not to ATP1B1-OD, although binding to ATP1B2-OD was significantly weaker than binding to normal ATP1B2 (0.36 +/- 0.16, $P < 0.05$) (**Figure 27 B**).
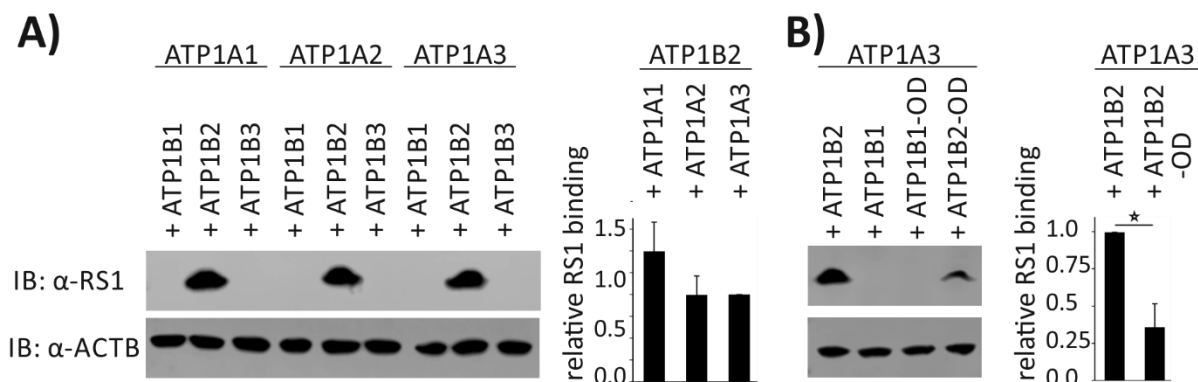
Figure 27: Binding of retinoschisin to Na/K-ATPases of different subunit combinations.
A) Hek293 cells were transfected with expression vectors for ATP1A1, ATP1A2 or ATP1A3 in combination with expression vectors for ATP1B1, ATP1B2 or ATP1B3. **B)** Hek293 cells were transfected with an expression vector for ATP1A3 in combination with an expression vector for ATP1B2, ATP1B1, or with expression vectors for ATP1B1 - OD (outer domain of ATP1B1, fused to inner and transmembrane domains of ATP1B2), or ATP1B2-OD (outer domain of ATP1B2, fused to inner and transmembrane domains of ATP1B1). 48 h after transfection, cells were incubated with retinoschisin containing Hek293 supernatant from a Hek293 line, which stably expresses retinoschisin. After 60 min of incubation cells were washed thoroughly and retinoschisin binding was assessed by subjecting cell pellets to Western blot analysis applying antibodies against retinoschisin. The ACTB immunoblot was performed as loading control. Densitometric signals for retinoschisin were normalized against ACTB and calibrated against binding to ATP1B2-ATP1A3 transfected cells. Data given are means + SD (n=3). Underlined asterisks mark statistically significant (* = P < 0.05) differences. (Plössl et al., 2017b)

To assure that the lack of retinoschisin binding to ATP1B1 and ATP1B3 containing Na/K-ATPases is not due to difficulties in expression or membrane trafficking of the artificially co-expressed subunits, expression as well as cell surface localization of the different Na/K-ATPases isozymes were analysed. Western blot analysis of transfected Hek293 cells with antibodies against the different Na/K-ATPase subunits revealed good expression of all heterologously expressed subunits (**Figure 28 A**). ATP1A1 was stained in all cells, since this subunit is endogenously expressed by Hek293 cells, but still strongest ATP1A1 signals were detected upon transfection with an ATP1A1 expression vector. Weak cross-staining of the ATP1A2 antibody was seen in ATP1A3 transfected cells and is likely due to sequence homologies of the α subunits (Pierce and Lingrel, 1994). All other Na/K-ATPase subunits showed specific immunoblot signals only in cells heterologously expressing the respective subunits.

Cell surface localization of Na/K-ATPases was analysed by two independent approaches, Western blot analyses of isolated cell surface proteins and FACS. For the first approach, cell surface proteins of Hek293 cells transfected with the different Na/K-ATPase subunit combinations were biotinylated and isolated *via* affinity chromatography against streptavidin. Western blot analysis with antibodies against the different Na/K-ATPase subunits revealed the presence of all heterologously expressed Na/K-ATPase subunits in the isolated cell surface

proteins, documenting membrane expression of all subunits (**Figure 28 B**). Notably, Na/K-ATPase β subunit isoforms in whole cell extracts showed several protein bands with a molecular weight between 25 and 55 kDa (**Figure 28 A**), reflecting different glycosylation intermediates of this subunit due to elongation and branching by the Golgi-resident glycosidases (Tokhtaeva et al., 2010). The Na/K-ATPase β subunit isoforms in isolated cell surface proteins only revealed one or two bands between 40-55 kDa (**Figure 28 B**), most likely representing the mature, fully processed ß subunit isoform exported to plasma membranes (Tokhtaeva et al., 2010).
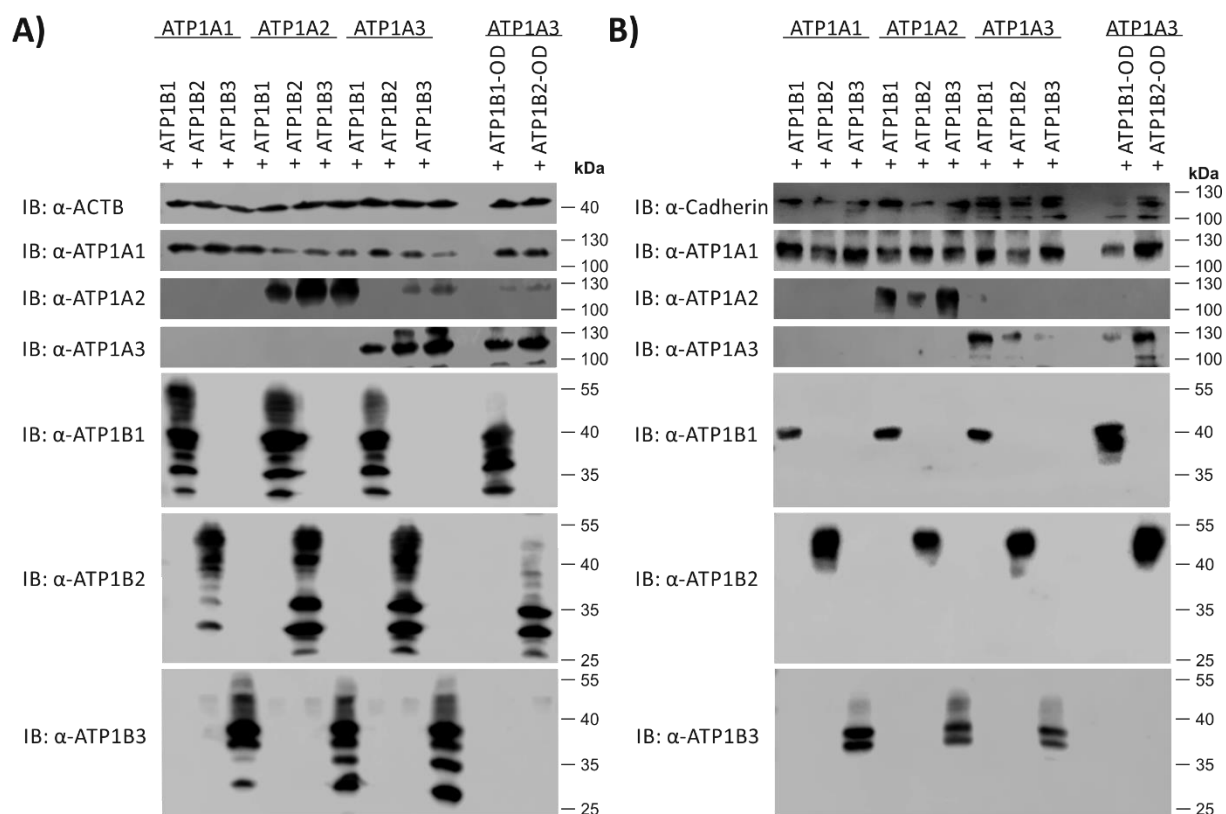
Figure 28: Protein expression and plasma membrane localization of heterologously expressed Na/K-ATPase subunit isoforms
Na/K-ATPase subunit combinations (α1-β1, α1-β2, α1-β3, α2-β1, α2-β2, α2-β3, α3-β1, α3-β2, or α3-β3, as well as α3 in combination with ATP1B1-OD or ATP1B2-OD) were heterologously expressed in Hek293 and protein expression was investigated 48 h after transfection. **A)** Hek293 cells were harvested, lysed, and subjected to Western blot analyses using antibodies against the different Na/K-ATPase subunits (ATP1A1, ATP1A2, ATP1A3 and ATP2B1, ATP1B2, ATP1B3). The ACTB immunoblot was performed as loading control. **B)** Cell surface proteins were biotinylated, purified by streptavidin affinity chromatography and analysed by Western blotting using antibodies against the different Na/K-ATPase subunits (ATP1A1, ATP1A2, ATP1A3 and ATP2B1, ATP1B2, ATP1B3). The pan-Cadherin (Cadherin) immunoblot was performed as loading control. (Plössl et al., 2017b)

In an independent approach to assess plasma membrane expression of Na/K-ATPase β subunit isoforms, whole Hek293 cells transfected with the different Na/K-ATPase subunit combinations were subjected to FACS analyses applying antibodies against ATP1B1, ATP1B2 and ATP1B3. FACS suitable antibodies against α subunits were not available in this study. ATP1B1, ATP1B2, and ATP1B3 were successfully detected on the cell surface by their

respective antibodies in the FACS experiments (**Figure 29**), confirming the observed results from Western Blot analyses of isolated cell surface proteins. However, ATP1B1-OD was not recognized in FACS analyses, in contrast to its detection in the isolated cell surface protein fractions by Western blot (**Figure 28 B**). A possible explanation for this discrepancy could be that ATP1B1-OD may display altered protein folding compared to normal ATP1B1. Proteins are not denatured before they are subjected to antibody staining in FACS, but they are when used in Western blot analyses. The epitope recognized by the anti-ATP1B1 antibody could be hidden in the native ATP1B1-OD constructs addressed in FACS but it could be accessible after denaturation for Western blot. This phenomenon has been observed for many other proteins before (e.g. Laman et al., 1993; McKnight et al., 1996).

FACS signals for ATP1B2-OD were different from those seen for non-mutated ATP1B2 which may also indicate a slight difference in the 3-D structure of the outer domain of the chimeric ATP1B2-OD construct compared to non-mutated ATP1B2.

A) Control (secondary antibody)
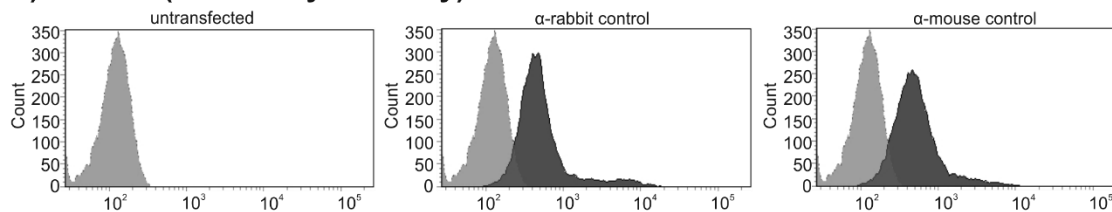
B) α-ATP1B1
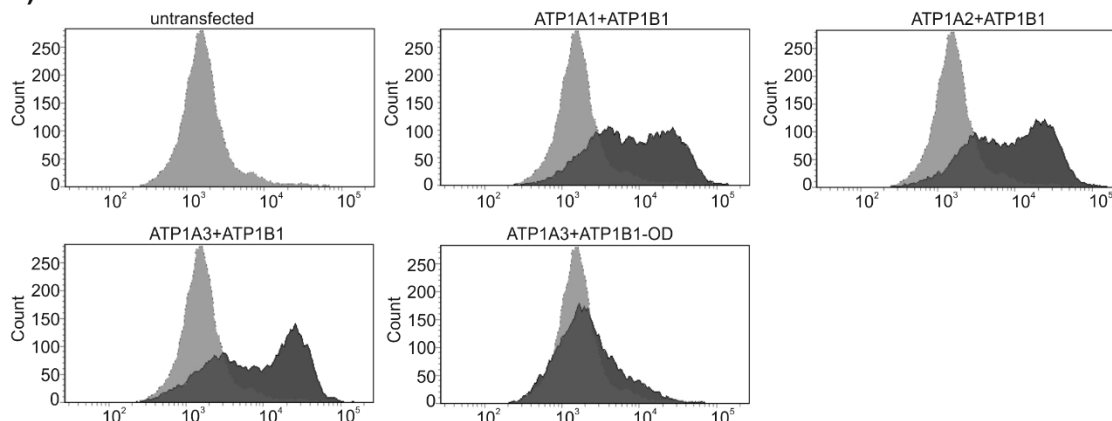
C) α-ATP1B2
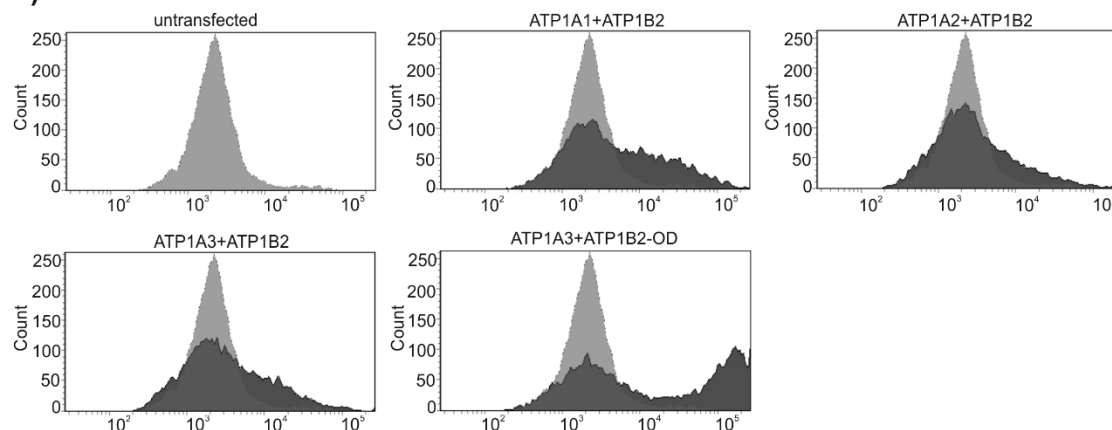
D) α-ATP1B3
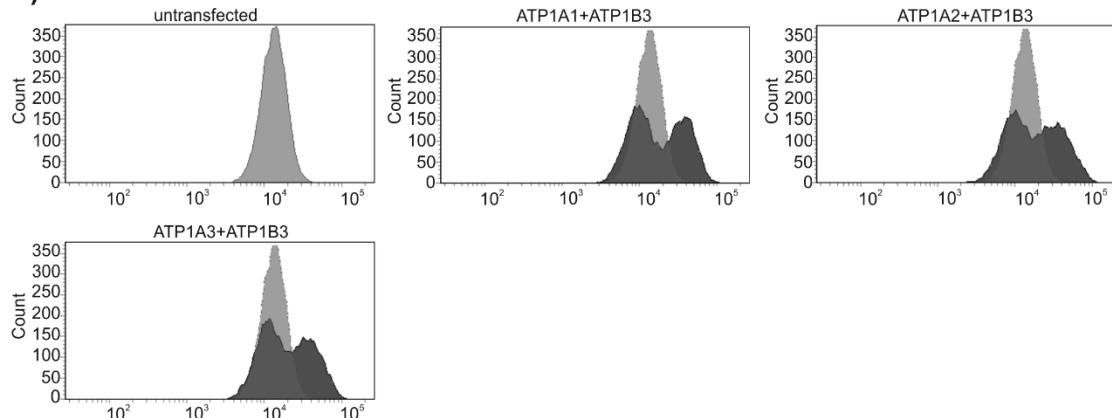
Figure 29: Analysis of cell surface expression of Na/K-ATPase subunit combinations by FACS
Hek293 cells were transiently transfected with the indicated constructs for different Na/K-ATPase subunit isozyme combinations and subjected to FACS analysis 48 h after transfection. **A)** Representative histograms of untransfected cells stained with secondary antibodies only (unstained control in light grey). **(B-D)** Representative histograms of cells transfected with the indicated Na/K-ATPase subunit isoform combinations stained with the indicated antibodies in combination with their corresponding secondary antibody (Figure modified from Plössl et al., 2017b).

4.6.2 Analysis von Hydrophobic Protein Surface Patches on ATP1B2 - Importance for Retinoschisin Binding

4.6.2.1 Bioinformatical Identification of Hydrophobic Protein-Protein Interaction Regions on ATP1B2

To further refine the retinoschisin binding region on ATP1B2, a cooperation with Prof. Dr. Rainer Merkl and Ms. Kristina Heyn (Institute for Biophysics and Physical Biochemistry, University of Regensburg, Germany) was established. By *in silico* prediction tools putative protein-protein interaction regions were identified on the ATP1B2 surface. Since the 3D structure of human ATP1B2 has not been resolved yet, a homology model was generated using the I-TASSER software (Zhang et al., 2008) and a known ß subunit structure from *Squalus acanthias* (PDB-ID 3a3y available at http://www.rcsb.org/pdb/explore.do?structureId=3a3y, accessed September 1st 2017) as template. The RMSD (Root-Mean-Square-Deviation) between the template and the model was 0.98 Å, which is an indicator for very good model quality. The PresCont Interface Prediction Tool (Zellner et al., 2012) was then used to identify putative hydrophobic protein-protein interaction sites on ATP1B2. Two different "docking patches", hydrophobic protein surfaces putatively involved in interaction processes, were identified by this approach (**Figure 30**), termed "Patch I" and "Patch II". Each patch consists of four individual sequence stretches as shown in **Table 41**.
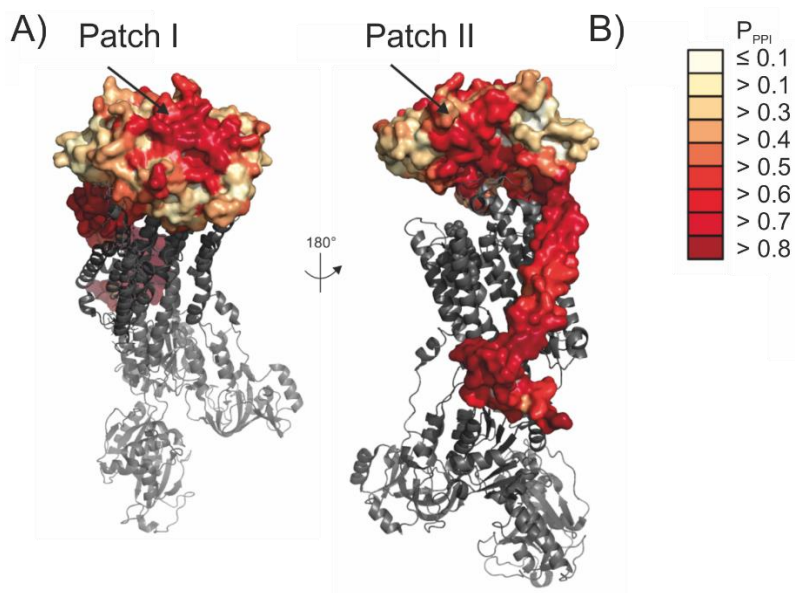
Figure 30: Docking Patch interface prediction
A) Aa residues in the ATP1B2 homology model are coloured according to a score. **B)** The p_{PPI} score represents the likelihood that a specific residue is part of a protein-protein interface. The transmembrane domain of ATP1B2 is composed of aa residues very similar to those found in interface regions and hence shows up as false positive prediction.
(Figure kindly provided by Kristina Heyn, Institute for Biophysics and Physical Biochemistry, University of Regensburg, Germany)

4.6.2.2 Binding of Retinoschisin to ATP1B2 Docking Patch Variants

To evaluate the importance of the predicted patches for the interaction between retinoschisin and the Na/K-ATPase, specific ATP1B2-ATP1B1 chimeras were generated. Since ATP1B1 is not capable of retinoschisin binding (shown in 4.6.1), the aa sequences of the computed docking patches in ATP1B2 were replaced by the corresponding aas of ATP1B1 (given in **Table 41**) applying site directed mutagenesis on the *ATP1B2* coding sequence.

Table 41: Characterization of computed ATP1B2 docking patches: Involved aas in ATP1B2 and corresponding aa sequence in ATP1B1.

aa Position in ATP1B2	aa Sequence in ATP1B2	Corresponding aa Sequence in ATP1B1	referred to as
Patch I			
aa 158-163	GNCSGI	GNCSGL	Patch I Region 1
aa 198-201	VTCA,	VQCT	Patch I Region 2
aa 246-249	VKFL	VQFT	Patch I Region 3
aa 213-221	NFVMFPANG	NVEYFGLGNSP	Patch I Region 4
Patch II			
aa 83-88	MIRPKT	TQIPQI	Patch II Region 1
aa 108-121	QKLNKFLEPYNDSI	LNIVRFLEKYKDSA	Patch II Region 2
aa 181-184	KMNR	KLNR	Patch II Region 3
aa 240	T	L	Patch II Region 4

Retinoschisin binding to the ATP1B2 docking patch variants was tested on Hek293 cells heterologously expressing ATP1A3 and the respective ATP1B2 variant. Efficient retinoschisin binding was seen to all ATP1B2 variants exhibiting ATP1B1 sequences in either of the 4 stretches of Patch I (Patch I Region 1, Region 2, Region 3 and Region 4 according to **Table 41**, labelled orange in **Figure 31 A**). Since the combined surface structure of several sequence stretches may be required for protein interaction, a complete ATP1B2 Patch I mutant, where all of the four regions from this patch were changed at once, was generated (Patch I Region 1+2+3+4, blue in **Figure 31 A**). No retinoschisin binding was seen to this complete ATP1B2-Patch I mutant. To further refine specific binding sites on Patch I, mutants were generated containing mutations in three of the four regions (Patch I Region 1+2+3, Patch I Region 1+2+4, Patch I Region 1+3+4 and Patch I Region 2+3+4, purple in **Figure 31 A**). Mutations of Patch I Region 1+2+3 still enabled efficient retinoschisin binding, suggesting that Patch I Region 1+2+3 is not the specific interaction site for retinoschisin binding. The other triple mutants did not show retinoschisin binding. Since those mutants share mutations in Patch I Region 4, double mutants of Patch I Region 4 and the other three regions were generated (Patch I Region 1+4, Patch I Region 2+4 and Patch I Region 3+4, red in **Figure 31 A**). Retinoschisin successfully bound to ATP1B2 mutated in Patch I Regions 2+4. Binding was also observed to ATP1B2 mutated in Patch I Region 1+4, although weaker than for normal ATP1B2. In contrast ATP1B2 mutated Patch I Region 3+4 failed to bind retinoschisin (**Figure 31 A**).

ATP1B2 variants mutated in Patch II were also generated. At first, binding was assessed to ATP1B2-variants exhibit mutations in either of the individual regions (orange in **Figure 31 B**). Efficient retinoschisin binding was seen to ATP1B2 mutated in Patch II Region 1 and Patch II Region 3. Patch II Region 2 and Patch II Region 4, however, failed to bind retinoschisin. A Patch II Region 1+3 double mutant (red in **Figure 31 B**) also effectively bound retinoschisin.
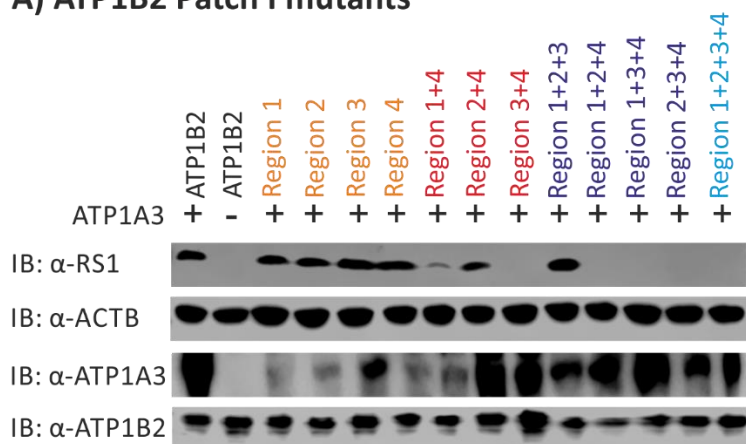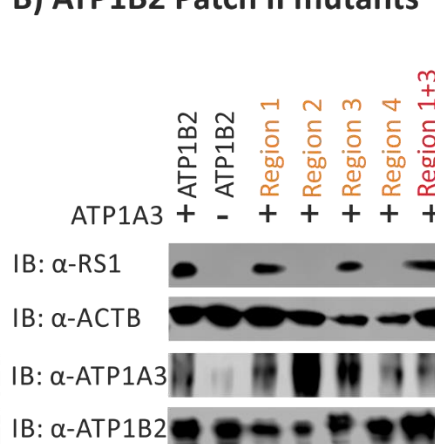
Figure 31: Binding of Retinoschisin to ATP1B2 Docking Patch Mutants
Hek293 cells were all transfected with expression vectors for ATP1A3 in combination with expression vectors for different ATP1B2 variants mutated in the Patch Regions depicted within the figure. **A)** ATP1B2 variants with different mutations of Patch I. **B)** ATP1B2 variants with different mutations of in Patch II. Hek293 cells transfected only with ATP1B2 served as negative control, ATP1A3-ATP1B2 expressing cells served as a positive control for retinoschisin binding. 48 h after transfection, cells were incubated with retinoschisin containing supernatant for 1 h and intensively washed afterwards. Retinoschisin binding to cell pellets was analysed by Western blot analyses with anti-retinoschisin antibodies. Heterologous ATP1A3 and ATP1B2 expression was confirmed by Western blotting with the respective antibodies. The ACTB staining served as loading control.

The binding assays with ATP1B2 variants mutated in Patch I or II revealed several mutants that were no longer able to bind retinoschisin (ATP1B2 variants exhibiting mutations in Patch I Regions 2 or 3 combined with Region 4, or in Patch II Regions 2 or 4). To test that the absent retinoschisin binding capacity of these ATP1B2 mutants is not a result of their decreased membrane expression, expression and cell surface localization of all ATP1B2 docking patch mutants was analysed by Western blotting and FACS analysis.

Analysis of ATP1B2 expression in total cell lysates from transfected Hek293 cells revealed good expression of all mutant constructs (**Figure 31 A**). Cell surface protein isolation showed that all ATP1B2-variants exhibiting mutations Patch I localize to the plasma membrane (**Figure 32 A**). However, in FACS analyses with an anti-ATP1B2 antibody, only ATP1B2 variants exhibiting mutations in individual Regions 1, 2, or 3 of Patch I were detected (**Figure 33**). The ATP1B2-epitope against which the antibody was generated (aa 115 to 141 of ATP1B2) overlaps for 6 aas with Region 2 of Patch I, but with none of the other regions in Patch I (or II). As the ATP1B2 variant mutated in Patch I Region 2 is detected in FACS analysis, the epitope for ATP1B2-antibody binding was thus not destroyed by the mutation. All other ATP1B2

variants mutated in Patch I were not recognized in FACS analyses (**Figure 33**). This again (as seen before for ATP1B1-OD), may be a result of altered protein folding of these ATP1B2 mutants which inhibits detection by the anti-ATP1B2 antibody in the folded state. Together, the two experimental setups (cell surface protein isolation and FACS experiments) thus indicate that protein structure of Patch I double, triple and complete mutants strongly differs from normal ATP1B2. Their effects on retinoschisin binding might thus not be caused by specific disruption of Patch I surface residues but by an overall alteration of ATP1B2 folding affecting more than Patch I (e.g. the anti-ATP1B2 epitope, aa 115-141).

All ATP1B2 variants mutated in Patch II were also expressed in transfected in Hek293 cells (**Figure 31 B**). Cell surface protein isolation of Patch II mutants revealed plasma membrane localization of all mutants despite Patch II Region 2 (**Figure 32 B**). This is in line with findings from FACS analysis, where cell surface staining was seen for all ATP1B2 Patch II mutants, but Patch II Region 2 (**Figure 34**).
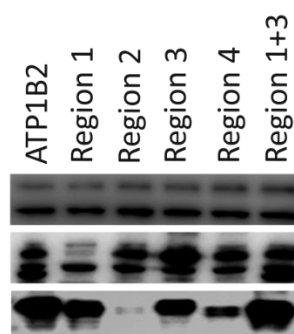
Figure 32: Cell surface protein isolation of ATP1B2 Docking Patch Mutants
Hek293 cells were transiently co-transfected with expression constructs for ATP1A3 and different ATP1B2 docking patch mutants **A)** Patch I, **B)** Patch II. Cell surface proteins were biotinylated, purified by streptavidin affinity chromatography and analysed by Western blotting using antibodies against the Na/K-ATPase subunits ATP1A3 and ATP1B2. The ATP1A1 immunoblot was performed as loading control.
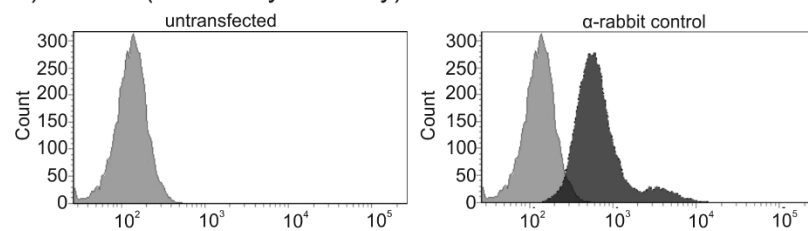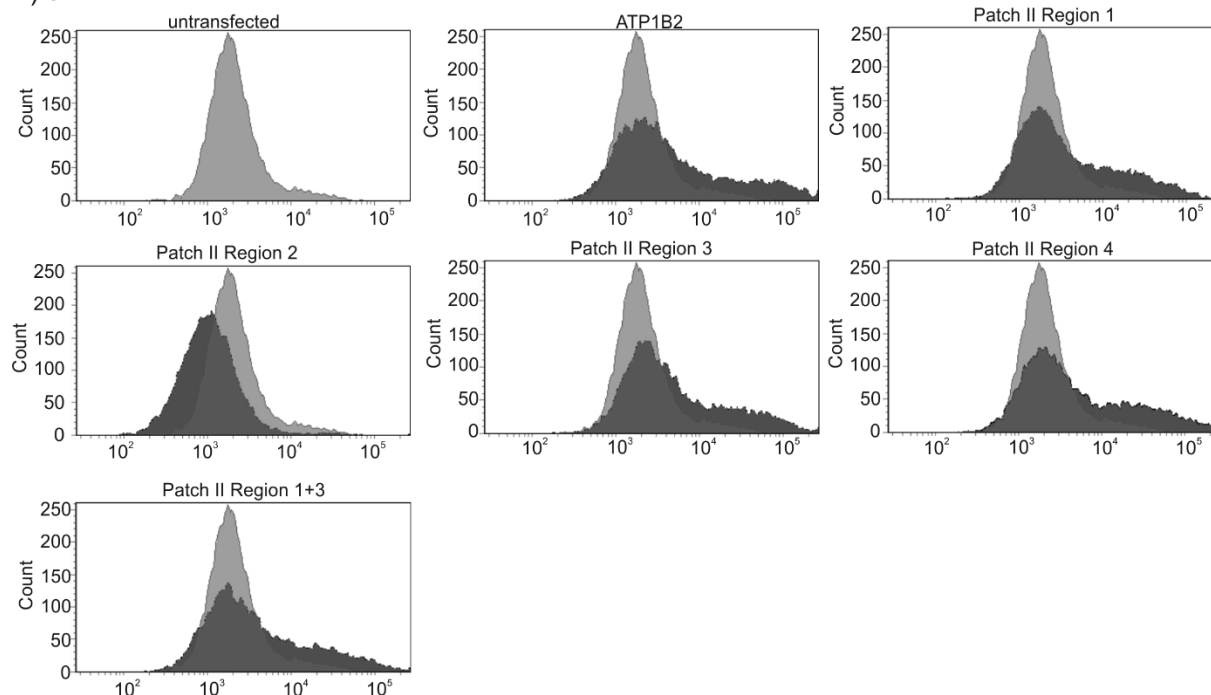
A) Control (secondary antibody)
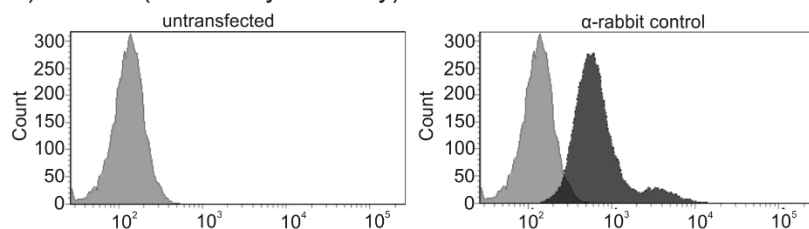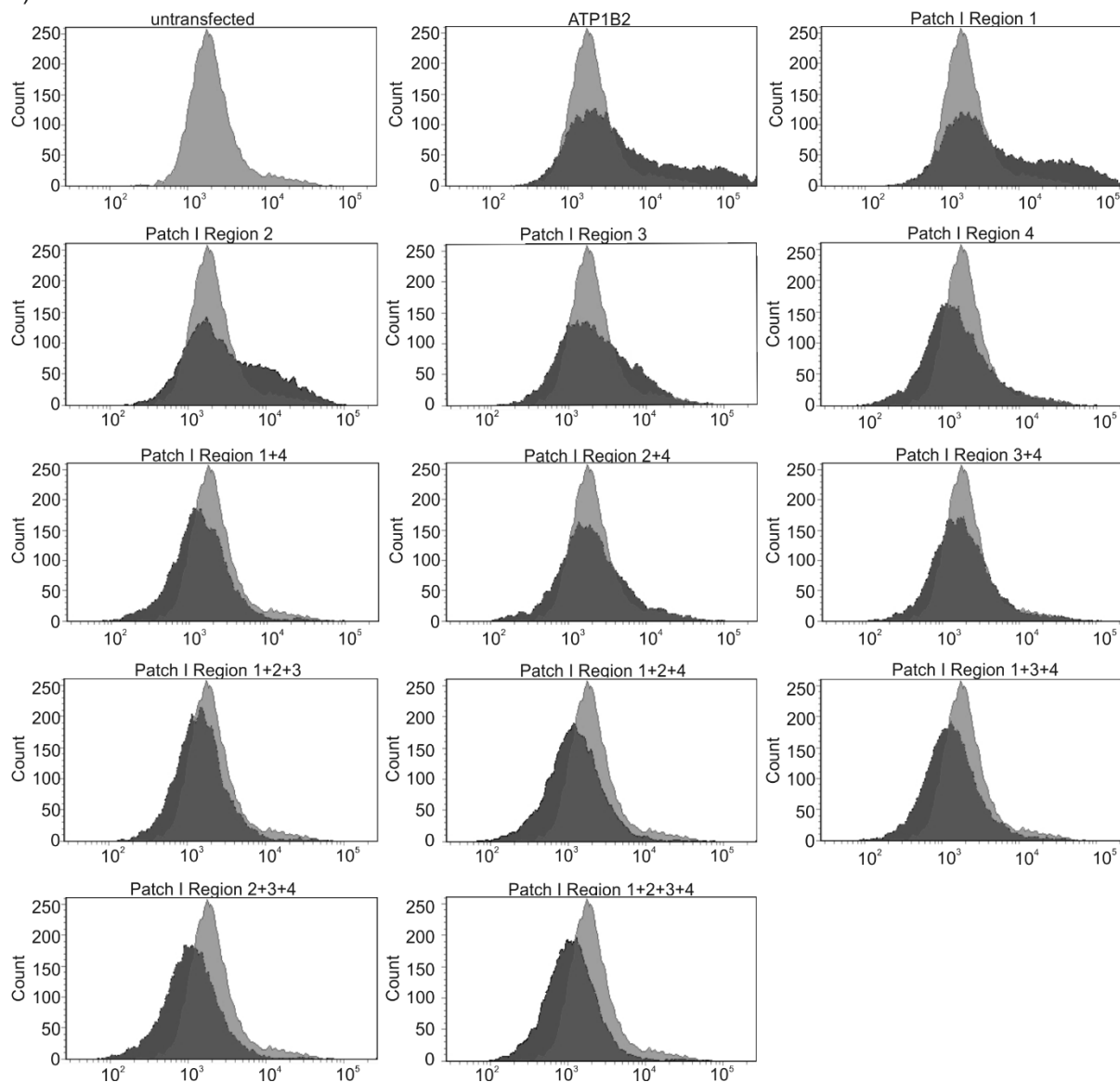
B) α-ATP1B2

Figure 33: FACS Analysis of ATP1B2 Docking Patch I mutants

Hek293 cells were transiently transfected with the indicated constructs for ATP1B2 Docking Patch mutants and subjected to FACS analysis 48 h after transfection.

A) Representative histograms of untransfected cells stained with secondary antibody only (unstained control in light grey). **B)** Representative histograms of cells transfected with the indicated Na/K-ATPase subunit isoform combinations and stained with the anti-ATP1B2 antibody. Light grey: histogram of untransfected Hek293 cells depicting unspecific background signals. Dark grey: histogram of transfected Hek293 cells.

Figure 34: FACS analysis of ATP1B2 Docking Patch II mutants

Hek293 cells were transiently transfected with the indicated constructs for different ATP1B2 Docking Patch II mutants and subjected to FACS analysis 48 h after transfection.

A) Representative histograms of untransfected cells stained with secondary antibody (unstained control in light grey). **B)** Representative histograms of cells transfected with the indicated Na/K-ATPase subunit isoform combinations stained with the anti-ATP1B2 antibody. Light grey: histogram of untransfected Hek293 cells depicting unspecific background signals. Dark grey: histogram of transfected Hek293 cells.

5   Discussion

XLRS is a common retinal dystrophy in young males, but the molecular mechanisms underlying XLRS pathogenesis are still unresolved. Therefore, the aim of this work was to elucidate molecular processes associated with XLRS. The work focused on the interaction between retinoschisin and its interaction partner in retinal membranes, the retinal Na/K-ATPase, a heterodimer consisting of ATP1A3 and ATP1B2.

The results revealed no influence of retinoschisin on Na/K-ATPase protein levels or membrane stability, as well as on Na/K-ATPase ion pump activity. In contrast, retinoschisin regulated Na/K-ATPase associated signaling pathways, specifically MAPK and Ca^{2+} signaling. This was revealed by following the activation of marker proteins and expression of target genes of these pathways in Western Blot or qRT-PCR analyses, respectively. Immunohistochemistry in retinal cryosections revealed an overlap of the retinoschisin-Na/K-ATPase complex and proteins involved in Na/K-ATPase signaling, confirming a potential regulation of signaling cascades *via* the retinoschisin-Na/K-ATPase complex.

Further studies testing an influence of retinoschisin on retinal homeostasis revealed no effects on cell viability, proliferation, or cell size of Y-79 cells. Apoptotic activity, assessed by qRT-PCR, caspase-3 activation and photoreceptor degeneration, in contrast, was decreased upon retinoschisin treatment in Y-79 cells and *Rs1h$^{-/Y}$* murine retinal explants.

Finally, a bioinformatics approach identified two putative retinoschisin interaction regions each consisting of 4 hydrophobic stretches on the retinal Na/K-ATPase. After mutating each of these stretches by site directed mutagenesis, retinoschisin binding assays identified aa residue T240 on ATP1B2 as being required for retinoschisin binding. This leaves this residue and its associated hydrophobic patch on ATP1B2 as a potential candidate for the retinoschisin interacting region on the retinal Na/K-ATPase.

5.1   Pathomechanism of the Retinoschisin Mutant RS1-C59S

The vast majority of *RS1* mutations results in a loss of secreted retinoschisin in the retina, representing true null alleles or leading to a failure in retinoschisin secretion (reviewed in Molday et al., 2012). RS1-C59S is one of the rare retinoschisin mutants which is secreted from cells. However, it can no longer form octamers, as these are stabilized by disulfide bonds between the cystein residues at aa positions 59 and 223 (Wu et al., 2005). A possible pathomechanism underlying RS1-C59S and other secreted retinoschisin mutants has not been described yet. Binding experiments conducted within this work revealed that in contrast to normal retinoschisin, RS1-C59S is not able to bind to retinal membranes and thus to interact

with the retinal Na/K-ATPase. Consequently, RS1-C59S also failed to show regulation of intracellular signaling or apoptosis as attributed to retinoschisin within this thesis work.

Several molecular mechanisms can explain the loss of binding capacity of RS1-C59S to the retinal Na/K-ATPase. In the retinoschisin octamer, C59 is a central component within the interface of two adjacent retinoschisin monomers, thus likely not accessible for the retinal Na/K-ATPase (Tolun et al., 2016). However, defective octamerization might lead to alterations in the 3-D structure of the single retinoschisin monomer, and thus the surface of the actual interaction site. Several studies suggest the exposed three spikes of retinoschisin as being responsible for retinoschisin binding to its interaction partner in the retina (Dyka et al., 2008, Molday et al., 2012, Ramsay et al., 2016). Spike regions of discoidin domains were previously shown to form a hypervariable cave which is involved in the interaction with a variety of interaction partners, whereas the core regions of discoidin domains are less variable and function as a scaffold for the spikes (Kiedzierska et al., 2007). Alterations of the scaffold structure by defective octamerization could thus negatively affect the folding of the spikes. An alternative explanation could be that multiple discoidin domains are required to enable binding of retinoschisin to retinal membranes. This assumption is strengthened by the fact that most discoidin domain containing proteins have either multiple discoidin domains within their polypeptide chain or assemble as oligomers (Baumgartner et al., 1998, Kiedzierska et al., 2007).

5.2   Effect of Retinoschisin on the Retinal Na/K-ATPase

Na/K-ATPase binding members of the FXYD protein family can influence the Na/K-ATPase complex at many levels, including overall protein expression of the α subunit, stability of the Na/K-ATPase complex as well as ion transport and substrate affinity of the α subunit (Garty et al., 2002, Jones et al., 2005, Jia et al., 2005, Lifshitz et al., 2006, Lifshitz et al., 2007, Mishra et al., 2011). Another Na/K-ATPase interacting protein, glycoprotein nonmetastatic melanoma protein B (GNMPB) was reported to modify Na/K-ATPase mediated signal transduction as well as ion pump activity upon binding to the Na/K-ATPase from the extracellular site (Ono et al., 2016). Furthermore, several intracellular proteins like caveolin (Liang et al., 2007; Quintas et al., 2010; Yosef et al., 2016), ankyrin, actin, and adducin (reviewed by Therien and Blostein, 2000) have been shown to interact with the Na/K-ATPase and modify its function, with regard to both ion transport as well as signal transduction. Similar to these proteins, retinoschisin could also act as a modulator of the retinal Na/K-ATPase.

At first, an effect of retinoschisin on retinal Na/K-ATPase levels was assessed within this work. A study from Jia and colleagues showed that Fxyd1 deficiency in mice reduces expression of the α2 subunit in heart tissues by 40 % (Jia et al., 2005). Other groups reported on increased

stability of FXYD associated Na/K-ATPase complexes (Lifshitz et al., 2007, Mishra et al., 2011). To test whether retinoschisin could similarly influence Na/K-ATPase protein levels or stability, $Rs1h^{-/Y}$ murine retinal explants or Hek293 heterologously expressing the retinal Na/K-ATPase were incubated with recombinant retinoschisin for up to 24 h. These experiments, however, did not reveal an effect of retinoschisin on retinal Na/K-ATPase protein expression in both model systems, neither in total cell lysate nor in enriched membrane fractions. These findings are in line with previous results, which showed no differences in retinal Na/K-ATPase levels in total cell extract or enriched membrane fractions from retina from $Rs1h^{-/Y}$ mice and wildtype mice (Friedrich et al., 2011).

Interestingly, IHC of $Rs1h^{-/Y}$ retinae compared to wildtype retinae revealed that retinoschisin deficiency alters Na/K-ATPase localization from a prominent staining in photoreceptor inner segments in the wildtype to a weak staining in inner segments but additional disperse staining in the nuclear layers of the $Rs1h^{-/Y}$ retina (Friedrich et al., 2011). This could imply that retinoschisin is responsible for anchoring the retinal Na/K-ATPase to specific membrane compartments. Local changes in Na/K-ATPase protein levels in different membrane compartments would not have been detectable in the experimental set-up used in this study, analysing total cell lysates and membrane fractions. Membrane trafficking to and protein stability in specific membrane compartments could rather be followed by FCS (fluorescence correlation spectroscopy) or FRAP (fluorescence recovery after photobleaching) measurements on fluorescently labelled Na/K-ATPase, methods that are frequently used to assess lateral diffusion or stability of membrane proteins (e.g. Gonzales Bardeci et al., 2016, Appelhans and Busch, 2017).

Several FXYD proteins were shown to influence Na/K-ATPase ion pump activity (Béguin et al. 1997, Arystarkhova et al. 1999, Therien et al., 1999, Pu et al., 2001, Garty et al., 2002, Jones et al., 2005, Lifshitz et al., 2006), a property which has also been suggested for GNMPB (Ono et al., 2016). It was thus tested whether retinoschisin could also influence Na/K-ATPase pump activity and/or substrate affinities. Of note, Na/K-ATPase ion pump dysregulation due to retinoschisin deficiency could provide an explanation for pathological changes seen in XLRS. On the one hand, Na/K-ATPase function is crucial for the maintenance and re-establishment of the transmembrane Na^+ gradient and is also a major determinant of neuronal resting membrane potentials (Blanco and Mercer, 1998, Dobretsov and Stimers, 2005). Specifically the α3 subunit has been attributed an important position in the clearance of intracellular Na^+ after neuronal excitation (Azarias et al., 2016). Hence, misregulation of the α3 containing photoreceptor Na/K-ATPase due to retinoschisin deficiency could be the cause of defective signal transmission from photoreceptors to bipolar cells, as seen in XLRS patients and mouse models (reviewed by Molday et al., 2012). On the other hand, dysregulation and malfunctioning of ion transport and hence disturbed ion homeostasis could also induce the formation of

extracellular cavities, as it has been observed for example in bestrophinopathies which are linked to Ca^{2+}- and volume regulated Cl^- channel dysfunction (Hartzell et al., 2008, Song and Dunaief, 2013). The fluid filled cystic cavities, as observed in the $Rs1h^{-/Y}$ mouse but also in XLRS patients (Eriksson et al. 2004, Weber et al. 2002, Xu et al. 2010), could thus be caused by osmotic changes due to disturbed ion homeostasis. However, in assays following the ion transport dependent ATP cleavage by the Na/K-ATPase as a measure for ion pump activity in $Rs1h^{-/Y}$ retinal membrane fractions, recombinant retinoschisin did not affect active ion pump activity or substrate affinities of the retinal Na/K-ATPase. A corresponding set of experiments comparing Na/K-ATPase activity in wildtype and $Rs1h^{-/Y}$ retinal membranes has been conducted by Melanie Royer during her Master's thesis at the Institute of Human Genetics, University of Regensburg. These experiments did also not reveal any influence of retinoschisin deficiency (published in Plössl et al., 2017b). Consistently, recombinant retinoschisin did not affect Rb^+ influx into oocytes heterologously expressing the human retinal Na/K-ATPase. Taken together, these data point against an influence of retinoschisin on Na/K-ATPase catalysed ion transport.

The second project of this thesis thus focused on an effect of retinoschisin on another Na/K-ATPase function, namely Na/K-ATPase mediated signaling. Various studies described an effect of the Na/K-ATPase on intracellular signaling pathways, specifically MAPK signaling, IP3/AKT signaling and Ca^{2+} signaling (reviewed in Aperia et al., 2016, Cui and Xie, 2017, Orlov et al., 2017). Intracellular, transmembrane or extracellular interaction partners like caveolin-1, FXYD family members, or GNMPB were reported to modify Na/K-ATPase signaling activity (e.g. Liu et al., 2008, Bai et al., 2016, Ono et al., 2016). It was thus assessed whether retinoschisin could exert a regulatory effect on Na/K-ATPase mediated signaling. Of note, the addition of recombinant retinoschisin had an immediate and significant influence on MAPK signaling in Y-79 cells and murine $Rs1h^{-/Y}$ retinal explants, reflected by decreased activity of MAPK cascade constituents C-RAF and ERK1/2. C-RAF deactivation occurred before ERK1/2 deactivation, which is in line with the established timeline of C-RAF and ERK1/2 activation in the ERK signaling cascade (Qi and Elion, 2005, Roskoski 2012). In addition, treatment with recombinant retinoschisin also decreased expression of MAPK target genes *C-FOS* and *EGR1* in both model systems. Interestingly, the RS1-C59S variant failed to regulate the investigated markers for MAPK activation. These data suggest that retinoschisin acts as a direct modulator of MAPK signaling in the retina, potentially *via* its effect on the retinal Na/K-ATPase. These data are consistent with results from expression profiling of the XLRS mouse revealing upregulation of MAPK signaling target genes and Erk1/2 activation at different postnatal stages (Gehrig et al., 2007).

Considering the importance of MAPK signaling on fundamental cellular processes like apoptosis, adhesion, proliferation, differentiation, or development (Kolkova et al., 2000, Chang

and Karin, 2001, Zhang and Liu, 2002), it may not be surprising that a variety of disease processes have been linked to MAPK dysregulation. Several retinal dystrophies, such as age-related macular degeneration (Dridi et al., 2012, SanGiovanni and Lee, 2013, Yating et al., 2015), diabetic retinopathy (Dong et al., 2014), or retinitis pigmentosa (Sekimukai et al., 2009, Kang et al., 2012), were linked to malfunctioning MAPK pathways. Also, neuronal degenerative diseases, like Alzheimer disease, Parkinson disease, or amyotrophic lateral sclerosis were associated with aberrant MAPK signaling (Gartner et al., 1999, Arendt et al., 2000, Holasek et al., 2005, Cali et al., 2013, Cali et al., 2014, Wang et al., 2014). The retinoschisin induced changes in MAPK pathway deactivation (to around 75 %) may seem rather small, but a similar effect size was observed for other ERK associated pathological processes: Early disease stages of Alzheimer disease present with 25 % less ERK1/2 activation in temporal cortex of healthy individuals compared to patients (Arendt et al., 1995). Similar effect sizes were also observed in a mouse model of ocular ischemic syndrome where 29 % less ERK1 and 21 % less ERK2 activation was seen in retinae of control mice than in the model (Du et al., 2016). Comparably small alterations in MAPK signaling were further observed in lymphocytes of Alzheimer and Parkinson patients (Wang et al., 2014) and in natural killer cells of Chronic Fatigue Syndrome patients (Huth et al., 2016).

The next experiments assessed an effect of retinoschisin on other Na/K-ATPase associated signaling cascades. Several studies suggested the non-receptor tyrosine kinase SRC to be an initial signal transmitter in Na/K-ATPase dependent signaling (e.g. Haas et al., 2000, Quintas et al., 2010). It was thus tested whether recombinant retinoschisin influences Src activation in murine $Rs1h^{-/Y}$ retinal explants. Treatment with recombinant retinoschisin, but not with RS1-C59S, indeed decreased Src activation. Moreover, the application of Src inhibitor PP2 almost completely abolished Erk1/2 activation in the retinal model system. These findings are consistent with the established time line and interdependency for Src and Erk1/2 activation by the Na/K-ATPase (Haas et al., 2002). Even though the differences in Src activation that were induced by retinoschisin treatment were statistically significant, they were rather small (14 % reduction compared to control). One explanation for this could be found within the α subunit isozyme composition of retinal Na/K-ATPases: 85 % of retinal Na/K-ATPases complexes contain α3, and about 15 % α1 (Schneider and Craig, 1990). Na/K-ATPases containing α3 were recently reported to activate ERK signaling in a Src independent manner (Madan et al., 2017). It would thus be conceivable that the rather small changes in Src activation seen upon retinoschisin treatment are a result of Src regulation by only α1 containing Na/K-ATPases. Alternatively, the retinal distribution of Src may play a role: Immunohistochemical analyses of murine wildtype retinae revealed that Src is indeed expressed in photoreceptor inner segments, the outer nuclear layer and the outer plexiform layer, which are all retinal layers also depicting retinoschisin expression (Molday et al., 2007, Friedrich et al., 2011). However,

strongest Src protein expression was detected in the inner nuclear and the inner plexiform layers where no retinoschisin was detected. This Src fraction is thus most likely not subjected to regulation by retinoschisin.

Addressing the remaining two Na/K-ATPase associated signaling pathways, recombinant retinoschisin did not influence PI3K/AKT signaling, but it showed an inhibitory effect on Ca^{2+} signaling: Activation of Camk2, a marker for activated Ca^{2+} signaling (Illario et al., 2003) was markedly reduced upon treatment with retinoschisin. Furthermore, inhibition of the IP3R, a central constituent in the Ca^{2+} signaling, by 2-APB resulted in a strong Erk1/2 deactivation, demonstrating an involvement of Ca^{2+} signaling in the regulation of the ERK pathway, which has been previously shown for other cell types (Illario et al., 2003, Rusciano et al., 2010). It is thus conceivable that retinoschisin modifies MAPK signaling *via* regulation of both Src and Ca^{2+} signaling in the retina. Nevertheless, Ca^{2+} signaling as such can also exert an influence in disease pathogenesis, as documented for Parkinson disease (Cali et al., 2014) and Alzheimer disease (Cali et al., 2013), or amyotrophic lateral sclerosis (Cali et al., 2013).

The assembly of Na/K-ATPase signaling complexes is reported to be significantly involved in the induction and regulation of Na/K-ATPase mediated signaling (Therien and Blostein, 2000; Xie and Askari, 2002, Xie and Cai, 2003; Wang et al., 2004; Yuan et al., 2005, Quintas et al., 2010, Reinhard et al., 2013). Thus, immunohistochemical analyses were performed to investigate colocalization of the retinal Na/K-ATPase complex with scaffolding proteins and intracellular signal transducers, contributing to Na/K-ATPase signal transmission. In several tissues, caveolin-1, was shown to concentrate Na/K-ATPases into caveolae, leading to the formation of so called "signaling microdomains" (Wang et al., 2004; Liang et al., 2007; Quintas et al., 2010; Bai et al., 2016). Immunohistochemical analyses of murine retina revealed an overlap of the retinoschisin-Na/K-ATPase complex with caveolin-1 in photoreceptor cells, but no enrichment of caveolin-1 along with the Na/K-ATPase, as it was observed for signaling microdomains in cultured cardiac myocytes, a kidney proximal tubule cell line, and cardiac T tubules (Liu et al., 2003, Liu and Askari, 2006, Cai et al., 2008) In contrast, a perfect colocalization was described for the Na/K-ATPase and ankyrin-B in the retina (Kizhatil et al., 2009). Of note, ankyrin-B was described to tether the IP3R and the Na/K-ATPase in a signaling complex which was capable of activating Ca^{2+} signaling in monkey kidney cells (Liu et al., 2008).

The conducted immunohistochemical analyses also revealed an overlap of the retinoschisin-Na/K-ATPase complex with Src. Although it is widely accepted that Src is one possible initial signal transmitter in Na/K-ATPase mediated signaling, the mechanism underlying signal transduction from the Na/K-ATPase to Src is controversially discussed: Some studies suggest a direct interaction between the Na/K-ATPase and Src (e.g. Wang et al., 2004; Tian et al.,

2005; Banerjee et al., 2015), while others were not able to verify these results and presented data refuting a direct interaction between the Na/K-ATPase and Src (e.g. Weigand et al., 2012; Clifford et al., 2013; Gable et al., 2014; Yosef et al., 2016). Similar to caveolin-1, the immunohistochemical data showed no enrichment of Src along with the Na/K-ATPase-retinoschisin complex at the photoreceptor membrane. Nevertheless, the Src fraction detected in photoreceptors could be affected by Na/K-ATPase signaling. Plc and the IP3R are implicated in the induction of Ca^{2+} signaling by the Na/K-ATPase (Aizman and Aperia, 2003, Miyakawa-Naito et al., 2003, Yuan et al., 2005, Liu et al., 2008). No specific enrichment of the IP3R and Plc was seen for plasma membrane regions of inner segments, but the retinoschisin-Na/K-ATPase complex overlapped with the IP3R as well as with Plc, bringing the Na/K-ATPase in close proximity to both signal transducers.

5.3   Effect of Retinoschisin on Retinal Homeostasis

Both MAPK and Ca^{2+} signaling pathways control important cellular events like degeneration, adhesion, proliferation, differentiation, or development (reviewed by Kolkova et al., 2000, Chang and Karin, 2001), which are also involved in XLRS pathogenesis (reviewed by Khan et al., 2001, Sikkink et al., 2007, Molday et al., 2012). Therefore, a possible influence of retinoschisin on cellular homeostasis was analysed. Retinoschisin treatment failed to show an influence on cell size, proliferation rate or viability of Y-79 cells. However, it revealed a protective effect against apoptosis in Y-79 cells and murine *Rs1h*[-/Y] retinal explants. This result is in line with previous studies, revealing increased, apoptosis induced retinal cell death in *Rs1h*[-/Y] mice compared to wildtype (Gehrig et al., 2006). Whether increased apoptosis under retinoschisin-deficiency might also be causative for the XLRS associated characteristic alterations in retinal homeostasis, schisis and defects in neuronal signal transmission, remains to be shown. Increased apoptosis is also observed in kidney cells of patients suffering from polycystic kidney disease (PKD), which, similar to the schisis in XLRS, is characterized by the formation of fluid filled cysts (Lanoix et al., 1996). Moreover, a mouse model deficient for the anti-apoptotic protein Bcl-2 shows cyst formation in the kidney (Veis et al., 1993, Sorenson et al., 1996). However, the interdependency of apoptosis and cyst formation is discussed controversially (Zhou and Kukes, 1996, Goilav 2011). Furthermore, apoptotic cell loss was observed in a variety of disorders associated with neuronal dysfunction (reviewed by Honig and Rosenberg, 2000, Mattson 2000). In particular, in amyotrophic lateral sclerosis (ALS), a disease characterized by loss of motor neurons in the spinal cord, analysis of human autopsy tissue revealed apoptotic cells in the spinal cord of ALS patients (Troost et al., 1995). Additionally, anti-apoptotic *Bcl-2* mRNA was downregulated and pro-apoptotic *Bax* mRNA was upregulated in spinal cord neurons of ALS patients (Mu et al., 1996). The importance of apoptotic cell death in ALS is further highlighted by the fact that overexpression of Bcl-2 and

administration of caspase inhibitors delays degeneration and death of motor neurons in an ALS mouse model (Kostic et al., 1997, Li et al., 2000). Interestingly, early stages of the disease are characterized by dysfunction of the neuromuscular junction, a specialized cholinergic synapse allowing signaling between muscle and nerve (Campanari et al., 2016).

5.4 Identification of the Retinoschisin Binding Site at the Na/K-ATPase

The importance of the retinal Na/K-ATPase consisting of ATP1A3 and ATP1B2 for anchoring retinoschisin to retinal plasma membranes has been established (Friedrich et al., 2011). In the last project of my thesis it was first addressed, whether retinoschisin binding requires Na/K-ATPase isozymes consisting of ATP1A3 and ATP1B2, or whether retinoschisin specifically interacts with only one of the two subunits. Therefore, nine different Na/K-ATPase α and ß subunit combinations (α1-β1, α1-β2, α1-β3, α2-β1, α2-β2, α2-β3, α3-β1, α3-β2, or α3-β3) were tested for their ability to bind retinoschisin. Only Na/K-ATPases containing the ß2 subunit were able to bind retinoschisin independent of the co-expressed α subunit. The ß1 and ß3 containing Na/K-ATPases, although experimentally confirmed to be expressed at the membrane, failed to bind retinoschisin. The finding that retinoschisin interacts with the extracellular domain of ATP1B2 is in line with previous data by Friedrich and colleagues who tested retinoschisin binding to different tissues like muscle, liver, kidney, brain, lung, heart and spleen (Friedrich et al., 2011). Besides retina, the only tissue which showed successful retinoschisin binding was brain, which, interestingly, was also shown to express ß2. All other tissues failed to bind retinoschisin and did not express ß2 (Friedrich et al., 2011).

The experimental data presented in this part of my thesis cannot fully exclude an interaction between retinoschisin and the α subunit. As all α subunits show a high extent of conservation (reviewed by Kaplan, 2002), retinoschisin interaction might be possible with all three α subunit isoforms tested in the study. However, it was shown that retinoschisin specificity is restricted to the binding of the ß2-subunit. In addition, X-ray crystallography analyses on the 3-D structure of the Na/K-ATPase revealed that the short extracellular domains of the α subunit are almost completely covered by the extracellular domain of the ß subunit (Morth et al., 2007), making an interaction of retinoschisin with these domains rather unlikely. Further analyses with ATP1B1-ATP1B2 chimeras narrowed down the retinoschisin interaction site to the extracellular domain of ß2. Bioinformatics analyses subsequently identified two potential protein interaction regions ("docking patches" I and II), which were then tested for their impact on retinoschisin-binding by generating ATP1B2-ATP1B1 chimeras at the identified regions. One artificially generated chimera harbouring a mutation at T240, a bioinformatically identified hotspot for protein interaction in docking patch II, seemed of particular importance for retinoschisin interaction. Protein isolation of cell surface proteins and FACS analyses revealed that the

ATP1B2-construct mutated at T240 (Patch II Region 4) was secreted and folded similar to normal retinoschisin. However, it failed to bind retinoschisin, which makes docking patch (Patch II) around residue T240 a likely interface for retinoschisin binding.

The mechanism of how retinoschisin binding to ß2 might affect signaling properties of the Na/K-ATPase is unclear. Interestingly, the ß2 subunit has been shown to differ from ß1 and ß3 when it comes to regulatory effects on the α subunit. Compared to the other two ß subunits, ß2 was shown to stabilize the Na/K-ATPase in its Na^+ bound E1P state. This modulatory effect was suggested to be dependent on the tilt angle of the ß2 transmembrane domain which also leads to a changed tilt angle in the extracellular domain of ß2 (Hilbers et al., 2016). Different tilt angles of the different ß subunits may alter interaction sites between the ß and the α subunit which are of importance for the kinetic properties of Na^+ binding (Hilbers et al., 2016). Likewise, retinoschisin binding to the ß2 could induce conformational changes which might alter the α-ß interaction site. As suggested by Hilbers et al., 2016, an altered α-ß interface could result in different enzymatic properties of the Na/K-ATPase, which may also include different signaling properties.

Taking into account the cog-wheel like octameric or even hexadecameric structure of retinoschisin (Tolun et al., 2016, Ramsay et al., 2016), retinoschisin might interact with more than one Na/K-ATPase simultaneously and may be capable of tethering a number of Na/K-ATPases together in clusters, as seen for Na/K-ATPase enrichment by its interaction with caveolin in caveolae (Liu et al., 2003). A mechanism like this could potentiate the regulatory properties of retinoschisin on Na/K-ATPase mediated signaling, as one molecule of retinoschisin could regulate more than one molecule of Na/K-ATPase.

5.5 Implications

Taken together, the present study provides novel insight into the pathomechanism of XLRS and highlights the importance of the retinal Na/K-ATPase as an interaction partner of retinoschisin. The data set obtained for the effect of retinoschisin on intracellular signaling and the overlap of the retinoschisin-Na/K-ATPase complex with intracellular signal transducers indicate the existence of a retinoschisin-Na/K-ATPase signalosome complex in the retina. Defective regulation of this signalosome complex could eventually result in aberrant regulation of cellular processes like apoptosis, and thus represent an initial step in XLRS pathogenesis. The interaction site of the retinal Na/K-ATPase to retinoschisin was refined to the extracellular domain of ATP1B2, suggesting the interface at a hydrophobic patch containing aa T240 in ATP1B2. Together, these novel findings may have implications for research into alternative therapeutic options for this progressive and currently untreatable disease. Specifically, strategies for preventing Na/K-ATPase dysregulation could be considered and are currently

also under investigation as novel treatment options for other diseases associated with aberrant activation of Na/K-ATPase signaling, such as cardiac fibrosis (reviewed by Fan et al., 2016). Passive immunization against marinobufagenin (MBG), as well as administration of anti-MBG antibodies or anti-Digoxin antibodies have been shown to attenuate fibrosis in models of cardiac and renal disease (Haller et al., 2014, Grigorova et al., 2016, reviewed by Fan et al., 2016). Additionally, a synthetic peptide, called NaKTide is proposed to inhibit Na/K-ATPase dependent SRC activation and was also shown to reduce cardiac fibrosis in mice (Li et al., 2009, Liu et al., 2016). A similar approach might also be feasible to reduce MAPK activation in XLRS retinae and thus represent a novel therapeutic option for XLRS.

6 References

Ackermann, U., & Geering, K. (1990). Mutual dependence of Na,K-ATPase alpha- and beta-subunits for correct posttranslational processing and intracellular transport. *FEBS Letters*, *269*(1), 105–8.

Aizman, O., & Aperia, A. (2003). Na,K-ATPase as a signal transducer. *Annals of the New York Academy of Sciences*, *986*, 489–96.

Aizman, O., Uhlen, P., Lal, M., Brismar, H., & Aperia, A. (2001). Ouabain, a steroid hormone that signals with slow calcium oscillations. *Proceedings of the National Academy of Sciences*, *98*(23), 13420–13424.

Antonicek, H., Persohn, E., & Schachner, M. (1987). Biochemical and functional characterization of a novel neuron-glia adhesion molecule that is involved in neuronal migration. *The Journal of Cell Biology*, *104*(6), 1587–95.

Antonicek, H., & Schachner, M. (1988). The adhesion molecule on glia (AMOG) incorporated into lipid vesicles binds to subpopulations of neurons. *The Journal of Neuroscience : The Official Journal of the Society for Neuroscience*, *8*(8), 2961–6.

Apaolaza, P. S., del Pozo-Rodríguez, A., Torrecilla, J., Rodríguez-Gascón, A., Rodríguez, J. M., Friedrich, U., … Solinís, M. A. (2015). Solid lipid nanoparticle-based vectors intended for the treatment of X-linked juvenile retinoschisis by gene therapy: In vivo approaches in Rs1h -deficient mouse model. *Journal of Controlled Release*, *217*, 273–283.

Apaolaza, P. S., del Pozo-Rodríguez, A., Solinís, M. A., Rodríguez, J. M., Friedrich, U., Torrecilla, J., … Rodríguez-Gascón, A. (2016). Structural recovery of the retina in a retinoschisin-deficient mouse after gene replacement therapy by solid lipid nanoparticles. *Biomaterials*, *90*, 40–49.

Aperia, A., Akkuratov, E. E., Fontana, J. M., & Brismar, H. (2016). Na $^+$-K $^+$-ATPase, a new class of plasma membrane receptors. *American Journal of Physiology - Cell Physiology*, *310*(7), C491–C495.

Appelhans, T., & Busch, K. B. (2017). Dynamic imaging of mitochondrial membrane proteins in specific sub-organelle membrane locations. *Biophysical Reviews*, *9*(4), 345–352.

Apushkin, M. A., & Fishman, G. A. (2006). Use of dorzolamide for patients with X-linked retinoschisis. *Retina*, *26*(7), 741–745.

Arendt, T., Holzer, M., Stöbe, A., Gärtner, U., Lüth, H. J., Brückner, M. K., & Ueberham, U. (2000). Activated mitogenic signaling induces a process of dedifferentiation in Alzheimer's disease that eventually results in cell death. *Annals of the New York Academy of Sciences*, *920*, 249–55.

Arystarkhova, E., & Sweadner, K. J. (1997). Tissue-specific expression of the Na,K-ATPase beta3 subunit. The presence of beta3 in lung and liver addresses the problem of the missing subunit. *The Journal of Biological Chemistry*, *272*(36), 22405–8.

Arystarkhova, E., Wetzel, R. K., Asinovski, N. K., & Sweadner, K. J. (1999). The gamma subunit modulates Na(+) and K(+) affinity of the renal Na,K-ATPase. *The Journal of Biological Chemistry*, *274*(47), 33183–5.

Azarias, G., Kruusmägi, M., Connor, S., Akkuratov, E. E., Liu, X.-L., Lyons, D., … Aperia, A. (2013). A specific and essential role for Na,K-ATPase α3 in neurons co-expressing α1 and α3. *The Journal of Biological Chemistry*, *288*(4), 2734–43.

Bai, Y., Wu, J., Li, D., Morgan, E. E., Liu, J., Zhao, X., … Liu, L. (2016). Differential roles of caveolin-1 in ouabain-induced Na $^+$/K $^+$ -ATPase cardiac signaling and contractility. *Physiological Genomics*, *48*(10), 739–748.

Ball, S. L., & Gregg, R. G. (2002). Using mutant mice to study the role of voltage-gated calcium channels in the retina. *Advances in Experimental Medicine and Biology*, *514*, 439–50.

Banerjee, M., Duan, Q., Xie, Z., Cowburn, D., Kuriyan, J., & Shapiro, J. (2015). SH2 Ligand-Like Effects of Second Cytosolic Domain of Na/K-ATPase α1 Subunit on Src Kinase. *PLOS ONE*, *10*(11), e0142119.

Baumann, L., Gerstner, A., Zong, X., Biel, M., & Wahl-Schott, C. (2004). Functional characterization of the L-type Ca2+ channel Cav1.4alpha1 from mouse retina. *Investigative Ophthalmology & Visual Science*, *45*(2), 708–13.

Baumgartner, S., Hofmann, K., Bucher, P., & Chiquet-Ehrismann, R. (1998). The discoidin domain family revisited: New members from prokaryotes and a homology-based fold prediction. *Protein Science*, *7*(7), 1626–1631.

Béguin, P., Wang, X., Firsov, D., Puoti, A., Claeys, D., Horisberger, J., & Geering, K. (1997). The γ subunit is a specific component of the Na,K-ATPase and modulates its transport function. *The EMBO Journal*, *16*(14), 4250–4260.

Berntson, A., Taylor, W. R., & Morgans, C. W. (2003). Molecular identity, synaptic localization, and physiology of calcium channels in retinal bipolar cells. *Journal of Neuroscience Research*, *71*(1), 146–51.

Berta, Á. I., Boesze-Battaglia, K., Magyar, A., Szél, Á., & Kiss, A. L. (2011). Localization of caveolin-1 and c-src in mature and differentiating photoreceptors: raft proteins co-distribute with rhodopsin during development. *Journal of Molecular Histology*, *42*(6), 523–533.

Blanco, G., Koster, J. C., Sánchez, G., & Mercer, R. W. (1995). Kinetic properties of the alpha 2 beta 1 and alpha 2 beta 2 isozymes of the Na,K-ATPase. *Biochemistry*, *34*(1), 319–25.

Blanco, G., & Mercer, R. W. (1998). Isozymes of the Na-K-ATPase: heterogeneity in structure, diversity in function. *The American Journal of Physiology*, *275*(5 Pt 2), F633-50.

Blanco, G. (2005). Na,K-ATPase Subunit Heterogeneity as a Mechanism for Tissue-Specific Ion Regulation. *Seminars in Nephrology*, *25*(5), 292–303.

Blaustein, M. P., Juhaszova, M., & Golovina, V. A. (1998). The cellular mechanism of action of cardiotonic steroids: a new hypothesis. *Clinical and Experimental Hypertension (New York, N.Y. : 1993)*, *20*(5–6), 691–703.

Bowles, K., Cukras, C., Turriff, A., Sergeev, Y., Vitale, S., Bush, R. A., & Sieving, P. A. (2011). X-Linked Retinoschisis: *RS1* Mutation Severity and Age Affect the ERG

Phenotype in a Cohort of 68 Affected Male Subjects. *Investigative Opthalmology & Visual Science*, *52*(12), 9250.

Boycott, K. M., Pearce, W. G., & Bech-Hansen, N. T. (2000). Clinical variability among patients with incomplete X-linked congenital stationary night blindness and a founder mutation in CACNA1F. *Canadian Journal of Ophthalmology. Journal Canadien D'ophtalmologie*, *35*(4), 204–13.

Brasil, O. F. M., da Cunha, A. L. G., de Castro, M. B., & Japiassú, R. M. (2011). Macular Hole Secondary to X-Linked Juvenile Retinoschisis. *Ophthalmic Surgery, Lasers, and Imaging*, *42 Online*, e4-5.

Bush, R. A., Zeng, Y., Colosi, P., Kjellstrom, S., Hiriyanna, S., Vijayasarathy, C., … Sieving, P. A. (2016). Preclinical Dose-Escalation Study of Intravitreal AAV-RS1 Gene Therapy in a Mouse Model of X-linked Retinoschisis: Dose-Dependent Expression and Improved Retinal Structure and Function. *Human Gene Therapy*, *27*(5), 376–389.

Bush, M., Setiaputra, D., Yip, C. K., & Molday, R. S. (2016). Cog-Wheel Octameric Structure of RS1, the Discoidin Domain Containing Retinal Protein Associated with X-Linked Retinoschisis. *PloS One*, *11*(1), e0147653.

Cai, T., Wang, H., Chen, Y., Liu, L., Gunning, W. T., Quintas, L. E. M., & Xie, Z.-J. (2008). Regulation of caveolin-1 membrane trafficking by the Na/K-ATPase. *The Journal of Cell Biology*, *182*(6), 1153–69.

Calì, T., Ottolini, D., & Brini, M. (2014). Calcium signaling in Parkinson's disease. *Cell and Tissue Research*, *357*(2), 439–454

Calì, T., Ottolini, D., & Brini, M. (2013). Calcium and Endoplasmic Reticulum-Mitochondria Tethering in Neurodegeneration. *DNA and Cell Biology*, *32*(4), 140–146.

Campanari, M.-L., García-Ayllón, M.-S., Ciura, S., Sáez-Valero, J., & Kabashi, E. (2016). Neuromuscular Junction Impairment in Amyotrophic Lateral Sclerosis: Reassessing the Role of Acetylcholinesterase. *Frontiers in Molecular Neuroscience*, *9*, 160.

Cereijido, M., Contreras, R. G., Shoshani, L., & Larre, I. (2012). The Na+-K+-ATPase as self-adhesion molecule and hormone receptor. *American Journal of Physiology - Cell Physiology*, *302*(3).

Chang, L., & Karin, M. (2001). Mammalian MAP kinase signalling cascades. *Nature*, *410*(6824), 37–40.

Clausen, M. J., Nissen, P., & Poulsen, H. (2011). The pumps that fuel a sperm's journey. *Biochemical Society Transactions*, *39*(3), 741–745.

Clausen, M. V., Hilbers, F., & Poulsen, H. (2017). The Structure and Function of the Na,K-ATPase Isoforms in Health and Disease. *Frontiers in Physiology*, *8*, 371.

Clifford, R. J., Kaplan, J. H., Sifre, M., Cidlowski, J., & Ellory, J. (2013). Human Breast Tumor Cells Are More Resistant to Cardiac Glycoside Toxicity Than Non-Tumorigenic Breast Cells. *PLoS ONE*, *8*(12), e84306.

Crambert, G., Hasler, U., Beggah, A. T., Yu, C., Modyanov, N. N., Horisberger, J. D., … Geering, K. (2000). Transport and pharmacological properties of nine different human Na, K-ATPase isozymes. *The Journal of Biological Chemistry*, *275*(3), 1976–86.

Cuba, J., & Gómez-Ulla, F. (2013). Fundus autofluorescence: Applications and perspectives. *Archivos de La Sociedad Española de Oftalmología (English Edition)*, *88*(2), 50–55.

Cuff, J. M., & Lichtman, M. A. (1975). The early effects of ouabain on potassium metabolism and rate of proliferation of mouse lymphoblasts. *Journal of Cellular Physiology*, *85*(2), 209–215.

Cui, X., & Xie, Z. (2017). Protein Interaction and Na/K-ATPase-Mediated Signal Transduction. *Molecules*, *22*(6), 990.

Day, N. S., Koutz, C. A., & Anderson, R. E. (1993). Inositol-1,4,5-trisphosphate receptors in the vertebrate retina. *Current Eye Research*, *12*(11), 981–991.

De Waard, M., Gurnett, C. A., & Campbell, K. P. (1996). Structural and functional diversity of voltage-activated calcium channels. *Ion Channels*, *4*, 41–87.

Dmitrieva, R. I., & Doris, P. A. (2003). Ouabain Is a Potent Promoter of Growth and Activator of ERK1/2 in Ouabain-resistant Rat Renal Epithelial Cells. *Journal of Biological Chemistry*, *278*(30), 28160–28166.

Dobretsov, M., & Stimers, J. R. (2005). Neuronal function and alpha3 isoform of the Na/K-ATPase. *Frontiers in Bioscience : A Journal and Virtual Library*, *10*, 2373–96.

Dong, N., Chang, L., Wang, B., & Chu, L. (2014). Retinal neuronal MCP-1 induced by AGEs stimulates TNF-α expression in rat microglia via p38, ERK, and NF-κB pathways. *Molecular Vision*, *20*, 616–28.

Dridi, S., Hirano, Y., Tarallo, V., Kim, Y., Fowler, B. J., Ambati, B. K., … Ambati, J. (2012). ERK1/2 activation is a therapeutic target in age-related macular degeneration. *Proceedings of the National Academy of Sciences*, *109*(34), 13781–13786.

Du, R., Wang, J., & Wang, Y. (2016). Role of RhoA/MERK1/ERK1/2/iNOS signaling in ocular ischemic syndrome. *Graefe's Archive for Clinical and Experimental Ophthalmology*, *254*(11), 2217–2226.

Dunn, K. W., Kamocka, M. M., & McDonald, J. H. (2011). A practical guide to evaluating colocalization in biological microscopy. *AJP: Cell Physiology*, *300*(4), C723–C742.

Dürr, K. L., Tavraz, N. N., Spiller, S., & Friedrich, T. (2013). Measuring Cation Transport by Na,K- and H,K-ATPase in Xenopus Oocytes by Atomic Absorption Spectrophotometry: An Alternative to Radioisotope Assays. *Journal of Visualized Experiments*, (72), e50201.

Dyka, F. M., & Molday, R. S. (2007). Coexpression and Interaction of Wild-type and Missense RS1 Mutants Associated with X-Linked Retinoschisis: Its Relevance to Gene Therapy. *Investigative Opthalmology & Visual Science*, *48*(6), 2491.

Dyka, F. M., Wu, W. W. H., Pfeifer, T. A., Molday, L. L., Grigliatti, T. A., & Molday, R. S. (2008). Characterization and Purification of the Discoidin Domain-Containing Protein Retinoschisin and Its Interaction with Galactose [†]. *Biochemistry*, *47*(35), 9098–9106.

Eakle, K. A., Kabalin, M. A., Wang, S. G., & Farley, R. A. (1994). The influence of beta subunit structure on the stability of Na+/K(+)-ATPase complexes and interaction with K+. *The Journal of Biological Chemistry*, *269*(9), 6550–7.

Eksandh, L., Andréasson, S., & Abrahamson, M. (2005). Juvenile X-Linked Retinoschisis with Normal Scotopic b-Wave in the Electroretinogram at an Early Stage of the Disease. *Ophthalmic Genetics*, *26*(3), 111–117.

Eriksson, U., Larsson, E., & Holmström, G. (2004). Optical coherence tomography in the diagnosis of juvenile X-linked retinoschisis. Acta Ophthalmologica Scandinavica, 82(2), 218–223.

X, F., J, X., & J, T. (2017). Reducing Cardiac Fibrosis: Na/K-ATPase Signaling Complex as a Novel Target. *Cardiovascular Pharmacology: Open Access*, *6*(1).

Fraternali, F., Cavallo, L., & Musco, G. (2003). Effects of pathological mutations on the stability of a conserved amino acid triad in retinoschisin. *FEBS Letters*, *544*(1–3), 21–26.

Friedrich, U., Stöhr, H., Hilfinger, D., Loenhardt, T., Schachner, M., Langmann, T., & Weber, B. H. F. (2011). The Na/K-ATPase is obligatory for membrane anchorage of retinoschisin, the protein involved in the pathogenesis of X-linked juvenile retinoschisis. *Human Molecular Genetics*, *20*(6), 1132–1142.

Gable, M. E., Abdallah, S. L., Najjar, S. M., Liu, L., & Askari, A. (2014). *Digitalis-induced cell signaling by the sodium pump: On the relation of Src to Na+/K+-ATPase. Biochemical and Biophysical Research Communications* (Vol. 446).

Gärtner, U., Holzer, M., & Arendt, T. (1999). Elevated expression of p21ras is an early event in Alzheimer's disease and precedes neurofibrillary degeneration. *Neuroscience*, *91*(1), 1–5.

Garty, H., Lindzen, M., Scanzano, R., Aizman, R., Fuzesi, M., Goldshleger, R., … Karlish, S. J. D. (2002). A functional interaction between CHIF and Na-K-ATPase: implication for regulation by FXYD proteins. *AJP: Renal Physiology*, *283*(4), F607–F615.

Geering, K. (2001). The functional role of beta subunits in oligomeric P-type ATPases. *Journal of Bioenergetics and Biomembranes*, *33*(5), 425–38.

Geering, K. (2006). FXYD proteins: new regulators of Na-K-ATPase. *AJP: Renal Physiology*, *290*(2), F241–F250.

Gehrig, A., Janssen, A., Horling, F., Grimm, C., & Weber, B. H. F. (2006). The role of caspases in photoreceptor cell death of the retinoschisin-deficient mouse. *Cytogenetic and Genome Research*, *115*(1), 35–44.

Gehrig, A., Langmann, T., Horling, F., Janssen, A., Bonin, M., Walter, M., … Weber, B. H. F. (2007). Genome-Wide Expression Profiling of the Retinoschisin-Deficient Retina in Early Postnatal Mouse Development. *Investigative Opthalmology & Visual Science*, *48*(2), 891.

Genead, M. A., Fishman, G. A., & Walia, S. (2010). Efficacy of Sustained Topical Dorzolamide Therapy for Cystic Macular Lesions in Patients With X-Linked Retinoschisis. *Archives of Ophthalmology*, *128*(2), 190.

George, N. D. L., Yates, J. R. W., & Moore, A. T. (1995). PERSPECTIVE X linked retinoschisis. *British Journal of Ophthalmology*, *79*, 697–702.

George, N. D., Yates, J. R., Bradshaw, K., & Moore, A. T. (1995). Infantile presentation of X linked retinoschisis. *The British Journal of Ophthalmology*, *79*(7), 653–7.

Gleghorn, L. J., Trump, D., & Bulleid, N. J. (2010). Wild-type and missense mutants of retinoschisin co-assemble resulting in either intracellular retention or incorrect assembly of the functionally active octamer. *Biochemical Journal*, *425*(1), 275–284.

Gloor, S., Antonicek, H., Sweadner, K. J., Pagliusi, S., Frank, R., Moos, M., & Schachner, M. (1990). The adhesion molecule on glia (AMOG) is a homologue of the beta subunit of the Na,K-ATPase. *The Journal of Cell Biology*, *110*(1), 165–74.

Goilav B. (2011). Apoptosis in polycystic kidney disease. *Biochimica et Biophysica Acta (BBA) - Molecular Basis of Disease*, *1812*(10), 1272–1280.

Golden, W. C., & Martin, L. J. (2006). Low-dose ouabain protects against excitotoxic apoptosis and up-regulates nuclear Bcl-2 in vivo. *Neuroscience*, *137*(1), 133–144.

González Bardeci, N., Angiolini, J. F., De Rossi, M. C., Bruno, L., & Levi, V. (2017). Dynamics of intracellular processes in live-cell systems unveiled by fluorescence correlation microscopy. *IUBMB Life*, *69*(1), 8–15.

Gu, X., Reagan, A., Yen, A., Bhatti, F., Cohen, A. W., & Elliott, M. H. (2014). Spatial and temporal localization of caveolin-1 protein in the developing retina. *Advances in Experimental Medicine and Biology*, *801*, 15–21.

Grayson, C., Reid, S. N., Ellis, J. A., Rutherford, A., Sowden, J. C., Yates, J. R., … Trump, D. (2000). Retinoschisin, the X-linked retinoschisis protein, is a secreted photoreceptor protein, and is expressed and released by Weri-Rb1 cells. *Human Molecular Genetics*, *9*(12), 1873–9.

Grigorova, Y. N., Juhasz, O., Zernetkina, V., Fishbein, K. W., Lakatta, E. G., Fedorova, O. V., & Bagrov, A. Y. (2016). Aortic Fibrosis, Induced by High Salt Intake in the Absence of Hypertensive Response, Is Reduced by a Monoclonal Antibody to Marinobufagenin. *American Journal of Hypertension*, *29*(5), 641–646.

Haas J. Ueber das Zusammenvorkommen von Veraenderungen der Retina und Choroidea. Arch Augenheilkd. 1898;37:343–348

Haas, M., Askari, A., & Xie, Z. (2000). Involvement of Src and Epidermal Growth Factor Receptor in the Signal Transducing Function of Na+/K+-ATPase. *Journal of Biological Chemistry*, *275*(36), 27832–7.

Haas, M., Wang, H., Tian, J., & Xie, Z. (2002). Src-mediated Inter-receptor Cross-talk between the Na $^+$/K$^+$-ATPase and the Epidermal Growth Factor Receptor Relays the Signal from Ouabain to Mitogen-activated Protein Kinases. *Journal of Biological Chemistry*, *277*(21), 18694–18702.

Haller, S. T., Drummond, C. A., Yan, Y., Liu, J., Tian, J., Malhotra, D., & Shapiro, J. I. (2014). Passive Immunization Against Marinobufagenin Attenuates Renal Fibrosis and Improves Renal Function in Experimental Renal Disease. *American Journal of Hypertension*, *27*(4), 603–609.

Hartzell, H. C., Qu, Z., Yu, K., Xiao, Q., & Chien, L.-T. (2008). Molecular physiology of bestrophins: multifunctional membrane proteins linked to best disease and other retinopathies. *Physiological Reviews*, *88*(2), 639–72.

Hazzalin, C. A., & Mahadevan, L. C. (2002). TRANSCRIPTIONMAPK-REGULATED TRANSCRIPTION: A CONTINUOUSLY VARIABLE GENE SWITCH? *Nature Reviews Molecular Cell Biology*, *3*(1), 30–40.

Hess, J., Angel, P., & Schorpp-Kistner, M. (2004). AP-1 subunits: quarrel and harmony among siblings. *Journal of Cell Science*, *117*(25).

Hilbers, F., Kopec, W., Isaksen, T. J., Holm, T. H., Lykke-Hartmann, K., Nissen, P., … Poulsen, H. (2016). Tuning of the Na,K-ATPase by the beta subunit. *Scientific Reports*, *6*, 20442. https://doi.org/10.1038/srep20442

Hlivko, J. T., Chakraborty, S., Hlivko, T. J., Sengupta, A., & James, P. F. (2006). The human Na,K-ATPase alpha4 isoform is a ouabain-sensitive alpha isoform that is expressed in sperm. *Molecular Reproduction and Development*, *73*(1), 101–115.

Holasek, S. S., Wengenack, T. M., Kandimalla, K. K., Montano, C., Gregor, D. M., Curran, G. L., & Poduslo, J. F. (2005). Activation of the stress-activated MAP kinase, p38, but not JNK in cortical motor neurons during early presymptomatic stages of amyotrophic lateral sclerosis in transgenic mice. *Brain Research*, *1045*(1–2), 185–198.

Honig L.S., Rosenberg R.N. (2000). Apoptosis and neurologic disease. *The American Journal of Medicine*, *108*(4), 317–330.

Horisberger, J.-D. (2004). Recent Insights into the Structure and Mechanism of the Sodium Pump. *Physiology*, *19*(6).

Howard, J. L., & Ridley, S. M. (1990). Acetyl-CoA carboxylase: a rapid novel assay procedure used in conjunction with the preparation of enzyme from maize leaves. *FEBS Letters*, *261*(2), 261–264.

Huang, L., Li, H., & Xie, Z. (1997). Ouabain-induced Hypertrophy in Cultured Cardiac Myocytes is Accompanied by Changes in Expression of Several Late Response Genes. *Journal of Molecular and Cellular Cardiology*, *29*(2), 429–437.

Huth, T. K., Staines, D., & Marshall-Gradisnik, S. (2016). ERK1/2, MEK1/2 and p38 downstream signalling molecules impaired in CD56dimCD16+ and CD56brightCD16dim/− natural killer cells in Chronic Fatigue Syndrome/Myalgic Encephalomyelitis patients. *Journal of Translational Medicine*, *14*(1), 97.

Iannaccone, A., Mura, M., Dyka, F. M., Ciccarelli, M. L., Yashar, B. M., Ayyagari, R., … Molday, R. S. (2006). An unusual X-linked retinoschisis phenotype and biochemical characterization of the W112C RS1 mutation. *Vision Research*, *46*(22), 3845–52.

Illario, M., Cavallo, A. L., Bayer, K. U., Di Matola, T., Fenzi, G., Rossi, G., & Vitale, M. (2003). Calcium/Calmodulin-dependent Protein Kinase II Binds to Raf-1 and Modulates Integrin-stimulated ERK Activation. *Journal of Biological Chemistry*, *278*(46), 45101–45108.

Jaisser, F., Jaunin, P., Geering, K., Rossier, B. C., & Horisberger, J. D. (1994). Modulation of the Na,K-pump function by beta subunit isoforms. *The Journal of General Physiology*, *103*(4), 605–23.

Jia, L.-G., Donnet, C., Bogaev, R. C., Blatt, R. J., McKinney, C. E., Day, K. H., … Tucker, A. L. (2005). Hypertrophy, increased ejection fraction, and reduced Na-K-ATPase activity in phospholemman-deficient mice. *American Journal of Physiology - Heart and Circulatory Physiology*, *288*(4).

Janssen, A., Min, S. H., Molday, L. L., Tanimoto, N., Seeliger, M. W., Hauswirth, W. W., … Weber, B. H. F. (2008). Effect of late-stage therapy on disease progression in AAV-mediated rescue of photoreceptor cells in the retinoschisin-deficient mouse. *Molecular Therapy : The Journal of the American Society of Gene Therapy*, *16*(6), 1010–7.

Jones, D. H., Li, T. Y., Arystarkhova, E., Barr, K. J., Wetzel, R. K., Peng, J., … Kidder, G. M. (2005). Na,K-ATPase from mice lacking the gamma subunit (FXYD2) exhibits altered Na+ affinity and decreased thermal stability. *The Journal of Biological Chemistry*, *280*(19), 19003–11.

Kang, M.-J., Chung, J., & Ryoo, H. D. (2012). CDK5 and MEKK1 mediate pro-apoptotic signalling following endoplasmic reticulum stress in an autosomal dominant retinitis pigmentosa model. *Nature Cell Biology*, *14*(4), 409–415.

Kaplan, J. G. (1978). Membrane Cation Transport and the Control of Proliferation of Mammalian Cells. *Annual Review of Physiology*, *40*(1), 19–41.

Kaplan, J. H. (2002). Biochemistry of Na,K-ATPase. *Annual Review of Biochemistry*, *71*(1), 511–535.

Khan, N. W., Jamison, J. A., Kemp, J. A., & Sieving, P. A. (2001). Analysis of photoreceptor function and inner retinal activity in juvenile X-linked retinoschisis. *Vision Research*, *41*(28), 3931–42.

Khandhadia, S., Trump, D., Menon, G., & Lotery, A. J. (2011). X-linked retinoschisis maculopathy treated with topical dorzolamide, and relationship to genotype. *Eye (London, England)*, *25*(7), 922–8.

Kiedzierska, A., Smietana, K., Czepczynska, H., & Otlewski, J. (2007). Structural similarities and functional diversity of eukaryotic discoidin-like domains. *Biochimica et Biophysica Acta (BBA) - Proteins and Proteomics*, *1774*(9), 1069–1078.

Kizhatil, K., Sandhu, N. K., Peachey, N. S., & Bennett, V. (2009). Ankyrin-B is required for coordinated expression of beta-2-spectrin, the Na/K-ATPase and the Na/Ca exchanger in the inner segment of rod photoreceptors. *Experimental Eye Research*, *88*(1), 57–64.

Kolkova, K., Novitskaya, V., Pedersen, N., Berezin, V., & Bock, E. (2000). Neural cell adhesion molecule-stimulated neurite outgrowth depends on activation of protein kinase C and the Ras-mitogen-activated protein kinase pathway. *The Journal of Neuroscience : The Official Journal of the Society for Neuroscience*, 20(6), 2238–46.

Kometiani, P., Li, J., Gnudi, L., Kahn, B. B., Askari, A., & Xie, Z. (1998). Multiple signal transduction pathways link Na+/K+-ATPase to growth-related genes in cardiac myocytes. The roles of Ras and mitogen-activated protein kinases. *The Journal of Biological Chemistry*, *273*(24), 15249–56.

Kostic, V., Jackson-Lewis, V., de Bilbao, F., Dubois-Dauphin, M., & Przedborski, S. (1997). Bcl-2: prolonging life in a transgenic mouse model of familial amyotrophic lateral sclerosis. *Science (New York, N.Y.)*, *277*(5325), 559–62.

Kotova, S., Vijayasarathy, C., Dimitriadis, E. K., Ikonomou, L., Jaffe, H., & Sieving, P. A. (2010). Retinoschisin (RS1) interacts with negatively charged lipid bilayers in the presence of Ca2+: an atomic force microscopy study. *Biochemistry*, *49*(33), 7023–32.

Kraus, D., Karlstetter, M., Walczak, Y., Hilfinger, D., Langmann, T., & Weber, B. H. F. (2011). Retinal expression of the X-linked juvenile retinoschisis (RS1) gene is controlled by an upstream CpG island and two opposing CRX-bound regions. *Biochimica et Biophysica Acta (BBA) - Gene Regulatory Mechanisms*, *1809*(4–6), 245–254.

Kühlbrandt, W. (2004). Biology, structure and mechanism of P-type ATPases. *Nature Reviews Molecular Cell Biology*, *5*(4), 282–295.

Kulikov, A., Eva, A., Kirch, U., Boldyrev, A., & Scheiner-Bobis, G. (2007). Ouabain activates signaling pathways associated with cell death in human neuroblastoma. *Biochimica et Biophysica Acta (BBA) - Biomembranes*, *1768*(7), 1691–1702.

Laman, J. D., Schellekens, M. M., Lewis, G. K., Moore, J. P., Matthews, T. J., Langedijk, J. P. M., … Claassen, E. (1993). A Hidden Region in the Third Variable Domain of HIV-1 IIIB gp120 Identified by a Monoclonal Antibody. *AIDS Research and Human Retroviruses*, *9*(7), 605–612.

Langer, G. A. (1972). Effects of Digitalis on Myocardial Ionic Exchange. *Circulation*, *46*(1).

Langmann, T., Lai, C. C. L., Weigelt, K., Tam, B. M., Warneke-Wittstock, R., Moritz, O. L., & Weber, B. H. F. (2008). CRX controls retinal expression of the X-linked juvenile retinoschisis (RS1) gene. *Nucleic Acids Research*, *36*(20), 6523–6534.

Lanoix, J., D'Agati, V., Szabolcs, M., & Trudel, M. (1996). Dysregulation of cellular proliferation and apoptosis mediates human autosomal dominant polycystic kidney disease (ADPKD). *Oncogene*, *13*(6), 1153–60.

Laursen, M., Gregersen, J. L., Yatime, L., Nissen, P., & Fedosova, N. U. (2015). Structures and characterization of digoxin- and bufalin-bound Na^+,K^+-ATPase compared with the ouabain-bound complex. *Proceedings of the National Academy of Sciences*, *112*(6), 1755–1760.

Lee, J. J., Kim, J. H., Kim, S. Y., Park, S. S., & Yu, Y. S. (2009). Infantile vitreous hemorrhage as the initial presentation of X-linked juvenile retinoschisis. *Korean Journal of Ophthalmology : KJO*, *23*(2), 118–20.

Lewis, T. S., Shapiro, P. S., & Ahn, N. G. (1998). Signal transduction through MAP kinase cascades. *Advances in Cancer Research*, *74*, 49–139.

Li, X., McClellan, M. E., Tanito, M., Garteiser, P., Towner, R., Bissig, D., … Elliott, M. H. (2012). Loss of caveolin-1 impairs retinal function due to disturbance of subretinal microenvironment. *The Journal of Biological Chemistry*, *287*(20), 16424–34.

Li, M., Ona, V. O., Guégan, C., Chen, M., Jackson-Lewis, V., Andrews, L. J., … Friedlander, R. M. (2000). Functional role of caspase-1 and caspase-3 in an ALS transgenic mouse model. *Science (New York, N.Y.)*, *288*(5464), 335–9.

Li, Z., Cai, T., Tian, J., Xie, J. X., Zhao, X., Liu, L., … Xie, Z. (2009). NaKtide, a Na/K-ATPase-derived Peptide Src Inhibitor, Antagonizes Ouabain-activated Signal Transduction in Cultured Cells. *Journal of Biological Chemistry*, *284*(31), 21066–21076.

Liang, M., Tian, J., Liu, L., Pierre, S., Liu, J., Shapiro, J., & Xie, Z.-J. (2007). Identification of a Pool of Non-pumping Na/K-ATPase. *Journal of Biological Chemistry*, *282*(14), 10585–10593.

Lifshitz, Y., Petrovich, E., Haviv, H., Goldshleger, R., Tal, D. M., Garty, H., & Karlish, S. J. D. (2007). Purification of the Human α2 Isoform of Na,K-ATPase Expressed in *Pichia pastoris*. Stabilization by Lipids and FXYD1 [†]. *Biochemistry*, *46*(51), 14937–14950.

Lifshitz, Y., Lindzen, M., Garty, H., & Karlish, S. J. D. (2006). Functional Interactions of Phospholemman (PLM) (FXYD1) with Na + ,K + -ATPase. Journal of Biological Chemistry, 281(23), 15790–15799

Liu, J., Tian, J., Chaudhry, M., Maxwell, K., Yan, Y., Wang, X., … Shapiro, J. I. (2016). Attenuation of Na/K-ATPase Mediated Oxidant Amplification with pNaKtide Ameliorates Experimental Uremic Cardiomyopathy. *Scientific Reports*, *6*(1), 34592.

Liu, L., & Askari, A. (2006). β-Subunit of cardiac Na+-K+-ATPase dictates the concentration of the functional enzyme in caveolae. *American Journal of Physiology - Cell Physiology*, *291*(4).

Liu, L., Mohammadi, K., Aynafshar, B., Wang, H., Li, D., Liu, J., … Askari, A. (2003). Role of caveolae in signal-transducing function of cardiac Na+/K+-ATPase. *American Journal of Physiology - Cell Physiology*, *284*(6).

Liu, L., Zhao, X., Pierre, S. V., & Askari, A. (2007). Association of PI3K-Akt signaling pathway with digitalis-induced hypertrophy of cardiac myocytes. *American Journal of Physiology - Cell Physiology*, *293*(5).

Liu, X., Špicarová, Z., Rydholm, S., Li, J., Brismar, H., & Aperia, A. (2008). Ankyrin B Modulates the Function of Na,K-ATPase/Inositol 1,4,5-Trisphosphate Receptor Signaling Microdomain. *Journal of Biological Chemistry*, *283*(17), 11461–11468.

Madan, N., Xu, Y., Duan, Q., Banerjee, M., Larre, I., Pierre, S. V., & Xie, Z. (2017). Src-independent ERK signaling through the rat α3 isoform of Na/K-ATPase. *American Journal of Physiology - Cell Physiology*, *312*(3).

Malik, N., Canfield, V. A., Beckers, M. C., Gros, P., & Levenson, R. (1996). Identification of the mammalian Na,K-ATPase 3 subunit. *The Journal of Biological Chemistry*, *271*(37), 22754–8.

Mansergh, F., Orton, N. C., Vessey, J. P., Lalonde, M. R., Stell, W. K., Tremblay, F., … Bech-Hansen, N. T. (2005). Mutation of the calcium channel gene Cacna1f disrupts calcium signaling, synaptic transmission and cellular organization in mouse retina. *Human Molecular Genetics*, *14*(20), 3035–3046.

Mattson, M. P. (2000). Apoptosis in neurodegenerative disorders. *Nature Reviews Molecular Cell Biology*, *1*(2), 120–130.

McKnight, A., Shotton, C., Cordell, J., Jones, I., Simmons, G., & Clapham, P. R. (1996). Location, exposure, and conservation of neutralizing and nonneutralizing epitopes on human immunodeficiency virus type 2 SU glycoprotein. *Journal of Virology*, *70*(7), 4598–606.

Miller, R. P., & Farley, R. A. (1988). All three potential N-glycosylation sites of the dog kidney (Na+ + K+)-ATPase beta-subunit contain oligosaccharide. *Biochimica et Biophysica Acta*, *954*(1), 50–7.

Mishra, N. K., Peleg, Y., Cirri, E., Belogus, T., Lifshitz, Y., Voelker, D. R., … Karlish, S. J. D. (2011). FXYD Proteins Stabilize Na,K-ATPase. *Journal of Biological Chemistry*, *286*(11), 9699–9712.

Miyakawa-Naito, A., Uhlén, P., Lal, M., Aizman, O., Mikoshiba, K., Brismar, H., … Aperia, A. (2003). Cell Signaling Microdomain with Na,K-ATPase and Inositol 1,4,5-Trisphosphate Receptor Generates Calcium Oscillations. *Journal of Biological Chemistry*, *278*(50), 50355–50361.

Molday, L. L., Hicks, D., Sauer, C. G., Weber, B. H., & Molday, R. S. (2001). Expression of X-linked retinoschisis protein RS1 in photoreceptor and bipolar cells. *Investigative Ophthalmology & Visual Science*, *42*(3), 816–25.

Molday, L. L., Wu, W. W. H., & Molday, R. S. (2007). Retinoschisin (RS1), the Protein Encoded by the X-linked Retinoschisis Gene, Is Anchored to the Surface of Retinal Photoreceptor and Bipolar Cells through Its Interactions with a Na/K ATPase-SARM1 Complex. *Journal of Biological Chemistry*, *282*(45), 32792–32801.

Molday, R. S. (2007). Focus on Molecules: Retinoschisin (RS1). *Experimental Eye Research*, *84*(2), 227–228.

Molday, R. S., Kellner, U., & Weber, B. H. F. (2012). X-linked juvenile retinoschisis: Clinical diagnosis, genetic analysis, and molecular mechanisms. *Progress in Retinal and Eye Research*, *31*(3), 195–212.

Morth, J. P., Pedersen, B. P., Toustrup-Jensen, M. S., Sørensen, T. L.-M., Petersen, J., Andersen, J. P., … Nissen, P. (2007). Crystal structure of the sodium–potassium pump. *Nature*, *450*(7172), 1043–1049.

Mu, X., He, J., Anderson, D. W., Springer, J. E., & Trojanowski, J. Q. (1996). Altered expression ofbcl-2 andbax mRNA in amyotrophic lateral sclerosis spinal cord motor neurons. *Annals of Neurology*, *40*(3), 379–386.

Murphy, L. O., & Blenis, J. (2006). MAPK signal specificity: the right place at the right time. *Trends in Biochemical Sciences*, *31*(5), 268–275.

Ono, Y., Tsuruma, K., Takata, M., Shimazawa, M., & Hara, H. (2016). Glycoprotein nonmetastatic melanoma protein B extracellular fragment shows neuroprotective effects and activates the PI3K/Akt and MEK/ERK pathways via the Na+/K+-ATPase. *Scientific Reports*, *6*, 23241.

Orlov, S., Klimanova, E., Tverskoi, A., Vladychenskaya, E., Smolyaninova, L., & Lopina, O. (2017). Na+i,K+i-Dependent and -Independent Signaling Triggered by Cardiotonic Steroids: Facts and Artifacts. *Molecules*, *22*(4), 635.

Ortel, T. L., Devore-Carter, D., Quinn-Allen, M., & Kane, W. H. (1992). Deletion analysis of recombinant human factor V. Evidence for a phosphatidylserine binding site in the second C-type domain. *The Journal of Biological Chemistry*, *267*(6), 4189–98.

Ou, J., Vijayasarathy, C., Ziccardi, L., Chen, S., Zeng, Y., Marangoni, D., … Sieving, P. A. (2015). Synaptic pathology and therapeutic repair in adult retinoschisis mouse by AAV-RS1 transfer. *Journal of Clinical Investigation*, *125*(7), 2891–2903.

Pagenstecher HE. Ueber eine unter dem Bilde der Netzhauterblosung verlaufende, erbliche Erkrankung der Retina. Graefes Arch Ophthalmol 1913; 86: 457-62.

Park, T. K., Wu, Z., Kjellstrom, S., Zeng, Y., Bush, R. A., Sieving, P. A., & Colosi, P. (2009). Intravitreal delivery of AAV8 retinoschisin results in cell type-specific gene expression and retinal rescue in the Rs1-KO mouse. *Gene Therapy*, *16*(7), 916–926.

Pedersen, P. L., & Carafoli, E. (1987). Ion motive ATPases. I. Ubiquity, properties, and significance to cell function. *Trends in Biochemical Sciences*, *12*, 146–150.

Plössl, K., Weber, B. H. F., & Friedrich, U. (2017). The X-linked juvenile retinoschisis protein retinoschisin is a novel regulator of mitogen-activated protein kinase signalling and apoptosis in the retina. *Journal of Cellular and Molecular Medicine*, *21*(4), 768–780. (a)

Plössl, K., Royer, M., Bernklau, S., Tavraz, N. N., Friedrich, T., Wild, J., … Friedrich, U. (2017). Retinoschisin is linked to retinal Na/K-ATPase signaling and localization. *Molecular Biology of the Cell*, mbc.E17-01-0064. (b)

Poole, S., Firtel, R. A., Lamar, E., & Rowekamp, W. (1981). Sequence and expression of the discoidin I gene family in Dictyostelium discoideum. *Journal of Molecular Biology*, *153*(2), 273–89.

Qi, M., & Elion, E. A. (2005). MAP kinase pathways. Journal of Cell Science, 118(16), 3569–3572.

Quintas, L. E. M., Pierre, S. V, Liu, L., Bai, Y., Liu, X., & Xie, Z.-J. (2010). Alterations of Na+/K+-ATPase function in caveolin-1 knockout cardiac fibroblasts. *Journal of Molecular and Cellular Cardiology*, *49*(3), 525–31.

Prasad, A., Wagner, R., & Bhagat, N. (2006) Vitreous hemorrhage as the initial manifestation of X-linked retinoschisis in a 9-month-old infant. *Journal of Pediatric Ophthalmology and Strabismus*, *43*(1), 56–8.

Price, E. M., & Lingrel, J. B. (1988). Structure-function relationships in the Na,K-ATPase alpha subunit: site-directed mutagenesis of glutamine-111 to arginine and asparagine-122 to aspartic acid generates a ouabain-resistant enzyme. *Biochemistry*, *27*(22), 8400–8.

Pu, H. X., Cluzeaud, F., Goldshleger, R., Karlish, S. J., Farman, N., & Blostein, R. (2001). Functional role and immunocytochemical localization of the gamma a and gamma b forms of the Na,K-ATPase gamma subunit. *The Journal of Biological Chemistry*, *276*(23), 20370–8.

Ramirez-Ortega, M., Maldonado-Lagunas, V., Melendez-Zajgla, J., Carrillo-Hernandez, J. F., Pastelín-Hernandez, G., Picazo-Picazo, O., & Ceballos-Reyes, G. (2006). Proliferation and apoptosis of HeLa cells induced by in vitro stimulation with digitalis. *European Journal of Pharmacology*, *534*(1–3), 71–76.

Reid, S. N. M., Yamashita, C., & Farber, D. B. (2003). Retinoschisin, a photoreceptor-secreted protein, and its interaction with bipolar and muller cells. *The Journal of Neuroscience : The Official Journal of the Society for Neuroscience*, *23*(14), 6030–40.

Reinhard, L., Tidow, H., Clausen, M. J., & Nissen, P. (2013). Na+,K+-ATPase as a docking station: protein–protein complexes of the Na+,K+-ATPase. *Cellular and Molecular Life Sciences*, *70*(2), 205–222.

Renner, A. B., Kellner, U., Fiebig, B., Cropp, E., Foerster, M. H., & Weber, B. H. F. (2008). ERG variability in X-linked congenital retinoschisis patients with mutations in the RS1 gene and the diagnostic importance of fundus autofluorescence and OCT. *Documenta Ophthalmologica*, *116*(2), 97–109.

Riss, T. L., Moravec, R. A., Niles, A. L., Duellman, S., Benink, H. A., Worzella, T. J., & Minor, L. (2004). *Cell Viability Assays*. *Assay Guidance Manual.* Eli Lilly & Company and the National Center for Advancing Translational Sciences.

Rodríguez, F. J., Rodríguez, A., Mendoza-Londoño, R., & Tamayo, M. L. (2005). X-linked retinoschisis in three females from the same family: a phenotype-genotype correlation. *Retina (Philadelphia, Pa.)*, *25*(1), 69–74.

Roskoski, R. (2012). ERK1/2 MAP kinases: Structure, function, and regulation. *Pharmacological Research*, *66*(2), 105–143.

Rusciano, M. R., Salzano, M., Monaco, S., Sapio, M. R., Illario, M., De Falco, V., … Vitale, M. (2010). The Ca2+-calmodulin-dependent kinase II is activated in papillary thyroid carcinoma (PTC) and mediates cell proliferation stimulated by RET/PTC. *Endocrine Related Cancer*, *17*(1), 113–123.

SanGiovanni, J. P., & Lee, P. H. (2013). AMD-Associated Genes Encoding Stress-Activated MAPK Pathway Constituents Are Identified by Interval-Based Enrichment Analysis. *PLoS ONE*, *8*(8), e71239.

Saldana, M., Thompson, J., Monk, E., Trump, D., Long, V., & Sheridan, E. (2007). X-linked retinoschisis in a female with a heterozygous RS1 missense mutation. *American Journal of Medical Genetics Part A*, *143A*(6), 608–609.

Sauer, C. G., Gehrig, A., Warneke-Wittstock, R., Marquardt, A., Ewing, C. C., Gibson, A., … Weber, B. H. F. (1997). Positional cloning of the gene associated with X-linked juvenile retinoschisis. *Nature Genetics*, *17*(2), 164–70.

Schneider, B. G., & Kraig, E. (1990). Na+, K(+)-ATPase of the photoreceptor: selective expression of alpha 3 and beta 2 isoforms. *Experimental Eye Research*, *51*(5), 553–64.

Schoner, W., & Scheiner-Bobis, G. (2007). Endogenous and exogenous cardiac glycosides and their mechanisms of action. *American Journal of Cardiovascular Drugs : Drugs, Devices, and Other Interventions*, *7*(3), 173–89.

Sekimukai, D., Honda, S., & Negi, A. (2009). RNA interference for apoptosis signal-regulating kinase-1 (ASK-1) rescues photoreceptor death in the rd1 mouse. *Molecular Vision*, *15*, 1764–73.

Sergeev Y., Bowles K., Ziccardi L, Sieving P. (2011). Molecular Modeling of Protein Structure, Biology of Disease and Clinical Electroretinography in Human X-Linked Retinoschisis (XLRS). In *Electroretinograms*. InTech.

Shamraj, O. I., & Lingrel, J. B. (1994). A putative fourth Na+,K(+)-ATPase alpha-subunit gene is expressed in testis. *Proceedings of the National Academy of Sciences of the United States of America*, *91*(26), 12952–6.

Shi, L., Jian, K., Ko, M. L., Trump, D., & Ko, G. Y.-P. (2009). Retinoschisin, a New Binding Partner for L-type Voltage-gated Calcium Channels in the Retina. *Journal of Biological Chemistry*, *284*(6), 3966–3975.

Shi, L., Ko, M. L., & Ko, G. Y.-P. (2017). Retinoschisin Facilitates the Function of L-Type Voltage-Gated Calcium Channels. *Frontiers in Cellular Neuroscience*, *11*, 232.

Shoshani, L., Contreras, R. G., Roldán, M. L., Moreno, J., Lázaro, A., Balda, M. S., … Cereijido, M. (2005). The Polarized Expression of Na+,K+-ATPase in Epithelia Depends on the Association between -Subunits Located in Neighboring Cells. *Molecular Biology of the Cell*, *16*(3), 1071–1081.

Shukla, D., Naresh, K. B., Rajendran, A., & Kim, R. (2006). Macular hole secondary to X-linked retinoschisis. *Eye*, *20*(12), 1459–1461.

Shyjan, A. W., Gottardi, C., & Levenson, R. (1990). The Na,K-ATPase beta 2 subunit is expressed in rat brain and copurifies with Na,K-ATPase activity. *The Journal of Biological Chemistry*, *265*(9), 5166–9.

Shyjan, A. W., & Levenson, R. (1989). Antisera specific for the alpha 1, alpha 2, alpha 3, and beta subunits of the Na,K-ATPase: differential expression of alpha and beta subunits in rat tissue membranes. *Biochemistry*, *28*(11), 4531–5.

Sikkink, S. K., Biswas, S., Parry, N. R. A., Stanga, P. E., & Trump, D. (2007). X-linked retinoschisis: an update. *Journal of Medical Genetics*, *44*(4), 225–32.

Skou JC (1957) The influence of some cations on an adenosine triphosphatase from peripheral nerves. Biochim Biophys Acta *23*:394–401

Song, D., & Dunaief, J. L. (2013). Retinal iron homeostasis in health and disease. *Frontiers in Aging Neuroscience*, *5*, 24.

Song, H., Lee, M. Y., Kinsey, S. P., Weber, D. J., & Blaustein, M. P. (2006). An N-terminal Sequence Targets and Tethers Na$^+$ Pump α2 Subunits to Specialized Plasma Membrane Microdomains. *Journal of Biological Chemistry*, *281*(18), 12929–12940.

Sorenson, C. M., Padanilam, B. J., & Hammerman, M. R. (1996). Abnormal postpartum renal development and cystogenesis in the bcl-2 (-/-) mouse. *The American Journal of Physiology*, *271*(1 Pt 2), F184-93.

Steiner-Champliaud, M.-F., Sahel, J., & Hicks, D. (2006). Retinoschisin forms a multi-molecular complex with extracellular matrix and cytoplasmic proteins: interactions with beta2 laminin and alphaB-crystallin. *Molecular Vision*, *12*, 892–901.

Sweadner, K. J., & Rael, E. (2000). The FXYD Gene Family of Small Ion Transport Regulators or Channels: cDNA Sequence, Protein Signature Sequence, and Expression. *Genomics*, *68*(1), 41–56.

Takada, Y., Fariss, R. N., Tanikawa, A., Zeng, Y., Carper, D., Bush, R., & Sieving, P. A. (2004). A Retinal Neuronal Developmental Wave of Retinoschisin Expression Begins in Ganglion Cells during Layer Formation. *Investigative Opthalmology & Visual Science*, *45*(9), 3302.

Takada, Y., Fariss, R. N., Muller, M., Bush, R. A., Rushing, E. J., & Sieving, P. A. (2006). Retinoschisin expression and localization in rodent and human pineal and consequences of mouse RS1 gene knockout. *Molecular Vision*, *12*, 1108–16.

Tantri, A., Vrabec, T. R., Cu-Unjieng, A., Frost, A., Annesley, W. H., & Donoso, L. A. (2004). X-linked retinoschisis: A clinical and molecular genetic review. *Survey of Ophthalmology*, *49*(2), 214–230.

Tang, F., Wang, Y., Hemmings, B., Rüegg, C., Xue, G. PKB/Akt-dependent regulation of inflammation in cancer. (2017). *Seminars in Cancer Biology*.

Therien, A. G., Karlish, S. J., & Blostein, R. (1999). Expression and functional role of the gamma subunit of the Na, K-ATPase in mammalian cells. *The Journal of Biological Chemistry*, *274*(18), 12252–6.

Therien, A. G., & Blostein, R. (2000). Mechanisms of sodium pump regulation. American Journal of Physiology. *Cell Physiology*, 279(3), C541-66.

Tian, J., Cai, T., Yuan, Z., Wang, H., Liu, L., Haas, M., … Xie, Z.-J. (2005). Binding of Src to Na+/K+-ATPase Forms a Functional Signaling Complex. *Molecular Biology of the Cell*, *17*(1), 317–326.

Tian, J., & Xie, Z. (2008). The Na-K-ATPase and calcium-signaling microdomains. *Physiology (Bethesda, Md.)*, *23*, 205–11.

Tokhtaeva, E., Munson, K., Sachs, G., & Vagin, O. (2010). N-glycan-dependent quality control of the Na,K-ATPase beta(2) subunit. *Biochemistry*, *49*(14), 3116–28.

Tokhtaeva, E., Sun, H., Deiss-Yehiely, N., Wen, Y., Soni, P. N., Gabrielli, N. M., … Dada, L. A. (2016). The *O*-glycosylated ectodomain of FXYD5 impairs adhesion by disrupting cell–cell trans-dimerization of Na,K-ATPase β_1 subunits. *Journal of Cell Science*, *129*(12), 2394–2406

Tolun, G., Vijayasarathy, C., Huang, R., Zeng, Y., Li, Y., Steven, A. C., … Heymann, J. B. (2016). Paired octamer rings of retinoschisin suggest a junctional model for cell-cell adhesion in the retina. *Proceedings of the National Academy of Sciences of the United States of America*, *113*(19), 5287–92.

Troost, D., Aten, J., Morsink, F., & de Jong, J. M. (1995). Apoptosis in amyotrophic lateral sclerosis is not restricted to motor neurons. Bcl-2 expression is increased in unaffected post-central gyrus. *Neuropathology and Applied Neurobiology*, *21*(6), 498–504.

Upmanyu, N., Dietze, R., Kirch, U., & Scheiner-Bobis, G. (2016). Ouabain interactions with the α4 isoform of the sodium pump trigger non-classical steroid hormone signaling and integrin expression in spermatogenic cells. *Biochimica et Biophysica Acta (BBA) - Molecular Cell Research*, *1863*(11), 2809–2819.

Vagin, O., Dada, L. A., Tokhtaeva, E., & Sachs, G. (2012). The Na-K-ATPasea1b1 heterodimer as a cell adhesion molecule in epithelia. *AJP: Cell Physiology*, *302*(9), C1271–C1281.

Valencia, A., Pestaña, A., & Cano, A. (1989). Spectroscopical studies on the structural organization of the lectin discoidin I: analysis of sugar- and calcium-binding activities. *Biochimica et Biophysica Acta*, *990*(1), 93–7.

Veis, D. J., Sorenson, C. M., Shutter, J. R., & Korsmeyer, S. J. (1993). Bcl-2-deficient mice demonstrate fulminant lymphoid apoptosis, polycystic kidneys, and hypopigmented hair. *Cell*, *75*(2), 229–40.

Verbakel, S. K., van de Ven, J. P. H., Le Blanc, L. M. P., Groenewoud, J. M. M., de Jong, E. K., Klevering, B. J., & Hoyng, C. B. (2016). Carbonic Anhydrase Inhibitors for the Treatment of Cystic Macular Lesions in Children With X-Linked Juvenile Retinoschisis. *Investigative Ophthalmology & Visual Science*, *57*(13), 5143–5147.

Vijayasarathy, C., Gawinowicz, M. A., Zeng, Y., Takada, Y., Bush, R. A., & Sieving, P. A. (2006). Identification and characterization of two mature isoforms of retinoschisin in murine retina. *Biochemical and Biophysical Research Communications*, *349*(1), 99–105.

Vijayasarathy, C., Sui, R., Zeng, Y., Yang, G., Xu, F., Caruso, R. C., … Sieving, P. A. (2010). Molecular Mechanisms Leading to Null-Protein Product from Retinoschisin (RS1) Signal-Sequence Mutants in X-Linked Retinoschisis (XLRS) Disease. *Human Mutation*, *31*(11), 1251–1260.

Vijayasarathy, C., Takada, Y., Zeng, Y., Bush, R. A., & Sieving, P. A. (2007). Retinoschisin Is a Peripheral Membrane Protein with Affinity for Anionic Phospholipids and Affected by Divalent Cations. *Investigative Opthalmology & Visual Science*, *48*(3), 991.

Vincent, A., Robson, A. G., Neveu, M. M., Wright, G. A., Moore, A. T., Webster, A. R., & Holder, G. E. (2013). A Phenotype–Genotype Correlation Study of X-Linked Retinoschisis. *Ophthalmology*, *120*(7), 1454–1464.

Walia, S., Fishman, G. A., Molday, R. S., Dyka, F. M., Kumar, N. M., Ehlinger, M. A., & Stone, E. M. (2009). Relation of response to treatment with dorzolamide in X-linked retinoschisis to the mechanism of functional loss in retinoschisin. *American Journal of Ophthalmology*, *147*(1), 111–115.e1.

Wang, H., Haas, M., Liang, M., Cai, T., Tian, J., Li, S., & Xie, Z. (2004). Ouabain Assembles Signaling Cascades through the Caveolar Na $^+$/K$^+$ -ATPase. *Journal of Biological Chemistry*, *279*(17), 17250–17259.

Wang, T., Waters, C. T., Rothman, A. M. K., Jakins, T. J., Römisch, K., & Trump, D. (2002). Intracellular retention of mutant retinoschisin is the pathological mechanism underlying X-linked retinoschisis. *Human Molecular Genetics*, *11*(24), 3097–105.

Wang S., Zhang C., Sheng X., Zhang X., Wang B., Zhang G.Peripheral expression of MAPK pathways in Alzheimer's and Parkinson's diseases. (2014). *Journal of Clinical Neuroscience*, *21*(5), 810–814. https://doi.org/10.1016/J.JOCN.2013.08.017

Wang, Y., Zhan, Y., Xu, R., Shao, R., Jiang, J., & Wang, Z. (2015). Src mediates extracellular signal-regulated kinase 1/2 activation and autophagic cell death induced by

cardiac glycosides in human non-small cell lung cancer cell lines. *Molecular Carcinogenesis*, *54*(S1), E26–E34.

Weber, B. H. F., Schrewe, H., Molday, L. L., Gehrig, A., White, K. L., Seeliger, M. W., … Molday, R. S. (2002). Inactivation of the murine X-linked juvenile retinoschisis gene, Rs1h, suggests a role of retinoschisin in retinal cell layer organization and synaptic structure. *Proceedings of the National Academy of Sciences*, *99*(9), 6222–6227.

Weber, B. H. F., & Kellner, U. (2007). X-Linked Juvenile Retinoschisis. In *Retinal Degenerations* (pp. 119–135). Totowa, NJ: Humana Press.

Weigand, K. M., Swarts, H. G. P., Fedosova, N. U., Russel, F. G. M., & Koenderink, J. B. (2012). Na,K-ATPase activity modulates Src activation: A role for ATP/ADP ratio. *Biochimica et Biophysica Acta (BBA) - Biomembranes*, *1818*(5), 1269–1273.

Wetzel, R. K., Arystarkhova, E., & Sweadner, K. J. (1999). Cellular and subcellular specification of Na,K-ATPase alpha and beta isoforms in the postnatal development of mouse retina. *The Journal of Neuroscience : The Official Journal of the Society for Neuroscience*, *19*(22), 9878–89.

Wieacker, P., Wienker, B., Mevorah, B., Dallapiccola, K., Davies, K., Ropers, H. (1984). "Linkage Relationships between Xg, Steroid Sulfatase (Sts) and Retinoschisis (Rs), Respectively, and a Cloned DNA-Sequence from the Distal Short Arm of the X-Chromosome." Cytogenet Cell Genet **37**(1-4): 608-608.

Whitmarsh, A. J. (2007). Regulation of gene transcription by mitogen-activated protein kinase signaling pathways. *Biochimica et Biophysica Acta (BBA) - Molecular Cell Research*, *1773*(8), 1285–1298.

Whitmarsh, A. J., & Davis, R. J. (1996). Transcription factor AP-1 regulation by mitogen-activated protein kinase signal transduction pathways. *Journal of Molecular Medicine (Berlin, Germany)*, *74*(10), 589–607.

Wolfensberger, T. J. (1999). The role of carbonic anhydrase inhibitors in the management of macular edema. *Documenta Ophthalmologica. Advances in Ophthalmology*, *97*(3–4), 387–97. 5

Wu, G., Cotlier, E., & Brodie, S. (1985). A carrier state of X-linked juvenile retinoschisis. *Ophthalmic Paediatrics and Genetics*, *5*(1–2), 13–7. Retrieved from

Wu, J., Akkuratov, E. E., Bai, Y., Gaskill, C. M., Askari, A., & Liu, L. (2013). Cell signaling associated with Na(+)/K(+)-ATPase: activation of phosphatidylinositide 3-kinase IA/Akt by ouabain is independent of Src. *Biochemistry*, *52*(50), 9059–67.

Wu, W. W. H., & Molday, R. S. (2003). Defective discoidin domain structure, subunit assembly, and endoplasmic reticulum processing of retinoschisin are primary mechanisms responsible for X-linked retinoschisis. *The Journal of Biological Chemistry*, *278*(30), 28139–46.

Wu, W. W. H., Wong, J. P., Kast, J., & Molday, R. S. (2005). RS1, a Discoidin Domain-containing Retinal Cell Adhesion Protein Associated with X-linked Retinoschisis, Exists as a Novel Disulfide-linked Octamer. *Journal of Biological Chemistry*, *280*(11), 10721–10730.

Xie, J., Ye, Q., Cui, X., Madan, N., Yi, Q., Pierre, S. V., & Xie, Z. (2015). Expression of rat Na-K-ATPase α2 enables ion pumping but not ouabain-induced signaling in α1-deficient porcine renal epithelial cells. *American Journal of Physiology - Cell Physiology*, *309*(6), C373–C382.

Xie, Z., Kometiani, P., Liu, J., Li, J., Shapiro, J. I., & Askari, A. (1999). Intracellular reactive oxygen species mediate the linkage of Na+/K+-ATPase to hypertrophy and its marker genes in cardiac myocytes. *The Journal of Biological Chemistry*, *274*(27), 19323–8.

Xie, Z., & Cai, T. (2003). Na+-K+-ATPase-Mediated Signal Transduction: From Protein Interaction to Cellular Function. *Molecular Interventions*, *3*(3), 157–168.

Xie, Z., & Askari, A. (2002). Na(+)/K(+)-ATPase as a signal transducer. *European Journal of Biochemistry*, *269*(10), 2434–9

Xu, J., Molday, L. L., Molday, R. S., & Sarunic, M. V. (2009). In vivo imaging of the mouse model of X-linked juvenile retinoschisis with fourier domain optical coherence tomography. *Investigative Ophthalmology & Visual Science*, *50*(6), 2989–93.

Yating, Q., Yuan, Y., wei, Z., Qing, G., xingwei, W., Qiu, Q., & Lili, Y. (2015). Oxidized LDL Induces Apoptosis of Human Retinal Pigment Epithelium Through Activation of ERK-Bax/Bcl-2 Signaling Pathways. *Current Eye Research*, *40*(4), 415–422.

Ye, G.-J., Budzynski, E., Sonnentag, P., Miller, P. E., Sharma, A. K., Ver Hoeve, J. N., … Chulay, J. D. (2015). Safety and Biodistribution Evaluation in Cynomolgus Macaques of rAAV2tYF-CB-hRS1, a Recombinant Adeno-Associated Virus Vector Expressing Retinoschisin. *Human Gene Therapy Clinical Development*, *26*(3), 165–176.

Ye, G.-J., Conlon, T., Erger, K., Sonnentag, P., Sharma, A. K., Howard, K., … Chulay, J. D. (2015). Safety and Biodistribution Evaluation of rAAV2tYF-CB-hRS1, a Recombinant Adeno-Associated Virus Vector Expressing Retinoschisin, in RS1-Deficient Mice. *Human Gene Therapy Clinical Development*, *26*(3), 177–184.

Yosef, E., Katz, A., Peleg, Y., Mehlman, T., & Karlish, S. J. D. (2016). Do Src Kinase and Caveolin Interact Directly with Na,K-ATPase? *Journal of Biological Chemistry*, *291*(22), 11736–11750.

Yuan, Z., Cai, T., Tian, J., Ivanov, A. V, Giovannucci, D. R., & Xie, Z. (2005). Na/K-ATPase tethers phospholipase C and IP3 receptor into a calcium-regulatory complex. *Molecular Biology of the Cell*, *16*(9), 4034–45.

Zellner, H., Staudigel, M., Trenner, T., Bittkowski, M., Wolowski, V., Icking, C., & Merkl, R. (2012). Prescont: Predicting protein-protein interfaces utilizing four residue properties. *Proteins: Structure, Function, and Bioinformatics*, *80*(1), 154–168.

Zeng, Y., Takada, Y., Kjellstrom, S., Hiriyanna, K., Tanikawa, A., Wawrousek, E., … Sieving, P. A. (2004). *RS-1* Gene Delivery to an Adult *Rs1h* Knockout Mouse Model Restores ERG b-Wave with Reversal of the Electronegative Waveform of X-Linked Retinoschisis. *Investigative Opthalmology & Visual Science*, *45*(9), 3279.

Zhang, Y. (2008). I-TASSER server for protein 3D structure prediction. *BMC Bioinformatics*, *9*, 40. https://doi.org/10.1186/1471-2105-9-40

Zhang, L., Zhang, Z., Guo, H., & Wang, Y. (2008). Na $^+$/K $^+$ -ATPase-mediated signal transduction and Na $^+$/K $^+$ -ATPase regulation. *Fundamental & Clinical Pharmacology*, *22*(6), 615–621.

Zhang, W., & Liu, H. T. (2002). MAPK signal pathways in the regulation of cell proliferation in mammalian cells. *Cell Research*, 12(1),

Zhou, X. J., & Kukes, G. (1998). Pathogenesis of autosomal dominant polycystic kidney disease: role of apoptosis. *Diagnostic Molecular Pathology : The American Journal of Surgical Pathology, Part B*, *7*(2), 65–8.

Zwaal, R. F., Comfurius, P., & Bevers, E. M. (1998). Lipid-protein interactions in blood coagulation. *Biochimica et Biophysica Acta*, *1376*(3), 433–53.

List of Abbreviations

Abbreviation	Meaning
µ	micro
µl	microliter
µM	micromolar
aa	amino acid
AAS	Atomic absorption spectroscopy
APS	Ammoniumpersulfate
ATP	Adenosintriphosphate
bp	base pair
BSA	Bovine Serum Albumine
C	cystein
cDNA	complementary DNA
Dapi	4',6-Diamidin-2-phenylindol
DMEM	Dulbecco`s Modified Eagle Medium
DMSO	Dimethylsulfoxide
DNA	Deoxyribonucleicacid
dNTP	Deoxynucleotidetriphosphate
E. coli	*Escherichia coli*
ECL	Enhanced chemiluminescence
EDTA	Ethylendiamintetraacetate
ER	Endoplasmatic reticulum
ERG	Electroretinogram
ERK	Extracelluar-signal regulated kinase
et al.	et aliter (and others)
FACS	Fluorescence activated cell sorting
FBS/FCS	Fetal bovine/calf serum
g	gram
G-418	Geneticin
h	hour
HRP	Horse radish peroxidase
IB	Immunoblot
IHC	Immunohistochemistry
INL	Inner nuclear layer
IPL	Inner plexiform layer
kb	kilobase
kDA	kilodalton
K_m	Michaelis Menten constant
l	liter
LB	Lysogeny broth
m	milli
M	molar
mAB	monoclonal antibody
MAPK	mitogen-activated protein kinase
min	minute
MM	Mastermix
mRNA	messenger riboculeicacid
n	nano
Na/K-ATPase	Sodium Potassium ATPase
NAD(P)H	Nicotinamide adenine dinucleotide phosphate
OD	Optical densitiy
ONL	Outer nuclear layer

OPL	Outer plexiform layer
P	postnatal
pAB	polyclonal antibody
PBS	Phosphate buffered saline
PCR	Polymerase chain reaction
Pen/Strep	Penicillin/Streptomycin
PFA	Paraformaldeyd
P_i	Orthophosphat
PVDF	Polyvinylidenfluorid
RNA	Ribonucleicacid
RS1	Retinoschisin
s	second
SDS	Sodium dodecyl sulfate
SDS-PAGE	sodium dodecyl sulfate polyacrylamide gel electrophoresis
Std	Standard
TBE	Tris Borat EDTA
TBS	Tris-buffered saline
TEMED	Tetramethylethylendiamine
Tris	Tris(hydroxymethyl)-aminomethan
V	Volt
WB	Western blot
WT	Wildtype
XLRS	X-linked juvenile retinoschisis

List of Figures

List of Tables

Acknowledgements

I would like to thank my supervisor Prof. Dr. Bernhard Weber for giving me the opportunity to do my PhD project at the Institute of Human Genetics and for providing a great and inspiring working environment throughout the whole project. I really appreciate all the suggestions and support I have gotten during my thesis work as well as getting the opportunity to present my work at international meetings.

Thanks to Prof. Dr. Christian Wetzel for mentoring my PhD project and for taking over the position of the second examiner of my thesis.

I would like to thank my collaborators at the University of Regensburg:

Prof. Dr. Rainer Merkl and Ms. Kristina Heyn for support with bioinformatics and computational analyses as well as fruitful discussions on the "Docking Patch" project.

Dr. Jens Wild for introducing me to FACS analysis and helping with data analysis and evaluation as well as preparation of the FACS data figures.

Prof. Dr. Karl Kunzelmann for providing initial support for establishing *Xenopus* oocytes as a model system for my project.

Prof. Dr. Rainer Schreiber for mentoring my PhD project as well as helping with establishing *Xenopus* oocytes as a model system.

Many thanks to Prof. Thomas Friedrich and his team at the Technical University of Berlin for carrying out experiments for the *Xenopus* project in their lab and for providing help with data analysis and presentation.

I would like to say a special thank you to Dr. Ulrike Friedrich for the dedication she put into this project and all her support, no matter if it was concerning experimental set-ups, data evaluation or writing and designing presentations, posters and manuscripts.

Thanks a lot, Lisa Parakenings, for excellent technical assistance and incredible valuable support with lab work.

I would also like to thank Denise Schmied for helping with and teaching me a lot about mouse work involved in this project.

Thanks to all my colleagues at the Institute of Human Genetics for providing a nice working environment and for the much appreciated tips and tricks when it came to lab work.

Thanks a lot to my family and friends for all their support and encouragement during the last few years of my degree.

Selbstständigkeitserklärung

Ich, Karolina Plößl, geboren am 30.12.1988 in Nabburg, erkläre hiermit, dass ich die vorliegende Arbeit ohne unzulässige Hilfe Dritter und ohne Benutzung anderer als der angegebenen Hilfsmittel angefertigt habe.

Die aus anderen Quellen direkt oder indirekt übernommenen Daten und Konzepte sind unter Angabe der Quelle gekennzeichnet. Insbesondere habe ich nicht die entgeltliche Hilfe von Vermittlungs- bzw. Beratungsdiensten (Promotionsberater oder andere Personen) in Anspruch genommen.

Die Arbeit wurde bisher weder im In- noch im Ausland in gleicher oder ähnlicher Form einer anderen Prüfungsbehörde vorgelegt.

Regensburg, 10.10.2017   Karolina Plößl